CHAPTER 1

INTRODUCTION

Fluid Catalytic Cracking (FCC) is one of the most efficient secondary processes to increase gross refinery margin (GRM). This process offers the greatest potential for increasing profitability in the entire refinery. FCC converts low- priced heavy feedstock into lighter, more valuable hydrocarbons such as liquefied petroleum gas (LPG) and gasoline. Coke is formed as a byproduct during the process along with dry gas, both of which are undesirable. The conversion and yield pattern strongly depend on the feedstock quality, operating conditions of the riser reactor-regenerator sections and the type of catalyst. The FCC process is very complex due to complicated hydrodynamics, heat transfer and mass transfer effects and complex cracking kinetics. These complex interactions coupled with economic importance of the unit have prompted many researchers to put their efforts on the modelling of FCC processes. Transport phenomena based mathematical models are the most popular because of their analytical description of the process in detail. Modeling is an iterative process and, therefore, leads to deeper understanding of the physics involved in the FCC process. Parametric sensitivity study helps in designing better control. Process optimization, which can be subsequently carried out, can lead to improved productivity by maximizing throughput and choosing optimal operating conditions. Optimizing online can help maximize long-term profits. Additionally, running a model simultaneously in parallel with the plant operation can help in monitoring the plant and its health.

1.1 FLUID CATALYTIC CRACKING UNIT

FCC units operate at high temperature and moderate pressure with finely divided silica/alumina based catalyst. One of the important advantages of FCC is the

ability of the catalyst to flow easily between the reactor and regenerator when fluidized with reaction mixture in vapor phase. Due to this fluidization of the catalyst, there is intimate interaction between the catalyst and hydrocarbons leading to more cracking reactions. The main components of FCCU are riser reactor and regenerator. The partially vaporized raw oil charge meets a stream of regenerated hot catalyst at the base of riser. The liquid droplets of the feed receive heat from the hot catalyst particles and almost instantaneously vaporize. As the vapors and catalyst particles move up the riser, the cracking reactions take place. Carbon generated during cracking reactions gets deposited on the catalyst surface and cracking activity progressively decreases. At the exit of the reactor, catalyst is separated from the reaction mass, adsorbed hydrocarbons stripped off in a stripper with the help of steam and the spent catalyst sent to regenerator. In the regenerator, the catalyst is continuously regenerated by burning off the coke deposited during the cracking reaction. Other auxiliary units such as feed preheat, air and flue gas systems are required for control and optimal operation of this unit for regenerating the catalyst.

1.1.1 FCC Feed

FCC processes the feedstock, which is obtained either from a refinery atmospheric distillation unit or vacuum distillation unit and normally has the boiling range from 650 0F (350 0C) to 1000+ 0F (550+ 0C). In addition, FCCU may also process heavy fractions from other conversion units (coker gas oil and hydrocracker fractionator bottoms) as part of the FCC feed blend. The feed is normally, heated to the desired reactor inlet temperature of 500 0F (260 0C to 700 0F (370 0C). The main fractionator bottoms pumparounds and /or fired heaters are usual sources of heat. The main feedstocks for FCC unit are as follows

- Straight- Run Feedstocks

- Flashed Distillate (~370-580 ^{0}C) from High Vacuum Units.
- Short Residue from High Vacuum Units.
- Light Long Residue (~370 +) from Crude Distillation Units

- Hydrogeneted Feedstocks
  - Hydrotreated Flashed Distillate
  - Hydrowax from Hydrocracker Bottom
  - Hydrogeneted Cycle Oils
- Miscellaneous
  - Heavy Gas Oil
  - Coker Gas Oil

In addition to fresh feed streams, FCCU may also recycle certain product streams, such as heavy cycle oil (HCO) and slurry settler. All these feedstocks and recycle strreams will have different properties and will therefore also have a different cracking behaviour in the FCCU.

1.1.2 Reactor-Regenerator Section

FCC feed enters at the bottom of the riser reactor through feed nozzle system as a mixture of vapors and liquid drops and makes contact with hot catalyst particles coming from the regenerator. Figure 1.1 shows a schematic of the FCC riser reactor and regenerator. Heat from the catalyst vaporizes the gas oil droplets and the cracking process, which occurs only in vapor phase at the catalyst surface. As a heavy molecule of gas oil cracks into several smaller hydrocarbon molecules, the vapor volume expands as it moves up the riser. These vapors carry the catalyst particles along with them at about the same velocity. The rate of vaporization of feed in the entry zone of the riser/reactor affects the cracking performance of the feed to a great

extant. The rate of cracking and yield of products are strongly dependent on the temperature and amount of catalyst.

The cracking process terminates in the riser reactor because of the deactivation of the catalyst due to the coke deposition on the catalyst surface as well as the short contact time between catalyst and vapor hydrocarbons in the riser reactor. The cracked hydrocarbons are separated from the catalyst in the cyclones which are located at the upper part of the reactor to prevent the catalyst particles from going along with the product stream. Finally, the cracked hydrocarbons, separated from the catalyst in the reactor and move overhead to the main fractionation column and gas plant. The main fractionator recovers the heavier products such as light cycle and decanted oil, from the gasoline and lighter products. The gas plant separates the main fractionator overhead vapors into gasoline, C3's, C4's and fuel gas.

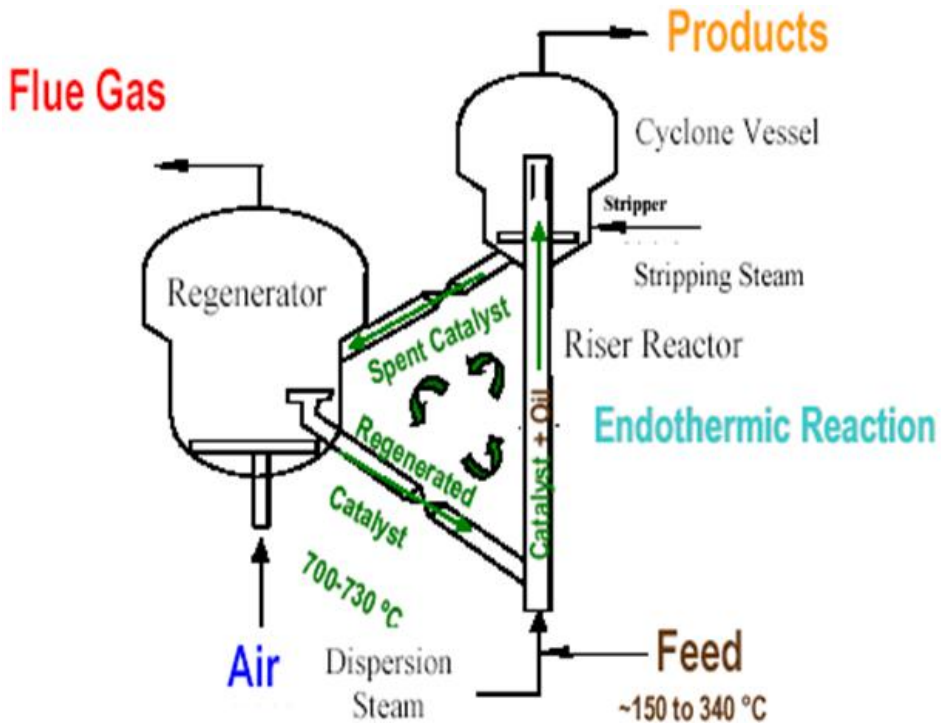

Figure 1.1: Schematic of riser reactor - regenerator

The catalyst falls down into the stripping section. Steam is used to strip the catalyst particles of the adsorbed hydrocarbons and the catalyst then flows down a

standpipe to the regenerator. A standpipe carries spent catalyst from reactor to mix with air at the base of the regenerator. The deposited coke on catalyst surface is burned in presence of air, which restores the catalyst activity. The flue gases are released in atmosphere after burning CO to CO2 in CO-boiler and removing catalyst particles in cyclones and scrubber unit. The regenerated catalyst flows down a standpipe to the reactor to meet the raw oil charge, and used as a heat carrier, provides heat required for endothermic cracking reactions and feed vaporization. This is the continuous cyclic process between regenerator and reactor.

1.2 MODELING OF FCC UNIT

The performance of the FCC units plays a major role in the overall economics of refinery plants. A small improvement in the operation or control of an FCC unit can result in impressive economic benefits. However, these can be achieved only if a satisfactory mathematical model is available which is analytical so that its optimization can lead to optimal operating conditions. A large number of researchers have examined this problem but because of the complexities involved, a completely satisfactory model has eluded each one so far. Because of a large number of components present in the FCC feed, a rigorous kinetic model is not possible. Therefore, the description of these complex reactions has been studied by lumping together a large number of chemical compounds. Modeling of FCC riser reactor is based on a specified number of lumps for feedstock and product yields rather than for individual molecules. These lumps are considered either on the basis of boiling range of the feedstock and corresponding products in the reaction system or based on type of hydrocarbon groups. Each type of hydrocarbons is assumed as one lump and the products are considered by different lumps according to their boiling range. Larger the number of lumps, more accurate will be the result but that requires still larger

number of rate parameters to be determined. This is seldom possible because of the cost associated with obtaining experimental data. Besides difficulties in developing a detailed kinetic model, other problems arise from the hydrodynamics which is no less complex. The partially vaporized feed enters the riser reactor through a system of pipes or nozzles which decide the liquid droplet sizes. These, in turn, decide the length of the riser required to completely vaporize the feed, which has profound influence on the reactor performance. Also, because of wall effect, the flow of vapors and catalyst particles is never plug flow type. Small catalyst particles may form loose agglomerates complicating heat and mass transfer. The slip between vapor and solid particles also completes the hydrodynamics. In view of these, the resultant hydrodynamics coupled with heat and mass transfer effects is very complex and no satisfactory hydrodynamic model is available.

1.3 SCOPE OF PRESENT WORK AND THESIS ORGANIZATION

As discussed above, a finite number of kinetic lumps are used to describe the reactions taking place in the FCC riser reactor. Two to six lump models considered feed as a single lump, which is too gross, and hence less than satisfactory. The ten or twelve lump kinetic models used by some researchers are quite elaborate and characterizes the feed not by a single lump but 6 to 8 lumps in terms of different hydrocarbon groups. However, the limitation of single lump representing feed is that the kinetics is valid only for the particular VGO with which the model parameters were estimated and is generally not applicable to other feeds especially if the composition is significantly different. Hence, a more realistic, a new ten lump kinetic model has been developed which is more general and applicable for various VGO with different properties. Moreover, the new ten lump kinetic model uses 6 lumps to describe the feed gas oil namely heavy and light paraffins, heavy and light naphthenes

and heavy and light aromatics. However, in day to day refinery operations, it is not possible to analyze every VGO stream in terms of these lumps before using in the FCC model. In the present work, an ANN model was sought to be developed, which relates the easily measurable properties of gas oil such as specific gravity, Conradson carbon residue (CCR), total sulfur, nitrogen and ASTM distillation temperatures to these kinetic lumps.

The main objectives have been identified that lead to a logical progression through the research:

I. Development of an Artificial Neural Network (ANN) model, which relates the simple feed properties such as specific gravity, CCR, total sulfur, nitrogen and ASTM distillation temperatures to the detailed composition of feed in terms of paraffins, naphthenes and aromatics.
II. Development of a new ten lump kinetic model for the riser reactor including estimation of kinetic parameters which when coupled with a regenerator model can simulate the behaviour of the FCC unit.
III. Combining the ANN model with the ten lump kinetic model along with a solution procedure into a simulation package for the prediction of FCC product yields from simple feed properties. This model should be feed composition invariant and be applicable to a variety of heavy gas oils.
IV. Comparison of present development with conventional five lump model results. Parametric sensitivity study with respect to operating conditions is desirable.

The research work done in this study has been organized into eight chapters. An outline of these chapters is as follows:

Chapter 1 provides an introduction to fluid catalytic cracking (FCC) with scope of present study and thesis organization.

Chapter 2 provides the literature review on modeling of FCC unit

Chapter 3 presents simulation of integrated five lump kinetic model for riser with a regenerator model. Also included is the parametric sensitivity study with respect to operating conditions of FCC unit.

Chapter 4 presents the experimental work required for ANN modeling. Also included are FCC yield data from an operating plant as well as from ASPEN FCC Simulator for kinetic modeling.

Chapter 5 includes the development of an artificial neural network model for predicting the FCC feed composition. The ANN model validation is also included in this chapter.

Chapter 6 presents the development of a new ten lump kinetic model with associated kinetic parameters estimation. A sensitivity study with respect to kinetic parameters is also included in this chapter.

Chapter 7 In this chapter, a simulator development based on the ten lump kinetics is discussed. The simulator predicted results are compared with plant experimental data for validation of the kinetic model. Also included in this chapter is a comparison of 10- lump model with 5 – lump model results.

Chapter 8 includes the conclusions drawn from the present study together with the recommendations for future work.

CHAPTER 2

LITERATURE REVIEW

Fluid catalytic cracking is a key unit in the refineries. It consists of a three-step process: reaction, product separation, and catalyst regeneration. In this cyclic process, gas oils are converted into lighter and more valuable products. The most important product from the FCC unit is gasoline, whose yield ranges between 46 and 51 wt% for standard feedstock and could increase to about 60 wt % for hydrotreated feedstock. The second commercial product is LPG whose yield is about 12 to 15 wt %. The operating conditions include high reaction temperatures in the range of 476 0C -525 0C (750 K-800 K) and pressure close to atmospheric conditions. The first unit in operation was model-1 from Standard Oil Development Co. (SOD, now Exxon Mobil) in 1942.This unit was composed of multiple small vessels and had a catalyst up-flow configuration in both the reactor and regenerator vessels. In 1947, UOP built the first unit as shown in Figure 2.1(a) that used the concept of spent catalyst stripping. In 1951, M. W. Kellogg introduced the Ortho-flow unit, composed of a low elevation regenerator and a high reactor with an internal stripper. In 1952, SOD introduced another FCC configuration, called model IV. This unit presented smaller vessels arranged side by side as per Figure 2.1(b) and was operated at higher pressure and internal velocities; catalyst flow control was done by changes in the differential pressure between the reactor and regenerator (U-bend concept) and by changes in the aeration in the spent catalyst entrance to the regenerator. The first riser cracking unit was proposed by Shell in 1957, and further introduced with high-activity zeolite catalysts in the 1960s. In 1961, Kellogg and Phillips developed first residue cracker on-stream at Borger, Texas. In 1972, Amoco Oil Co. invented high-temperature regeneration. In 1979, Exxon introduced the Flexicracking unit as per Figure 2.1(c)

that maintained a side-by-side arrangement but included a riser with an elevated stripper/disengager vessel and a lower elevation regenerator (Murcia, 1992).

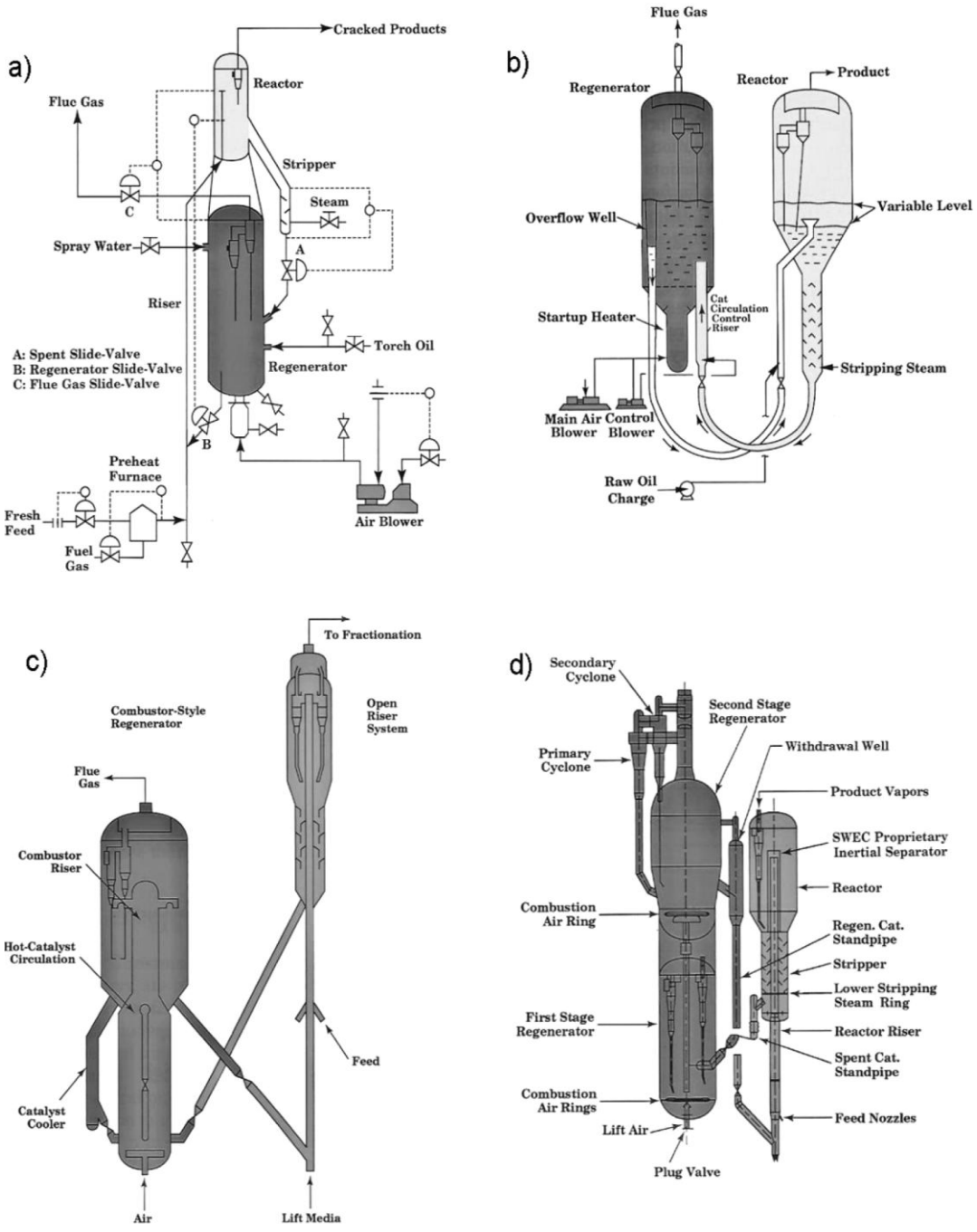

Figure 2.1: Scheme of different FCC units (a) UOP stacked unit (b) model IV (c) Exxon Flexicracking unit (d) R2R residue unit (Pinheiro et al., 2012).

In 1981, Total Petroleum, USA developed its residue FCC unit (R2R Unit, now licensed by Axens/IFP and Stone and Webster), presenting a Side-by-side

configuration with a two-stage regeneration system without catalyst cooling, which occurs in two separate stacked vessels, and a straight riser reactor with a proprietary feed injection system and an internal exit separation system shown in Figure 2.1(d). In 1983, Mobil reported first commercial use of ZSM-5 octane /olefins additive in FCC and further installed closed cyclone systems in 1985. In 1994, Coastal Corporation conducted commercial test of ultra short residence time with selective cracking. The recent developments in FCC technology have also been implemented to satisfy the increasing propylene demand with a second riser in the FCC complex to which the light cracked naphtha produced in the first riser is sent for further processing (Wang et al., 2008 and Li et al., 2007).

The riser reactor engineering is one field that is still under research, because of its complexity due the complex reaction kinetics, hydrodynamics and its strong interaction with regenerator etc. Modeling is an important tool to understand or simplify the complexity. Therefore, many researchers have put their efforts into the modeling of this highly complex process. Over the last few decades FCC modelling has evolved considerably with the inclusion of more and more details of the physics involved thereby significantly improving its prediction capability. However, the development of a satisfactory hydrodynamic model and accounting for heat and mass transfer effects are far from complete.

2.1 FCC FEED CHARACTERIZATION

The most common of the conventional FCC feed is vacuum gas oil which is typically a hydrocarbon material having boiling range 343-552 °C and is a product stream of vacuum fractionation of atmospheric residue. Heavy or residual feeds, i.e., boiling above 499 °C, are also processed in FCC units.

A complete hydrocarbon-type analysis of the paraffins, naphthenes and the

aromatics from an FCC feedstock can provide sufficient data to permit the engineer to find correlations between the feed composition and product distributions. In addition, the feed characterization can assist in the development of reliable kinetic and fluid dynamic models in order to optimize the FCC reactors (Liguras and Allen, 1989; Avidan and Shinar, 1990; Weekman, 1979; Froment and Bischoff, 1979).However, isolation, identification, and characterization of the hydrocarbon components in heavy oil fractions is a very complicated task (Dooley et al., 1974). For this reason, the standard analysis usually performed in refinery laboratories is not sufficient to give a good quantitative and qualitative prediction of chemical composition of a given feedstock. To simplify this problem, a separation technique was developed for the characterization and identification of the non- aromatic fraction of a light and a heavy FCC feedstock (gas-oil) but this process is unable to separate paraffins from naphthenes (Lappas et al., 1997a). Further research by the same authors allowed them to separate the non- aromatics in terms of paraffins and naphthenes (Lappas et al., 1997b) with a good match of paraffinic components but found naphthenic mixture to be very complicated for a detailed characterization. Otterstedt et al., (1986) also reviewed the problems associated with FCC feed characterization due to heavy oil fractions.

Physical feed characterization can be readily performed even in the field laboratory in terms of specific gravity and ASTM distillation. It may also be characterized using mass spectrometry (MS), NMR and HPLC. Characterizing a FCC feedstock involves determining both its chemical and physical properties. Because sophisticated analytical techniques, such as mass spectrometry, are not practical on a daily basis, physical properties are used. These provide qualitative measure of the feed composition. The refinery laboratory is usually equipped to carry out these

physical property tests on a routine basis (Sadeghbeigi, 2000; Riazi et al., 1980). The most widely used properties are:

- API Gravity
- Distillation
- Aniline Point
- Refractive Index (RI)
- Bromine Number (BN) and Bromine Index (BI)
- Viscosity
- Conradson Carbon Residue

A typical refinery laboratory is not equipped to conduct PONA and other chemical analyses on a routine basis. However, physical properties such as API gravity and distillation are easy to measure. As a result, empirical correlations have been developed to estimate chemical properties from these physical analyses. Some correlations have been developed which use some physical properties and predict chemical composition of the feed. The widely used correlations available in open literature include (Sadeghbeigi, 2000 and Speight, 2001):

- K Factor
- TOTAL
- n-d-M Method
- API Method

The **K factor** is a very useful indication of feed crackability. The K factor relates to the hydrogen content of the feed. It is normally calculated using feed distillation and gravity data, and measures aromaticity relative to paraffinicity. Higher K values indicate increased paraffinicity and more crackability. The K factor does not provide information as to the ratio of naphthene and paraffin contents. The ratio of

naphthenes to paraffins can vary considerably with the same K values. K value is the ratio of the cube root of a boiling temperature to gravity. There are two widely used methods to calculate the K factor: Kw (or Watson K) and the Kuop (or UOP K).

The **TOTAL** correlation calculates aromatic carbon content, hydrogen content, molecular weight, and refractive index using routine laboratory tests.

The **n-d-M** correlation is an ASTM (D-3238) method that uses refractive index (n), density (d), average molecular weight (MW), and sulfur (S) to estimate the percentage of total carbon distribution in the aromatic ring structure (CA), naphthenic ring structure (CN), and paraffin chains (CP). Both refractive index and density are either measured or estimated at 20°C (68°F). Note that the n-d-M method calculates the percent of carbon in the aromatic ring structure and not the total carbon; for example, if there is a toluene molecule in the feed, n-d-M predicts six aromatic carbons (86 %) versus the actual seven carbons.

The **API method** is a generalized method that predicts mole fraction paraffinic, naphthenic, or aromatic compounds for an olefin-free hydrocarbon. The development of the equations is based on dividing the hydrocarbons into two molecular ranges: heavy fractions (200 < MW < 600) and light fractions (70 < MW <200).

Riazi (2005) developed a more accurate, generalized method to predict fractional composition of paraffins, naphthenes, and aromatics contained in both light and heavy petroleum fractions. Viscosity, specific gravity, and refractive index of the fractions were used as input parameters. The authors claimed better prediction with their correlations than those of existing methods such as the n-d-M method.

The simple correlations presented above do a reasonable job of defining hydrocarbon type and distribution in FCC feeds. Each correlation provides

satisfactory results within the range for which it was developed. However, these are not completely satisfactory for studying FCC reaction kinetics.

The reaction kinetics can be better accounted for if hydrocarbon groups and their relative properties were available. Typically an FCC feed can be realistically characterized in terms of paraffins, naphthenes, simple aromatics and condensed ring aromatics, each of four groups can be further divided into heavy and light fractions. However, such an analysis of FCC feed, usually heavy gas oil, vacuum gas oil is by no means a simple task and cannot be undertaken by field laboratories. Therefore, it is important to develop more reliable correlation or model to characterize wide range of FCC feeds in terms of various hydrocarbon groups. Once the feed composition is known, kinetic models can be developed to predict product yields.

2.2 CATALYST AND CRACKING MECHANISM

Understanding some basic principles regarding fluid catalytic cracking (FCC) catalyst performance is important to understanding catalyst technology. Besides providing sites for cracking reaction to take place, modern FCC catalyst carries out a variety of other functions. The burning of coke on the catalyst in the regenerator provides all the process heat requirements:

- Heating the hydrocarbon feed up to the reaction temperature
- Providing for the endothermic heat of cracking
- Compensating for all the unit's heat losses
- Pre-heating the air from the air blower to the regenerator.

Thus, the catalyst must have the thermal stability to maintain particle and catalytic integrity under severe regenerator conditions. It must have the physical strength to maintain particle morphology under severe impact and erosion forces so that it remains in the unit, and it must have the proper flow characteristics to

allow it to readily flow between the regenerator and the reactor. On the reactor side, the catalyst must have sufficient activity to carry out catalytic conversion of the hydrocarbon feed before any significant amount of thermal cracking occurs. The catalyst usually consists of active zeolite crystals and active alumina particles embedded in a silica-alumina or purely alumina framework.

The catalytic cracking reactions can be classified into two broad categories; primary cracking of the feedstock molecules and secondary rearrangement and re-cracking of the cracked products. The catalyst promotes the primary cracking reaction mechanism, which can be explained by the carbonium ion theory. After the feed comes in contact with the regenerated catalyst, the first step is the vaporization of the feed. The theory then explains the formation of intermediate positively charged organic species, called carbocation (carbenium ion) which are initiated by the active/acidic sites (either Bronsted or Lewis acid sites) of the cracking catalyst.

The primary reaction in catalytic cracking is the β-scission reaction that occurs by breakage of the β C-C bond with the positive charge; thus, an olefin and a new carbocation are obtained. The new carbocation is now free to react with another paraffin molecule and continue the β-scission reaction. As the reaction proceeds, smaller olefins and paraffins are produced from the original larger feedstock hydrocarbon molecules. The reaction ends when the carbocation loses a proton to the catalyst and is converted to an olefin or the carbocation picks up a hydride ion from a donor, such as the coke, and is converted into a paraffin (Sadeghbeigi, 2000; Ancheyta, 2011; Bartholomew and Farrauto, 2005).

1. **Primary Reactions:** Cracking (β-scission) is the primary reaction, which involves only a single molecule. Cracking of the original large gas-oil molecule is a primary reaction. Such reactions can be:

- Paraffin ⟶ Smaller paraffin + Olefin
- Alkyl naphthene ⟶ Naphthene + Olefins
- Alkyl aromatic ⟶ Aromatic + Olefin
- Multi ring naphthene ⟶ Alkylated lesser-ring naphthene

2. **Secondary reactions:** These reactions involve bimolecules.

- Olefin + Paraffin ⟶ Paraffin + Olefin
- Olefin + Naphthene ⟶ Paraffin + Aromatic
- Olefin + Olefin ⟶ Paraffin + Diolefin

A number of secondary acid-catalyzed reactions are as below (Pinheiro et al 2012):

- Isomerization (rearrangement of the carbon skeleton)

  -alkene → branched alkene

- Hydrogen transfer (intermolecular hydride shift)

  -cycloalkane + alkenes → aromatic + alkanes
  -coke precursor + alkenes → coke + alkanes

- Cyclization (intramolecular or self alkylation)
- Intermolecular alkylation
- Condensation Reaction

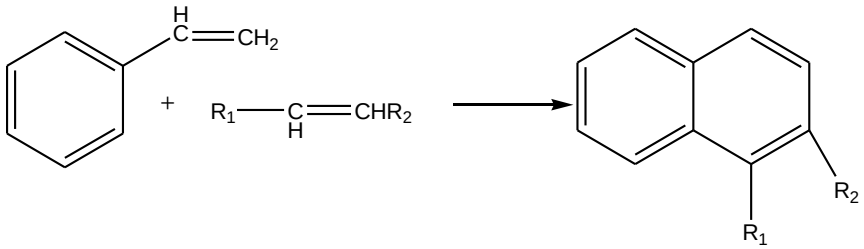

Reaction Mechanism

- Carbenium ions are formed by the addition of a proton (H+) from the catalyst Bronsted acid sites to an olefin or by a removal of a hydride ion (H^-) from a paraffin by the catalyst Lewis acid sites

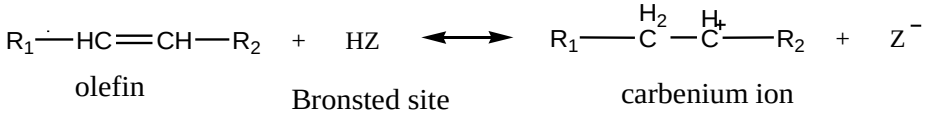

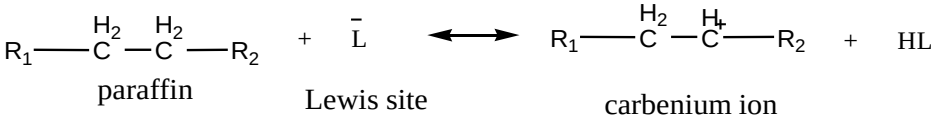

- Carbonium ions are formed by the addition of a hydrogen ion (H^+) to a paraffin molecule via direct attack of proton from the catalyst Bronsted acid sites.

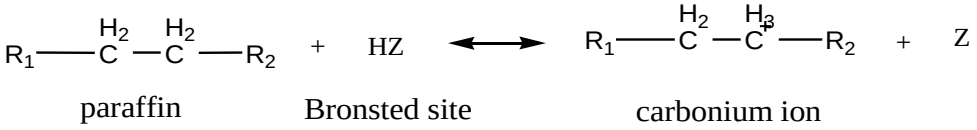

The carbonium ion's charge is not stable and it is just an intermediate step before it is converted to a carbenium ion and paraffin:

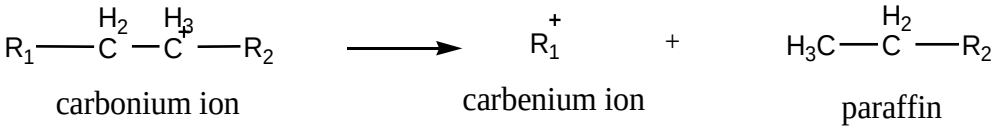

Carbenium ion chain type mechanism

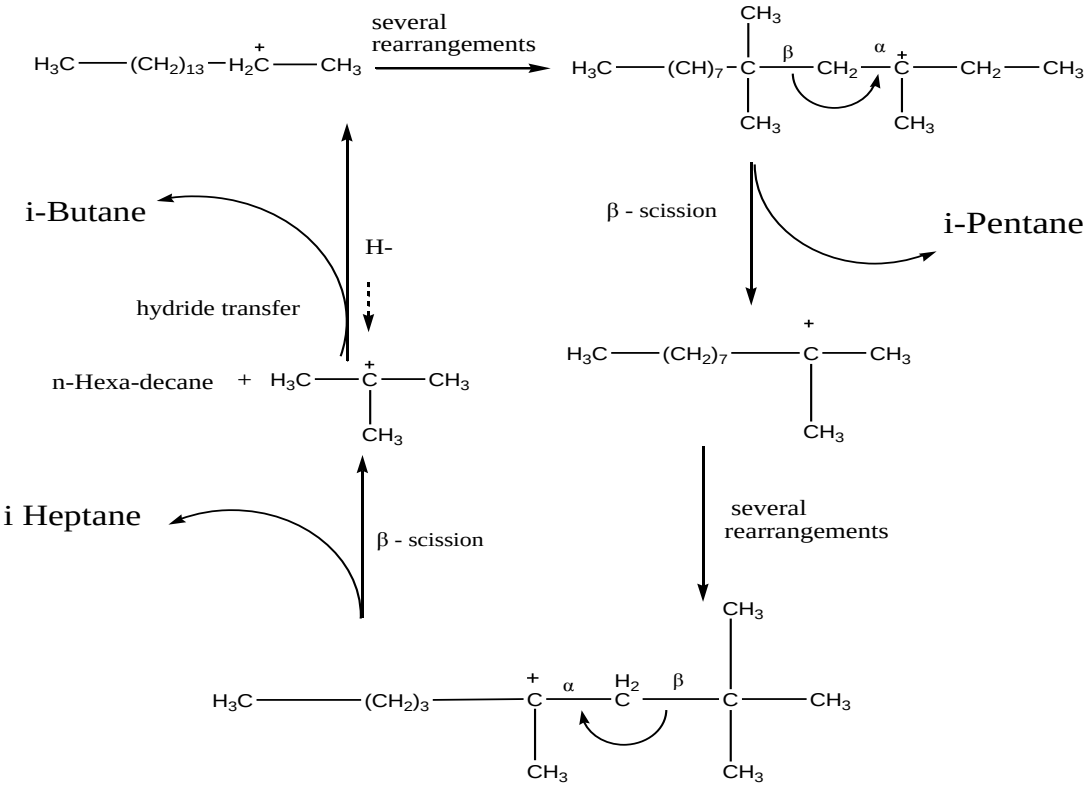

2.3 RISER REACTOR KINETIC MODEL

The complexity of the heavy gas oil composition due to very large number of components makes it extremely difficult to characterize these components individually and their kinetics at molecular level. Therefore, the complex reactions occurring in the process are generally described by grouping a large number of components known as kinetic lumps and defining the reaction network in terms of these lumps. So far, only a limited number of lumps have been considered by researchers to describe the feed as well as the products. Many kinetic models are available in the literatures which use 2, 3, 4, 5, 6, 8, 10 or 12 lumps. Weekman (1968) developed the first kinetic model of catalytic cracking conversion in isothermal fixed, moving and fluid bed reactors. The model accounted for conversion of gas oil into gasoline + lighter fractions. Weekman(1969) again developed a model to describe the feed and product yield distribution in terms of three lumped components: the gas oil, the gasoline and the remaining C_4s, dry gas and coke as shown in Figure 2.2. This model was used to study the effect of reaction time on the products, which showed that the time averaged gasoline yield is always less than the instantaneous gasoline yield because of the smoothing effect of time averaging. Weekman and Nace (1970) used a similar three lump kinetic scheme based on the theory of Wei and Prater (1963), to develop a kinetic model for FCC riser reactor. The authors considered gas oil cracking to be second order where gasoline cracking is the first order reaction.

A four- lump kinetic model (Figure 2.3) was proposed by several researchers using coke as a separate lump (Lee et al., 1989a; Gianetto et al., 1994; Blasetti and de Lasa, 1997). These authors also considered second order kinetics for gas oil cracking and first order kinetics for the gasoline. The main advantage of this model is its ability to predict coke production. This four lump model was used by various authors to

develop correlations and carry out different parametric studies and different aspects of FCC modeling because of its simplicity of material and energy equations and ease of formulation of kinetic scheme (Farag et al., 1993; Zheng, 1994; Ali et.al., 1997; Blasetti and de Lasa 1997; Gupta and Subba Rao, 2001). Krishnaiah et al., (2007) developed a steady state four lump reactor model coupled with regenerator model, which consisted of a high density fluidized bed known as dense bed and a dilute bed. The dilute bed again was considered to have two phases, the emulsion phase and the bubble phase (Krishna and Parkin, 1985). The model was validated with the data from Ali et al.,(1997) and was subsequently used to find the effect of cat/ oil , air flow rate and gas oil inlet temperature on FCC performance. A four lump kinetic scheme was also used by Abul-Hamayel, (2002) to estimate the kinetic parameters for high severity fluidized catalytic cracking. Five lump kinetic models (Figure 2.4) developed by Ancheyta et al (1999), and Bollas et al. (2007a) included seven and nine rate constants respectively. The advantage of these models is their ability to predict liquefied petroleum gas (LPG) and dry gas yields separately from the other lumps. Ancheyta et al. (1997) estimated the reaction parameters in the 3, 4 and 5 lump kinetic models and later in 1998 (Ancheyta et al. (1998) developed some correlations for predicting the effect of feedstock properties on catalytic kinetic parameters. These correlations gave good predictions of gasoline and gas plus coke yields. Dave and Saraf, (2003) investigated an integrated reactor- regenerator model using five kinetic lumps with nine cracking reactions in the riser reactor. Later, Dasila et al., (2012c) modified the model of Dave and Saraf, (2003) particularly for the regenerator and reported parametric sensitivity analysis with respect to operating parameters. Corella, (2004) discussed a kinetic model with selective deactivation of the catalyst and found it to be more accurate and realistic as compared to the kinetic

model with non - selective catalyst deactivation. In all the 2, 3, 4, 5, 6 and 7 lump models (Figures 2.2 to 2.6) the feed has been characterized in terms of a single kinetic lump. Larocca et al. (1990) used another 5-lump model where gas oil was split into paraffins, naphthenes, and aromatics. This model is similar to that studied by Coxson and Bischoff (1987) which is essentially a 10-lump model grouped into six pseudo components. In more detailed ten or twelve lump kinetic models, the feed is characterized by several hydrocarbon groups such as paraffins, naphthenes, aromatics and carbon atom substituted aromatic rings with different lumping schemes. In these models, 6 to 8 kinetic lumps are used to characterize feed and intermediate products (Jacob et al., 1976; Gross et al., 1976; Cerqueira et al., 1997; Ellis et al., 1998; Kumar et al., 1995).

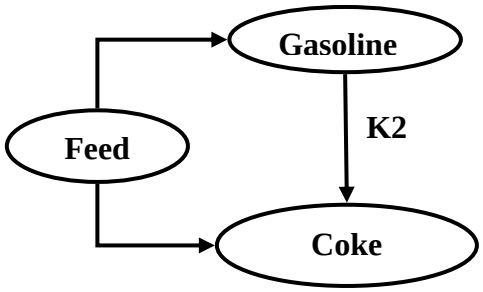

Figure 2.2: Three- lump model (Weekman and Nace, 1970)

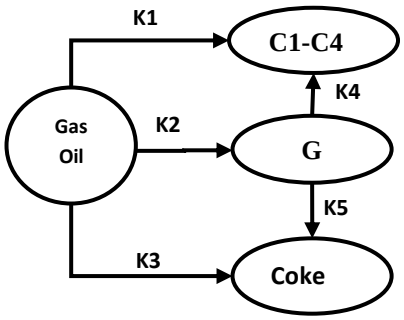

Figure 2.3: Four- lump model (Lee et al., 1989a)

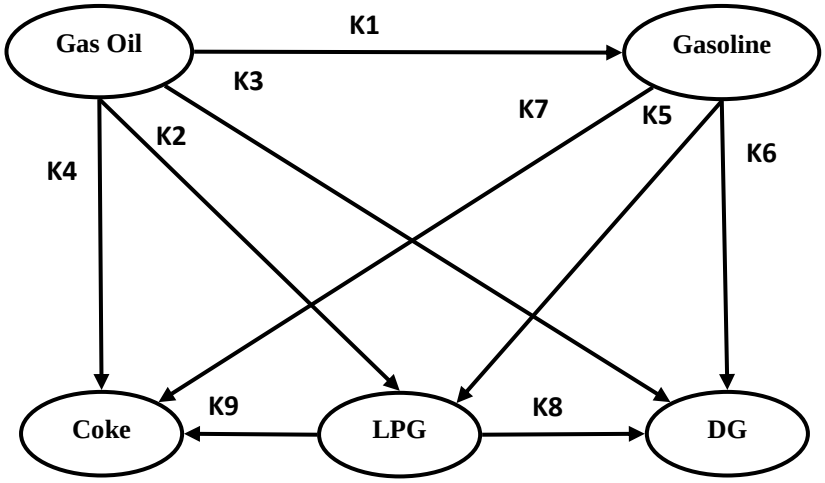

Figure 2.4: Five lump kinetic Scheme (Bollas et al., 2007a)

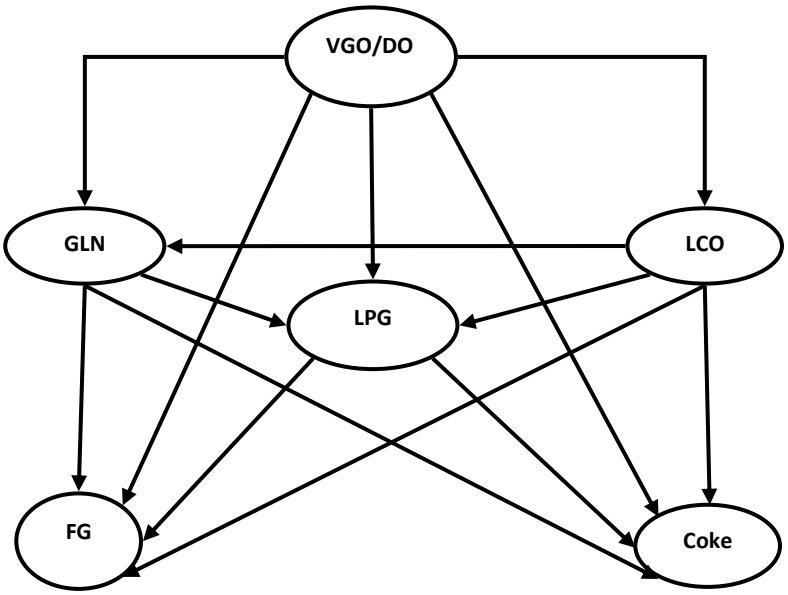

Figure 2.5: Six lump kinetic scheme (Takatsuka et al., 1987)

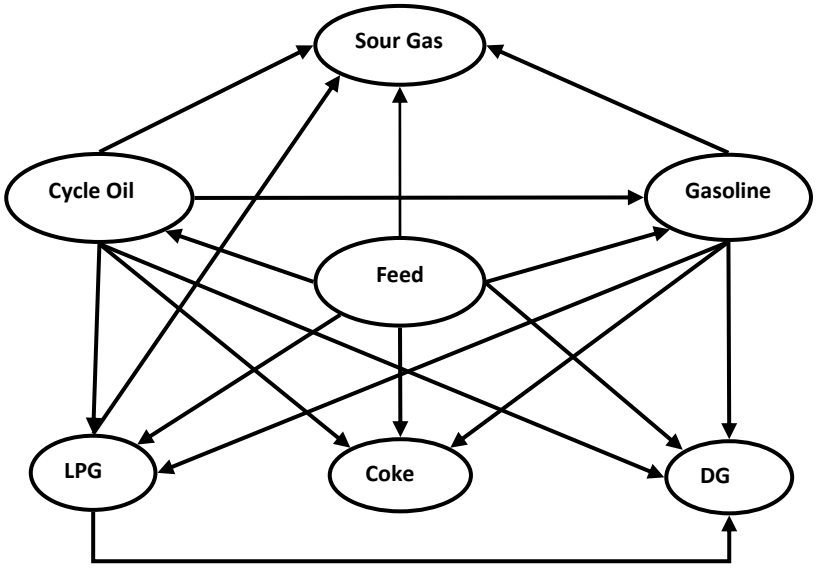

Figure 2.6: Seven lump scheme (Maya- Yescas et al., 2005)

An 8-lump kinetic model by Chen et al., (2007) which contained 21 kinetic parameters was proposed to describe the secondary reaction process of fluid catalytic cracking (FCC) of gasoline. The 10-lump kinetic scheme (Figure 2.7) developed by Jacob et al. (1976) was incorporated in an FCC process simulator called CRACKER (Kumar et al, 1995). Dewachtere, et al., (1996) combined the 10-lump model with a fluid dynamics model to simulate the feed injection zone in an FCC riser. They found that the feed nozzle with an included angle of 45° produced the most uniform temperature profile at the riser bottom. Theologos et al., (1999) observed that due to very small interaction time between feed and catalyst particles, the performance could be improved if the feed enters the riser reactor in vapour form. Gupta and Rao,(2001) proposed an atomization-modeling scheme by considering the initial feed droplet size at nozzle's exit, as well as droplet size reduction along with vaporization. Later, in 2003, the same authors extended their 4-lump riser model to the entire reactor-regenerator system, to study the effect of feed atomization on the performance of the

unit at constant coke yield. They observed that with smaller drop size the overall performance of the unit improved resulting in increased conversion at lower operating temperatures.

Many researchers extended the simple 3, 4, 5 lump kinetic schemes into more detailed kinetic schemes such as 11-lump model (Sa et al., 1985; Zhu et al., 1985), 12-lump model shown in Figure 2.8 (Cerqueira et al., 1997), 13- lump model (Sa et al., 1995; Gao et al., 1999), and 19- lump model (Pitault et al., 1994).

A detailed kinetic model based on pseudo-components description of the feed and products has been proposed by Gupta et al., (2007). This model was later incorporated with a 3-phase, one dimensional heat transfer model to account for the heat effects in the riser reactor (Gupta and Kumar, 2008). The kinetic parameters were estimated by a semi-empirical approach based on normal probability distribution. While their model more realistically describes the reaction kinetics than any other scheme, the parameters estimation method needs improvement. A mathematical model was also developed by Arandes et al., (2000) which is useful for predicting the behavior of FCC units both under steady and unsteady conditions. Fei et al., (1997) developed kinetic models using different lumping schemes for both riser and downer in fluid catalytic cracking process.

Other detailed kinetic scheme based on "structure oriented lumping" (SOL) approach proposed by Quann and Jaffe, 1992 and 1996 and Christensen et al., (1999) was based on an extensive network of reactions between lumps that are represented as an assembly of molecular building blocks. Another detailed kinetic model for catalytic cracking, based on a single-event approach, has been proposed by Feng et al., (1993) and Quintana-Solorzano etal., (2010). This modeling technique aims at retaining the full detail of the reaction pathways of all individual feed components and reaction

intermediates, by describing the reaction network in terms of elementary steps. Therefore, this requires a very detailed characterization of feeds and products, which is generally not available in industry, and is also computationally more demanding than the lumped models. Berry et al., (2004) developed a two dimensional hydrodynamic model and coupled it with the four kinetic lump model of Gianetto et al., (1994). An integrated reactor- regenerator model of FCC unit was presented by Fernandes et al. (2007) to describe the steady state and dynamic behavior of the unit. This model considered six lump cracking kinetics adapted from Takatsuka et al., (1987). This model was later modified to describe the UOP FCC unit with a high-efficiency regenerator, which differs mainly in the configuration of the regeneration section.

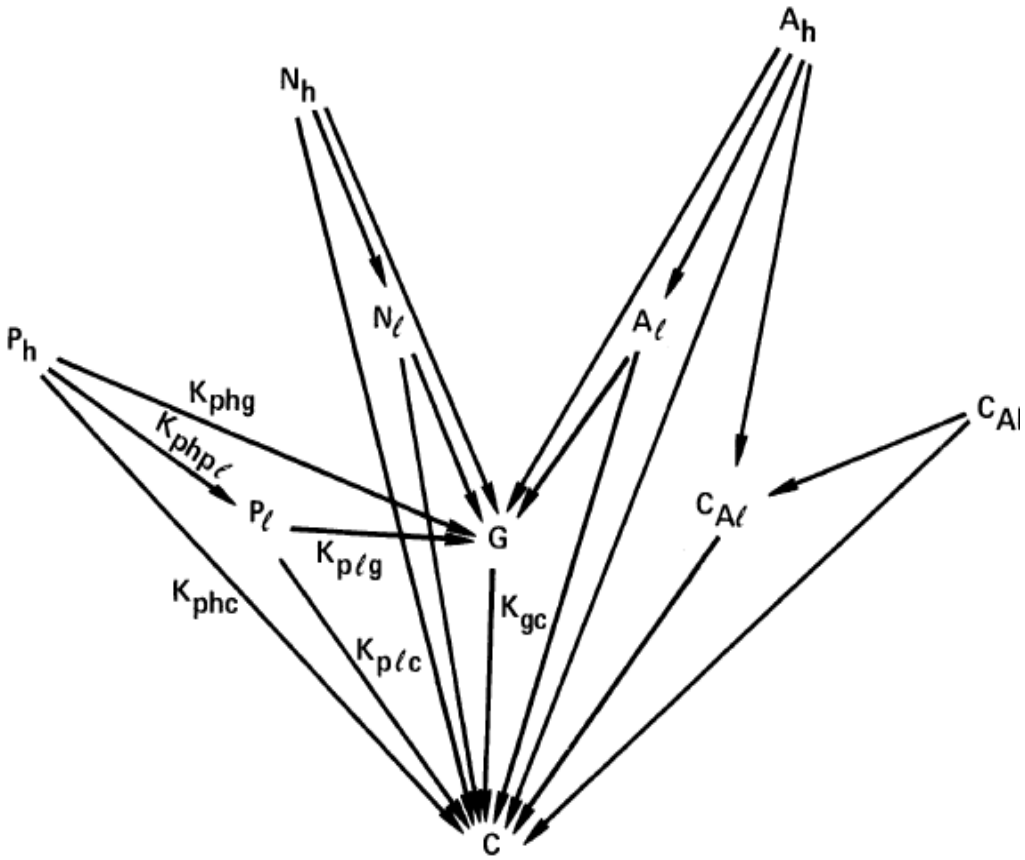

Figure 2.7: Ten lump kinetic scheme (Jacob et al., 1976)

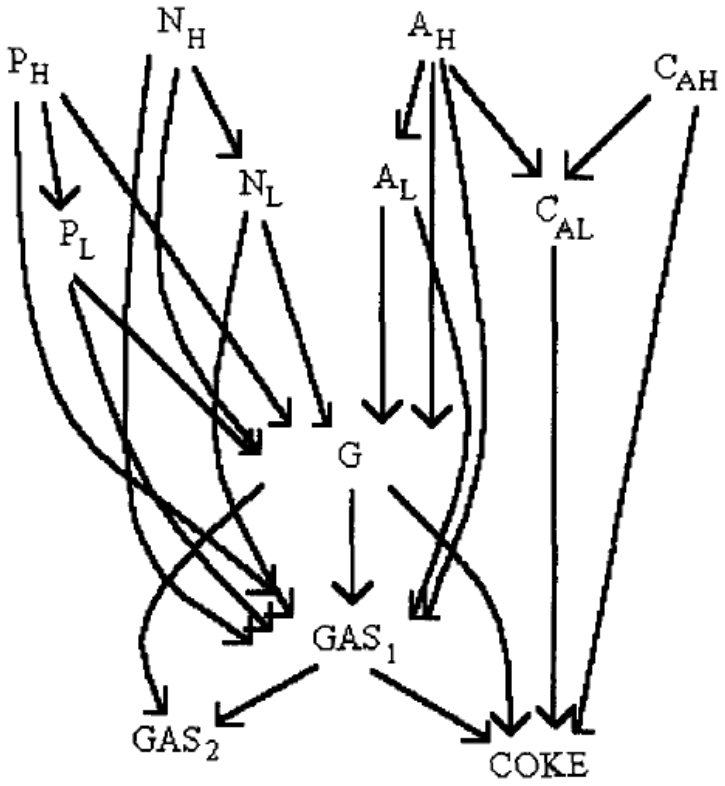

Figure 2.8: Twelve lump kinetic scheme (Cerqueira et al., 1997)

2.4 CATALYST DEACTIVATION AND COKE FORMATION

Any heterogeneous catalyst can be deactivated mainly due to two types of causes: physical and chemical. The first includes phenomena such as sintering, occlusion, loss of active surface etc. Indeed, chemical causes are the main problem and can be subdivided into three categories:

- Chemical degradation–reaction of a compound with the catalytic phase, causing its destruction or loss of reactivity. The main agents are alkaline metals which neutralize the acid sites and steam that causes dealumination, which destroys the zeolite framework.
- Poisoning—it expresses the irreversible adsorption (chemisoption) of impurities on the catalyst active sites. This leads to a permanent reduction of the activity. In the FCC process, the main poisons are basic nitrogen compounds.

- Fouling—this is due to the deposition of coke and other inorganic materials such as metals and their composites. These compounds block the porous structure and the access to the active sites (Froment, 2001).

Industrially used zeolites are normally sufficiently stable to avoid these processes in the range of operating conditions for which they were designed. The same happens with cracking catalysts: their physical stability would allow continuous operation for several months. The catalyst deactivation in commercial fluid catalytic cracking (FCC) occurs both reversibly and irreversibly. The irreversible catalyst deactivation occurs due to the presence of both metal (nickel and vanadium) and nonmetal (sulfur, nitrogen oxygen) contaminants. These contaminants present in the FCC feed, irreversibly but slowly adsorb or modify the active sites through chemical reactions. Fresh catalyst has to be added periodically to make up for the lost catalyst . Coke gets deposited on the catalyst due to undesired side reactions taking place in FCC, and affects the intrinsic activity by covering sites and blocking pores. This loss of activity due to coke deposition is very fast but is reversible and the catalyst can be regenerated easily by burning off the coke deposited on the catalyst surface. Due to the cyclic nature of the process, the catalyst particles may break, producing fines that will result in particulate emissions and loss of fines because of catalyst attrition. In order to maintain the catalyst activity, fresh catalyst addition is required frequently. The age distribution of catalyst particles also affects the activity of the catalyst in cracking reactions (Stockwell and Wieland, 2000 ; Bayerlein et al., 1990). At any instant of time , the catalyst in the reactor is composed of a mixture of young (low metal concentration, high activity) and old (high metal concentration, low activity) catalyst particles. This mixture of young and old catalyst from an industrial FCC unit is called equilibrium catalyst (Cerqueira et al., 2008).

2.4.1 Modeling of the Catalyst Deactivation

FCC catalyst deactivation is a complex process due to presence of minor impurities the feed, catalyst composition and process operation. Coke deposition on the catalyst particles is the dominant cause of catalyst deactivation in FCC units. Many studies on modeling of catalyst deactivation have been carried out in the recent decades to better understand the deactivation phenomena taking place during hydrocarbon transformations over acid zeolites and industrial FCC catalysts (Cerqueira et al., 2008). The catalyst deactivation function, usually expressed in terms of an effectiveness factor, Ø, is typically based on a function dependent on time-on-stream, represented by the catalyst residence time, or a function dependent on coke content of catalyst, represented by the catalyst coke mass fraction (Alsabei et al., 2008). These two different approaches to modeling catalyst deactivation are: time-on stream concept and coke on catalyst function.

I. Time- on- stream concept

Most of the popular models on deactivation are based on the time-on stream concept. In this concept, there is no specific function that can be used for the deactivation. Several empirical equations were employed by various researchers to fit their experimental data. However, there are two functions that fit the experimental data quite well: power function and exponential function. The catalyst deactivation factor is difficult to determine because every kinetic test provokes coke fouling. It is often pre-defined as an exponential or a hyperbolic function of the time on stream, whose parameters are fitted to the experimental results, together with the kinetic constants. The exponential function is more widely used. This approach may be misleading because time is not the physical cause of deactivation and it is not possible to use the same function for reactors with different times on stream (i.e. micro reactor

and riser) (Landeghem et al., 1996). For a fixed bed reactor, first order catalyst decay function was proposed by Weekman and Nace, (1970)

$$\emptyset = \mathrm{Exp}(-\alpha\, t_c)$$

where α is the catalyst decay velocity constant and t_c represents the time that the catalyst has been exposed to oil vapours. Another correlation for catalyst deactivation coefficient was proposed by Pitault et al., (1994) and Jacob et al., (1976).

$$\emptyset = {}^{\alpha}/_{(1+\beta * t_c{}^{\gamma})}$$

where, $\beta = 12$, $\gamma = 0.76$

Nam and Kittrell, (1984) addressed this issue and concluded that time-on-stream functions have the advantage of simultaneously allowing more than one deactivation mechanisms. Kung et al., (2000) prepared a very active hydrocarbon cracking catalyst by steam treatment of Y zeolite for understanding the enhanced cracking activity. However, the extent of enhancement in activity compared to a non-steamed sample depends on the reaction condition. Corella et al. (1985) studied the catalyst decay for a wide range of contact times (2 to 200 sec) considering homogeneous and non-homogeneous catalyst surfaces and showed that the order of deactivation kinetics decreases with the contact time, taking values 3, 2, and 1, successively. They further justified the change of order of deactivation with different contact times by showing the discrepancy in the values of these constants obtained by Weekman (1968) and Nace et al., (1971) for relatively large contact times and Shah et al., (1977) and Parakos et al., (1976) for short contact times. Corella et al., (1986) determined the kinetic parameters of cracking and of deactivation for a given feed-catalyst system. Corella and Menendez, (1986) developed a model in which the catalyst surface was assumed to be non-homogeneous with acidic sites of varying strength. Larocca et al., (1990) reported that the catalyst deactivation can be

represented by both an exponential decay function and a power decay function with an average exponent of 0.1-0.2. Corella (2004) discussed the modeling of the kinetics of selective deactivation of the catalysts. A selective deactivation kinetic model uses different activity, deactivation function, and or deactivation order for each reaction in the network. Although these represent the reality better than the nonselective models, the selective deactivation models may not be useful because of the complexity and handling difficulties.

Kraemer et al., (1991) used the data from two different experimental reactors and showed that exponential decay function or power law function could equally represent the data; however, the power law assumes the unrealistic limit of infinite catalyst activity at zero time-on-stream and requires two parameters to describe deactivation. They further concluded that the simple first order decay function is an effective model for describing the catalyst activity decay for short reaction times (less than 20 seconds).Several other workers(Voorhies, 1945; Wojciechowski, 1968; Nace, 1970; Gross et al., 1976) used various empirical functions for accounting for the catalyst decay based on time-on- stream. Froment and Bischoff (1979) proposed a mechanistic based model considering catalyst decay rate a function of the fraction of active sites and the concentration of the reactants.

II. Coke on catalyst function

In Coke on catalyst function concept, Yingxun (1991) proposed a correlation between catalyst deactivation function and amount of coke for catalytic cracking of vacuum gas oil.

$$\emptyset = (1 + 51C_c)^{-2.78}$$

where Cc is amount of coke of catalyst. The first empirical correlation for this coke formation in the catalytic cracking of gas oil were made by Voorhies (1945) that depends on the catalyst residence time as follows:

$$C_c = m.\theta^n$$

where m, and n are the constants and depends on the feed and θ is the catalyst residence time in the reactor. The exponent of θ is close to 0.5.

2.4.2 Coke Formation

Coke formation has an important role in the heat balance of FCC unit and the performance of the catalyst, conversion and product selectivity. However, different types of coke do not have the same influence on the cracking activity, e.g. depending on the feedstock characteristics; catalytic coke may have a greater influence on catalyst activity than additive coke. There are five main types of coke identified in catalytic cracking (Cerqueira., 1997 and 2008)

- Catalytic coke—from condensation and dehydrogenation.
- Catalyst-to-oil coke—hydrocarbons entrained in the small pores and not removed by the stripper.
- Thermal coke—formed by a free radical mechanism, it is important at high reaction temperatures and also yields hydrogen. It is less important than catalytic coke due to the low extent of thermal cracking at typical FCC conditions
- Additive coke (or Conradson coke)—from heavy molecules already present in the feed. Its amount correlates directly with the Conradson carbon residue (residue remaining after the fuel has been pyrolysed by raising the temperature to 800 ◦C).
- Contaminant coke—from dehydrogenation catalyzed by Ni, Fe and V.

Catalytic coke is apparent cause of the loss of catalyst activity due to the adsorption of poly nuclear aromatic compounds and olefins which polymerize with time to form a coke deposit.

This catalytic coke is dependent on the following four factors (Guisnet and Magnoux, 1997 and 2001):

- **Charge properties**: Results show that the presence of alkenes and aromatics in the feed substantially increases the rate of coke formation.
- **Operating conditions**: Temperature has a significant role both on the formation rate and on the composition of coke. At low temperatures, close to 250 ◦C, the H/C ratio is similar to that of the reactants and the coke molecules formed are strongly dependent on the charge. On the other hand, at high temperatures (relevant case for the FCC process), coke is highly poly aromatic (low H/C ratio) and the nature of the reactants is not as important. Coke formation reactions, due to their bimolecular nature, are favored by high reactant partial pressures.
- **Zeolite acidity**: The acid site density is also a relevant factor in coke formation. As the proximity of the acid sites increases, the faster will coke formation occur thereby deactivating the catalyst.
- **Zeolite porous structure**: The pore structure is the main parameter determining the composition of coke formed with zeolites at high temperatures. Zeolites with small cages form smaller molecules like anthracenes or pyrenes, whereas zeolites with large cages allow bulkier compounds to be produced.

2.4.3 Coke Formation Mechanisms

Coke formation is a bimolecular reaction that proceeds via carbenium ions.

Reactions as that produce unsaturates and multi-ring aromatics are main coke producers (Figure 2.9). For typical catcrackers, an optimum temperature will produce minimum coke yield. At low temperature, coke formed mainly because the carbenium

ions do not desorb. At high temperature, coke is formed mainly due to olefin polymerization. In addition, instant coke and stripper coke contribute as well to the total coke. Stripper coke consists of adsorbed and entrained hydrocarbons that are not removed by the stripping steam. A typical coke forming reaction is shown below:

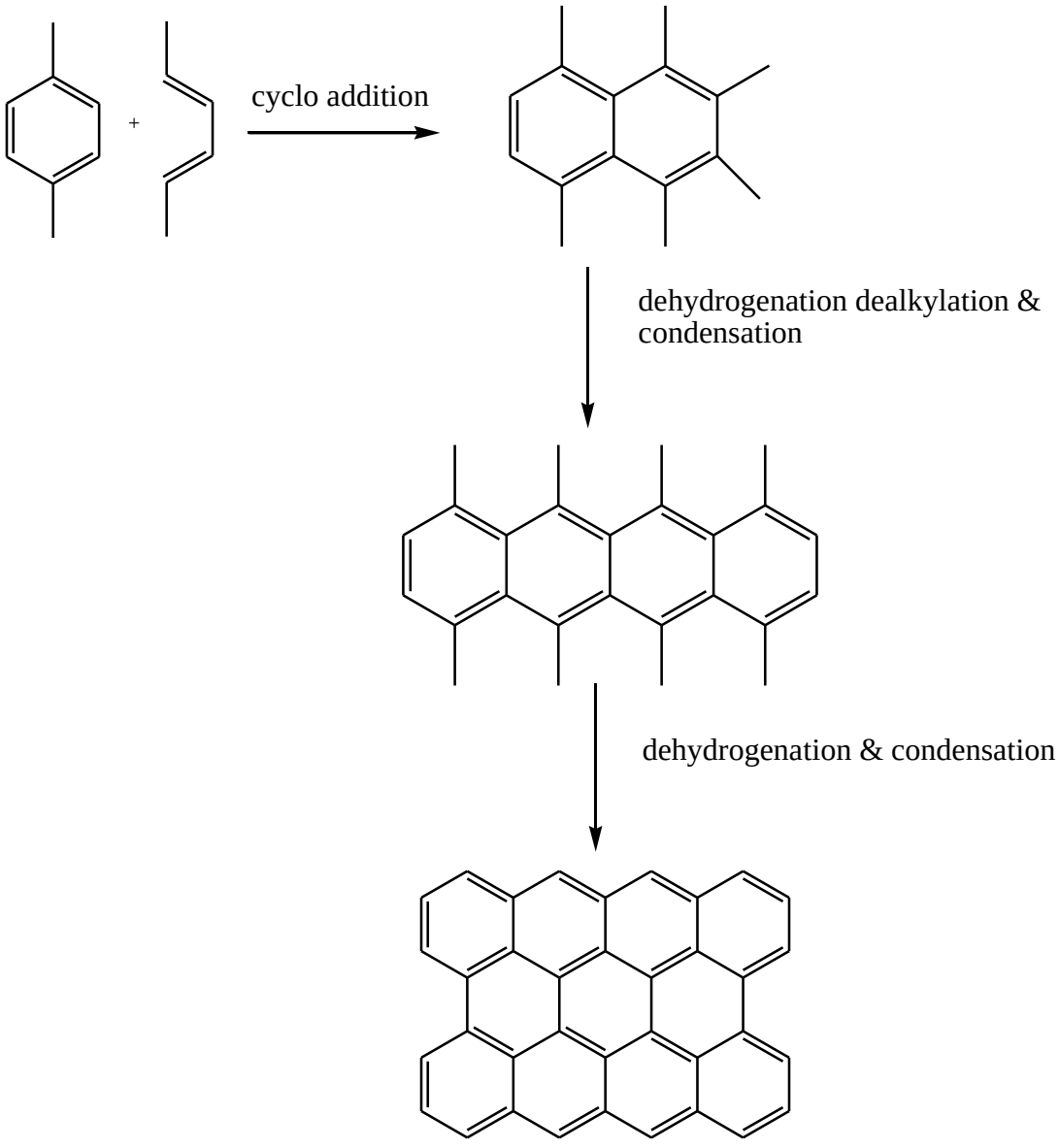

Figure 2.9: Coke formation

2.5 HYDRODYNAMICS OF RISER REACTOR

Shuyan et al., (2008) developed a hydrodynamic model to analyze the behavior of hydrocarbon vapours and catalyst in FCC riser. This model was coupled

with a four-lump kinetic model to investigate the effects of the cluster porosity, inlet velocity, and cluster formation on cracking reactions. Distributions of temperature, gases, and gasoline both from a catalyst particle cluster and from an isolated catalyst particle were presented. Simulated results showed that the cracking reactions from VGO to gasoline, gas, and coke on clusters are slower than those on the isolated particles, but faster for the reactions from gasoline to gas and coke. Particle clustering reduced the reaction rates from VGO to gasoline, gas, and coke but increased the reaction rates from gasoline to gas and coke. Gao et al., (1999) developed a hydrodynamic two-phase, turbulent flow model and coupled it with a thirteen lump kinetic scheme. The authors demonstrated that excessive cracking occurred beyond the 10 m riser height resulting in the increase of by-products yield at the expense of desirable products. They further extended their model to three-phase flow (Gao et al., 2001) by incorporating the effect of feed vaporization into their two-phase model which explained the synergetic effects of hydrodynamics, heat transfer, and feed vaporization on FCC reactions. Gidaspow and Huilin (1998) experimentally measured the solids pressure inside the circulating fluid bed (CFB) riser. This information coupled with a hydrodynamic model could be used for predicting the particle and expand to full form hydrocarbons velocity distribution profiles inside the CFBs. van der Meer et al. (1999) studied the dimensionless groups for hydrodynamic scaling of a CFB. The authors demonstrated that at least five dimensionless groups were required

for full hydrodynamic scaling of a CFB. Geometry of the CFB riser has been found to have considerable influence on the hydrodynamics of circulating fluidized beds (Brereton and Stromberg, 1986; Jin et al., 1988; Schnitzlein and Weinstein, 1988). The detailed solid voidage profiles and solid velocity profiles were obtained with the aid of an optical fiber probe in CFB risers of square cross-section (Zhou et al., 1994 and 1995) and solids flow patterns was measured in laboratory scale riser reactor of square cross-section Van der Meer et al. (2000). However, a satisfactory hydrodynamic model which accounts for heat and mass transfer effects is still not available.

2.6 REGENERATOR MODEL

An FCC regenerator usually consists of a large fluidized bed reactor with coke combustion kinetics and complex hydrodynamics. The deposited coke on catalyst surface during the cracking reactions in riser is burned off in the regenerator in presence of air. These coke combustion reactions taking place in the regenerator are strongly exothermic. There are usually two regions in the regenerator: the dense phase and the dilute phase (freeboard). The dilute phase is the region above the dense phase up to the cyclone inlet, and has a substantially lower catalyst concentration. The dense bed is all the catalyst contained below the established bed level, where, almost all reactions occur. The larger catalyst particles are separated from the gas in the dilute phase and fall back to the bed. Any catalyst particles that do not separate in the dilute phase enter into the regenerator cyclones. Catalyst entering the cyclones is separated by centrifugal force with the larger particles being returned to the bed via the cyclone

diplegs. Catalyst fines too small to be separated by the cyclones are carried out of the regenerator with the flue gas.

The design distance between the cyclone inlet and the surface of the dense bed is determined by the Transport Disengaging Height (TDH) shown in Figure 2.10.

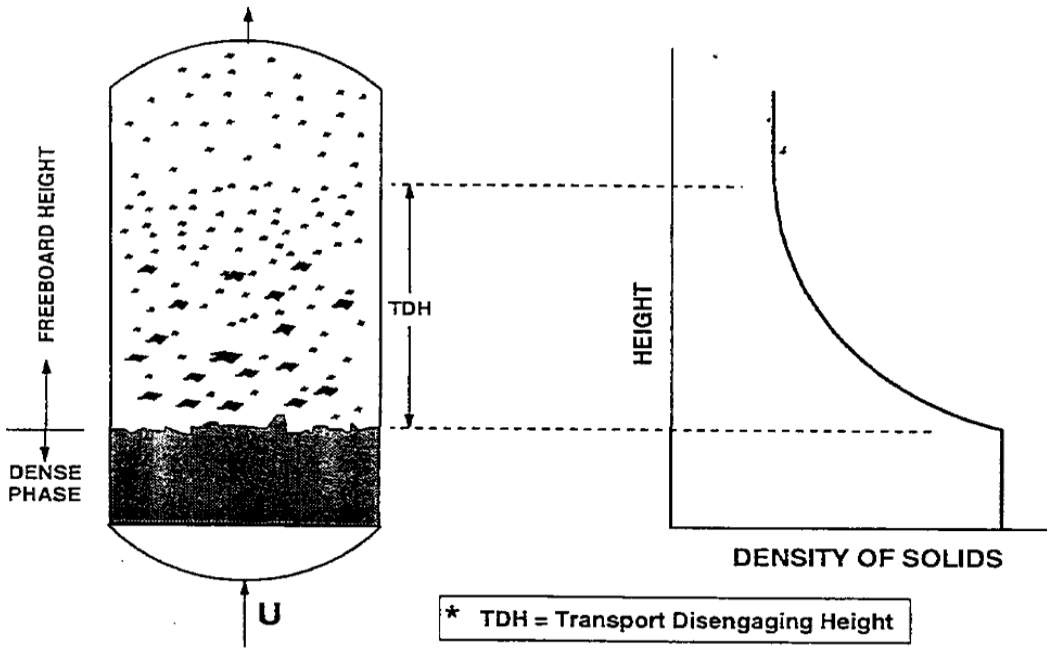

Figure 2.10: Schematic depiction of TDH

The TDH is a function of the superficial gas velocity, vessel diameter, and the particle size distribution. The amount of catalyst entrained in the gas above a fluidized bed decreases with the height above it. A given particle reaches a distance above the bed where gravitational forces overcome the upward drag forces of the gas, and the particle falls back to the bed. The smaller the particle, the greater the distance. A height is reached where the amount of entrained solids becomes constant, no more particles are overcome by gravitational forces. The particles here are too small to settle. The TDH, determines what minimum distance above the bed the cyclones inlets must be placed, other considerations for setting the cyclone design inlet level include dense bed level variations and minimum required dipleg length. To account

for these considerations, the cyclone inlet height will be greater than the actual TDH. If a regenerator is operated in such a manner that the distance between the catalyst bed and the cyclone inlet is less than the TDH, the catalyst density at the cyclone inlet will be higher. This will increase the catalyst loading to the cyclone and potentially increase catalyst losses from the cyclone.

The regenerator has two main functions: it restores catalyst activity and supplies the endothermic heat required to crack the feed in the riser. The spent catalyst activity is resorted in the regenerator by combustion of deposited coke in presence of air. Usually, coke is consists of various chemical components (C, H, N, S) but the hydrocarbons (C, H) are dominant. Therefore, coke is formulated by CHx, where x is a constant ratio of carbon and hydrogen (x = constant), the hydrogen combustion reaction is complete and instantaneous (Equation 2.5). These coke combustion reactions are considered mainly two types: one forming carbon monoxide and another carbon dioxide (Equation 2.1 and 2.2). Beyond the combustion reactions, oxidation of CO to produce CO2 also consumes the available oxygen in the regenerator. This CO oxidation may take the form of either homogeneous oxidation in the gas phase or heterogeneous oxidation in the presence of oxidation promoters (Arbel et al., 1995; Avidan, 1993; Avidan and Shinnar, 1990). The main combustion reactions in the regenerator are as follows:

$$C + \frac{1}{2}O_2 \xrightarrow{k1} CO \quad (2.1)$$

$$C + O_2 \xrightarrow{k2} CO_2 \quad (2.2)$$

$$CO + \frac{1}{2}O_2 \xrightarrow{k3c} CO_2 \quad \text{Heterogeneous CO Combustion} \quad (2.3)$$

$$CO + \frac{1}{2}O_2 \xrightarrow{k3h} CO_2 \quad \text{Homogeneous CO combustion} \quad (2.4)$$

$$H_2 + \frac{1}{2}O_2 \xrightarrow{k4} H_2O \quad (2.5)$$

The catalyst in the regenerator is fluidized with the hot air entering through an air distributor at the bottom. Many models with complete riser reactor and regenerator configuration have been proposed based on different sets of assumptions with respect to the kinetics of cracking reactions and hydrodynamics (Arbel et al., 1995; Bollas et al., 2007b; Bai et al., 1998), whereas other models concern themselves only with the regenerator (Krishna and Parkin, 1985 and Lee et al., 1989b; de Lasa and Grace, 1979). These regenerator models focus on the dense bed which is characterized by bubbles rising through an emulsion phase. A first non isothermal grid model to study the steady state behavior of FCC regenerator was described by Errazu et al. 1979 ; de lasa et al., 1981. The grid region is the gas feed zone at the bottom of the fluidized bed, where the gas is not yet dispersed as bubbles but flows as jets that will break down to bubbles in the highest part of the catalyst bed. The jets are assumed to be well mixed in the radial direction and to follow a plug flow regimen in the axial direction. The emulsion and the bubbles in the grid region are assumed to be perfectly mixed. Krishna and Parkin, 1985, subdivided the dense region in terms of two phases: bubble phase and emulsion phase. The bubble phase is free of catalyst particles whereas in emulsion phase, gas and catalyst particles are fully mixed. Kunnii and Levenspiel, (1990) also proposed the three phase model (bubble bed model) that assumes the presence of a thin layer around the bubble, with less solid content than the emulsion (the cloud) and a similar zone being pulled up by the bubble (the wake) . Lee et al., (1989b) applied three different models (two-phase, grid, and bubbling-bed) of the dense region of a typical regenerator and compared them with experimental results of an industrial plant. They concluded that the bubbling-bed model gives the smallest error in describing the experimental data.

The mathematical model for the regenerator consists of mass balances and energy balances for both the dense and dilute region. The mathematical modeling was done with some basic assumptions. The rate of the carbon combustion is first order with respect to the carbon-on catalyst and oxygen partial pressure. The rate of CO oxidation is also expressed as being first order with respect to the partial pressure of CO and half order with respect to the partial pressure of O2 for both homogeneous and catalytic oxidation reactions. The overall rate expression for the CO oxidation can be obtained by adding the rates of homogeneous and heterogeneous oxidation reactions. Coke burning was calculated from the observed oxygen concentration and CO2 /CO product ratio. In the dense region, the catalysts or solids were assumed as a CSTR and gases were in plug flow while in dilute bed, both the phases were in plug flow. (Krishna and Parkin, 1985; Lee et al., 1989b; Arbel et al.,1995; Morley and de Lasa 1987 and 1988; Avidan and Shinnar, 1990).

A detailed dynamic model of the regenerator as standalone unit was proposed by Faltsi-Saravelou and Vasalos, (1991a and 1991b), which is applicable to particles of Geldart groups A (which is the case of FCC catalyst) and B. Their model includes a rigorous description of the hydrodynamics of a fluidized bed using the two-phase theory and a detailed combustion kinetic model that considers carbon, hydrogen, and sulfur combustion. Later, Penteado et al., (2003) proposed a dynamic model concerning only the regenerator of an industrial FCC unit. Their model includes both the dense region and the dilute region.

CHAPTER 3

FIVE LUMP KINETIC MODEL

A steady state model was developed for simulating the performance of an industrial fluid catalytic cracking (FCC) unit which was subsequently used in parametric sensitivity studies. The simulator includes five lump kinetic model for the riser reactor and a two-phase model regeneration system. Mass and energy balances were performed for each of these sections and simulation results were compared with the plant data available in the literature. Model predictions were found to be in close agreement with the reported data. Finally this validated model was used for studying the effects of independent variables such as feed preheat temperature (T_{feed}) and feed flow rate (F_{feed}) on the unit performance at either fixed regenerated catalyst temp/regenerator temp (T_{rgn}) or constant reactor outlet temperature (ROT). The catalyst circulation rate (CCR) was automatically adjusted to keep the ROT constant with varying the independent variables feed preheat temperature while the air rate adjusted for keeping the regenerator temperature constant which consequences the dependency of both dependent and independent variables on the unit performance. The air flow rate to the regenerator was also an independent variable during the parametric sensitivity analysis and its effect on FCC performance was investigated at constant T_{feed}, F_{feed} and CCR.

3. 1 RISER MODEL

A 5-kinetic lump reaction scheme proposed by Bollas et al. 2007a and shown in Figure 3.1 has been adopted in the present study. The feed is represented by only one lump as gas oil while the products are lumped as gasoline, LPG, Dry Gas and Coke. The total number of kinetic reactions for the five lump kinetic model are nine.

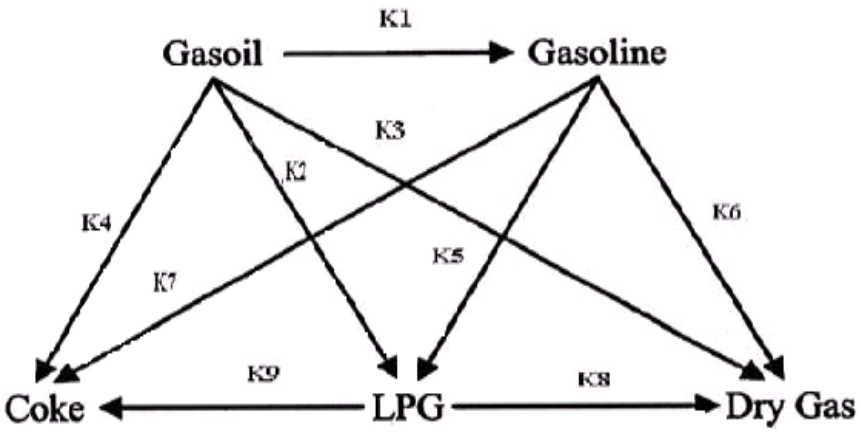

Figure 3.1: Five lump kinetic scheme

The following assumptions were made for the modeling of FCC riser reactor:

1. Gases and catalyst are in plug flow in the riser reactor
2. Gas oil cracking is a second order reaction but cracking of gasoline and LPG are first order reactions.
3. There are no radial temperature gradients in the gas and solid phases.
4. As the catalyst particles are very small (20 – 80 μm) and the vaporized gas oil carries catalyst particles at high velocities, slip factor is assumed to be unity.
5. Dry gases produce no coke.
6. Catalyst deactivation is non-selective and related to coke on catalyst only.
7. The solid catalyst particles are in thermal equilibrium with the gaseous mixture at all times.

Tables 3.1 to 3.4 provide plant operating data, design data and thermodynamic and other data (Dave and Saraf, 2003; Kasat et al., 2002)

Table 3.1: Input Data Used in the Simulation

Parameters	Numerical Value
F_{feed} (kg/sec)	32.14
F_{rgc} (kg/sec)	208.33
T_{feed} (K)	625.1
P_{ris} (atm)	2.546
P_{rgn} (atm)	2.68
F_{air} (kmol/sec)	0.57
T_{air} (K)	493.9

Table 3.2: Thermodynamic and Other Parameters Used in the Simulation of FCC Unit

Parameters	Numerical Value
$C_{p,c}$ (kj/kg K)	1.003
$C_{p,fl}$ (kj/kg K)	3.430
$C_{p,v}$ (kj/kg K)	3.390
$C_{p,N2}$ (kj/kg K)	30.530
$C_{p,o2}$ (kj/kg K)	32.280
$C_{p,h2o}$ (kj/kg K)	36.932
$C_{p,co}$ (kj/kg K)	30.850
$C_{p,co2}$ (kj/kg K)	47.400
ΔH_{evp} (kj/kg)	350.0
H_{co} (kJ/kmol)	$1.078 * 10^5$
H_{co2} (kJ/kmol)	$3.933 * 10^5$
H_{h2o} (kJ/kmol)	$2.42 * 10^5$
X_{pt}	0.10
ρ_c (kg/m^3)	1089.0
C_H (kg H_2/kg	0.165
D_p (ft)	$2.0 * 10^{-4}$
MW $_{Gas\ Oil}$	350
MW $_{Gasoline}$	114
MW $_{LPG}$	58
MW $_{Dry\ Gas}$	30
MW $_{Coke}$	12

Table 3.3: Design Data Used for the Simulation of FCC Unit

Parameters	**Numerical Value**
Riser Length (m)	36.965
Riser Diameter (m)	0.684
Regenerator Length (m)	19.344
Regenerator diameter (m)	4.522
Catalyst Inventory in the Regenerator(kg)	34000
Height of the cyclone inlet(ft)	49

Table 3.4: Kinetic and Thermodynamic Parameters Used for Reactor Modeling

Rate Constant	Reaction	Frequency Factor*	Activation Energy(kJ/kmol)	Heat of Reaction(kJ/kmol)
k1	Gas Oil →	18579.9	57540	45000
k2	Gas Oil →	3061.1	52500	159315
k3	Gas Oil →	532.14	49560	159315
k4	Gas Oil→	39.04	31920	159315
k5	Gasoline→	65.4	73500	42420
k6	Gasoline →	0.00	45360	42420
k7	Gasoline →	0.00	66780	42420
k8	LPG →	0.32	39900	2100
k9	LPG →	0.19	31500	2100

*m^6 / (kg catalyst) (kmol gas oil) for reactions (1) to (4) and m^3/(kg catalyst) (s) for reactions (5) to (9)

3.1.1. Riser Model Equations

a. The mass balance for the j^{th} lump over a differential element of height dh

$$\frac{dF_j}{dh} = A_{ris}H_{ris}(1-\varepsilon)\rho_c \sum_{i=1}^{9}\left(\alpha_{kj}\right)_i r_i \tag{3.1}$$

Rate equations for each of the nine reactions is as follows:

$$r_i = k_{0i}\exp\left(-\frac{E_i}{RT}\right)C_j{}^2\phi \qquad \text{for i} = 1,2,3,4 \text{ and j} = 1 \tag{3.2}$$

$$r_i = k_{0i}\exp\left(-\frac{E_i}{RT}\right)C_j\phi \qquad \text{for i} = 5,6,7 \text{ and j} = 2 \tag{3.3}$$

b. Enthalpy balance across the same differential element of the riser

$$\frac{dT}{dh} = \frac{A_{ris}H_{ris}\rho_c(1-\varepsilon)}{F_{rgc}C_{p_c}+F_{feed}C_{p_{fv}}}\sum_{i=1}^{9} r_i(-\Delta H_i) \tag{3.5}$$

$$T(h=0) = \frac{F_{rgc}C_{p_c}(T_{rgn}-10.0)+F_{feed}C_{p_{fl}}T_{feed}-\Delta H_{evp}F_{feed}-Q_{loss,ris}}{F_{rgc}C_{p_c}+F_{feed}C_{p_{fv}}} \tag{3.6}$$

c. Gas oil properties in the riser reactor are calculated by the following equations:

$$MW_g = \sum_{j=1}^{5} X_j MW_j \quad (3.7)$$

$$\rho_v = \frac{P_{ris} MW_g}{RT} \text{ and } \varepsilon = \frac{F_{feed}/\rho_v}{F_{feed}/\rho_v + F_{rgc}/\rho_c} \quad (3.8)$$

Stripper Modeling

$$T_{sc} = ROT - \Delta T_{sc} \quad (3.9)$$

$$F_{sc} = F_{rgc} + C_{sc} \quad (3.10)$$

The aim of stripper is to remove residual hydrocarbons from catalyst surface after cracking reactions. Being a minor unit, no effort was made to rigorously model this unit. The spent catalyst temperature and flow rate ware calculated from the model equations 3.9 and 3.10. A temperature drop of 10K was assumed across the stripper unit.

3.1.2 Catalyst Deactivation

The catalyst activity (ϕ) was related to coke concentration on the catalyst and proposed by Yingxun (1991) for catalytic cracking of vacuum gas oil is as follows:

$$\phi = (1 + 51C_c)^{-2.78} \quad (3.11)$$

where Cc is the weight percent carbon and is dependent on catalyst residence time (Voorhies et al, 1945):

$$C_c = m.\Theta^n \quad (3.12)$$

Θ is the catalyst residence time in minutes and m and n are the constants and depend on the feed. The exponent of Θ is close to 0.5.

3.2 REGENERATOR MODEL

The regenerator has two regions, a dense and dilute phase. The deactivated catalyst, after steam stripping of hydrocarbons, enters the regenerator where all

hydrogen in the coke is converted into steam. Carbon can be converted to either CO or CO2. The heat of combustion raises the temperature of the catalyst recycling from the regenerator. The heat of combustion released in the regenerator is therefore the most critical item in any such simulation. The following assumptions are made in the development of the regenerator model (Dave and Saraf, 2003; Kasat et al, 2002; Krishna et al 1985; De Lasa, 1979, McFarlane et al 1995) .

1. The gases are in plug flow through bed and in thermal equilibrium with surrounding bed.
2. Catalyst in dense bed is well mixed and isothermal with uniform carbon on catalyst.
3. Kinetics of the coke combustion assumes catalyst particles to be of 60 μm size.
4. Resistance to mass transfer from gas to catalyst phase is negligible.
5. Mean heat capacities of gases and catalyst are assumed to remain constant over the temperature range encountered
6. All entrained catalyst is returned via cyclones.

The coke combustion, reactions 3.13 and 3.14 are proportional to Crgc and Po2. The CO combustion, reactions 3.15 and 3.16, are proportional to Po2 and Pco and take place through two parallel paths, heterogeneous and homogeneous. The hydrogen combustion, reaction 3.17 is complete and immediate and the hydrogen weight fraction in the coke is constant. The main combustion reactions in the regenerator are as follows:

$$C + \frac{1}{2}O_2 \xrightarrow{k11} CO \qquad (3.13)$$

$$C + O_2 \xrightarrow{k12} CO_2 \qquad (3.14)$$

$$CO + \frac{1}{2}O_2 \xrightarrow{k13c} CO_2 \qquad \text{Heterogeneous CO Combustion} \tag{3.15}$$

$$CO + \frac{1}{2}O_2 \xrightarrow{k13h} CO_2 \qquad \text{Homogeneous CO combustion} \tag{3.16}$$

$$H_2 + \frac{1}{2}O_2 \xrightarrow{k14} H_2O \tag{3.17}$$

The following rate expressions for the combustion reactions in the regenerator in kmol / (m^3.sec) are:

$$r_{11} = (1-\varepsilon)\rho_c k_{11}\frac{C_{rgc}}{MW_c}P_{O2} = (1-\varepsilon)\rho_c k_{11}\frac{C_{rgc}}{MW_c}\frac{f_{o2}}{f_{tot}}P_{rgn} \tag{3.18}$$

$$r_{12} = (1-\varepsilon)\rho_c k_{12}\frac{C_{rgc}}{MW_c}P_{O2} = (1-\varepsilon)\rho_c k_{12}\frac{C_{rgc}}{MW_c}\frac{f_{o2}}{f_{tot}}P_{rgn} \tag{3.19}$$

$$r_{13} = k_{13}P_{O2}P_{CO} = \left(X_{pt}(1-\varepsilon)\rho_c k_{3h} + \varepsilon k_{13h}\right)P_{O2}P_{CO} = \left(X_{pt}(1-\varepsilon)\rho_c k_{13c} + \varepsilon k_{13h}\right)\frac{f_{o2}f_{co}}{f_{tot}}{P_{rgn}}^2 \tag{3.20}$$

where $x_{pt,}$ is the relative combustion rate simulating the addition of promoter.

The CO2/CO ratio in the gas leaving the dense bed is a function of the bed temperature, residence time, carbon- on-catalyst, and equilibrium metals on catalyst. The presence of CO promoter catalyzes CO oxidation and raises CO2/CO ratio. The CO in the dense bed exit is also oxidized in the dilute bed in presence of entrained catalyst.

The initial ratio of CO/CO2 at the catalyst surface is given by equation 3.21 (Weisz, 1966) and k_c is the overall coke combustion rate.

$$\left(\frac{CO}{CO_2}\right)_{Surface} = \frac{k_{11}}{k_{12}} = \beta_c = \beta_{c0}\exp\left(\frac{-E_\beta}{RT}\right) \tag{3.21}$$

$$k_c = k_{11} + k_{12} = k_{c0}\exp\left(-\frac{E_c}{RT}\right) \tag{3.22}$$

$$k_{11} = \frac{\beta_c k_c}{\beta_c + 1} = \frac{\beta_c k_{c0}\exp\left(-\frac{E_c}{RT}\right)}{\beta_c + 1} \tag{3.23}$$

$$k_{12} = \frac{k_c}{\beta_c + 1} = \frac{k_{c0}\exp\left(-\frac{E_c}{RT}\right)}{\beta_c + 1} \tag{3.24}$$

$$k_{13c} = k_{13c0}\exp\left(-\frac{E_{13c}}{RT}\right) \quad (3.25)$$

$$k_{13h} = k_{13h0}\exp\left(-\frac{E_{13h}}{RT}\right) \quad (3.26)$$

3.2.1. Dense Phase Model Equations

The regenerator dense bed consists of two phases, the gases phase and catalyst phase (solid phase), where as the gases are assumed to be moving in plug flow, the catalyst phase is assumed to be well mixed. In this model it is assumed that there is no resistance to mass transfer of gaseous components between gas phase and catalyst phase (Krishna and Parkin, 1985).

a. The Gas Phase Material Balance:

The material balances across a differential elemental of height, dz, of dense bed are as follows:

$$\frac{dF_{O2}}{dz} = -A_{rgn}\left(\frac{r_{11}}{2} + r_{12} + \frac{r_{13}}{2}\right) \quad (3.27)$$

$$\frac{dF_{CO}}{dz} = -A_{rgn}(r_{13} - r_{11}) \quad (3.28)$$

$$\frac{dF_{CO2}}{dz} = A_{rgn}(r_{12} + r_{13}) \quad (3.29)$$

$$\frac{dF_{N2}}{dz} = 0 \quad (3.30)$$

Initial Conditions (at z=0) for Dense Bed Modeling:

$$F_{H20} = \left(C_{sc} - C_{rgc}\right)\frac{C_H}{MW_c} \quad (3.31)$$

$$F_{O2} = 0.21F_{air} - \frac{1}{2}F_{h2o} \quad (3.32)$$

$$F_{CO} = F_{co2} = 0 \quad (3.33)$$

$$F_{N2} = 0.79\,F_{air} \quad (3.34)$$

$$F_{tot} = F_{O2} + F_{CO} + F_{CO2} + F_{H2O} + F_{N2} \quad (3.35)$$

b. Carbon Mass Balance:

Under the assumption that all the entrained catalyst returns to the dense bed, it is possible to write an overall carbon balance for the regenerator.

$$\frac{dCrgc}{dt} = \frac{1}{Wrgn}[(F_{sc}\,C_{sc} - \; F_{rgc}C_{rgc})(1 - C_H) \;\; + \left(F_{CO(Zbed)} + F_{CO_2(Zbed)}\right) MW_c \qquad (3.36)$$

For constant Crgc in dense bed, $\frac{dCrgc}{dt}$ = 0, as catalyst is in CSTR.

$$F_{sc}\;C_{sc}(1 - C_H) \;\; = \; F_{rgc}C_{rgc}(1 - C_H) \;\; + \left(F_{CO(Zbed)} + F_{CO_2(Zbed)}\right) MW_c$$

$$C_{rgc} = \frac{\left[F_{sc}C_{sc}(1-C_H) - \left(f_{CO(Zbed)} + f_{CO_2(Zbed)}\right)MW_c\right]}{F_{rgc}(1-C_H)} \qquad (3.37)$$

c. Energy Balance

Similar to the carbon mass balance, the catalyst temperature is also constant (catalyst is in CSTR and $\frac{dT_{rgn}}{dt} = 0$) in dense bed, so overall heat balance in the dense bed is given by the following equation:

$$\frac{dT_{rgn}}{dt} = \frac{1}{W_{rgn}C_{p,c}}\left[(Q_C + Q_H + Q_{air} + Q_{sc} + Q_{ent}) - \left(Q_{rgc} + Q_{sg} + Q_{loss,rgn}\right)\right] \qquad (3.38)$$

Heat balance across the regenerator dense bed is given by the following equation:

$$Q_c + Q_H + Q_{air} + Q_{sc} + Q_{ent} = Q_{rgc} + Q_{sg} + Q_{loss} \qquad (3.39)$$

Where,

$$Q_c = F_{co(Zbed)}H_{co} + F_{co2(Zbed)}H_{co2} \qquad (3.40)$$

$$Q_H = F_{H2o}H_{H2o} \qquad (3.41)$$

$$Q_{air} = F_{air}C_{P_{air}}(T_{air} - T_{base})$$

$$SQ_{sc} = F_{sc}C_{P_{sc}}(T_{sc} - T_{base}) \qquad (3.43)$$

$$Q_{rgc} = F_{rgc}C_{P_c}\left(T_{rgn} - T_{base}\right) \qquad (3.44)$$

$$Q_{sg} = F_{co2(Zbed)}C_{P_{co2}} + F_{co(Zbed)}C_{P_{co}} + F_{o2(Zbed)}C_{P_{o2}} + F_{H2o}C_{P_{H2o}} + F_{N2} \qquad (3.45)$$

$$Q_{ent} = F_{ent}C_{P_c}\left(T_{dil(Zbed)} - T_{base}\right) \qquad (3.46)$$

The final equation for the dense bed temperature is :

$$T_{rgn} = T_{base} + \frac{F_{co(Zbed)}H_{co} + F_{co2}H_{co2} + F_{H2o}H_{H2o} + F_{air}C_{P_{air}}(T_{air} - T_{base}) + F_{sc}C_{P_c}(T_{sc} - T_{base}) + Q_{loss,rgn}}{F_{rgc}C_{P_c} + F_{co2(Zbed)}C_{P_{co2}} + F_{co(Zbed)}C_{P_{co}} + F_{o2}C_{P_{o2}} + F_{H2o}C_{P_{H2o}} + F_{N2}C_{P_{N2}}} \qquad (3.47)$$

d. Evaluation of Bed Characteristics :

$$\rho_g = \frac{P_{rgn}}{RT_{rgn}} \tag{3.48}$$

$$u = \frac{F_{air}}{\rho_g A_{rgn}} \tag{3.49}$$

$$\varepsilon_{den} = \frac{0.305u_1+1}{0.305u_1+2} \quad \text{Ewell and Gadmer, 1978} \tag{3.50}$$

$$\rho_{c,dense} = \rho_c(1-\varepsilon_{den}) \tag{3.51}$$

$$\rho_{c,dilute} = \text{Max}[0,(0.582u1-0.878)] \quad \text{(lb/ft3),from McFarlane et al., 1995} \tag{3.52}$$

Void fraction in the dilute phase:

$$\varepsilon_{dil} = \frac{\rho_{c,dil}}{\rho_c} \tag{3.53}$$

$$F_{ent} = p_{c,dil}A_{rgn}u \tag{3.54}$$

Dense Bed Height:

The regenerator dense bed height is calculated by the given correlation McFarlane et al., 1995

$$z_{bed} = \min\left[z_{cyc}, \left(2.85 + 0.8u + \frac{W_{reg} - p_{c,dilute}A_{rgn}\,z_{cyc}}{A_{rgn}p_{c,dense}}\right) * \left(\frac{1}{1-\text{pc, dilute/pc, dense}}\right)\right]$$

3.2.2 Dilute Phase Model Equations

The Dilute bed is described as a lean phase where entrained catalyst particles and gases evolve in a plug flow pattern. The material and energy balance equations from Kasat et al., 2002 for the dilute bed regenerator are presented as follows:

a. Material Balance

$$\frac{dF_{O2}}{dz} = -A_{rgn}\left(\frac{r_{11}}{2} + r_{12} + \frac{r_{13}}{2}\right) \tag{3.55}$$

$$\frac{dF_{CO}}{dz} = -A_{rgn}(r_{13} - r_{11}) \tag{3.56}$$

$$\frac{dF_{CO2}}{dz} = A_{rgn}(r_{12} + r_{13}) \tag{3.57}$$

$$\frac{dF_C}{dz} = -A_{rgn}(r_{11} + r_{12}) \tag{3.58}$$

b. Energy Balance

$$\frac{dT_{dil}}{dz} = \frac{1}{C_{P_{tot}}}\left(H_{CO}\frac{dF_{CO}}{dz} + H_{CO2}\frac{dF_{CO2}}{dz}\right) = \frac{A_{rgn}}{C_{P_{tot}}F_{tot}}\ [H_{CO}(r_{11} - r_{12}) + H_{CO2}(r_{11} - r_{12})] \quad (3.59)$$

$$C_{P_{tot}} = \frac{C_{P_{N2}}F_{N2} + C_{P_{O2}}F_{O2} + C_{P_{CO}}F_{CO} + C_{P_{CO2}}F_{CO2} + C_{P_{H2o}}F_{H2o} + C_{P_c}F_{ent}}{F_{tot}}$$

3.3 SIMULATION PROCEDURE FOR CONTINUOUS REACTOR - REGENERATOR OPERATION

A simulator has been developed where the coupled riser reactor and regenerator model equations have been assembled along with solution procedures. These have been computer coded using C programming language. The ordinary differential equations and nonlinear algebraic equations for material and energy balance are solved by using a Runge Kutta fourth order integration scheme and Successive Substitution methods respectively. The solution of these equations starts with initially guessed values of regenerated catalyst temperature (T_{rgn}) and coke on regenerated catalyst (Crgc), the product yields are, then, calculated at the outlet of the reactor. Subsequently the temperature of spent catalyst and coke on spent catalyst are calculated. The regenerator consists of the two beds: dense bed and dilute bed. The spent catalyst enters into the regenerator dense bed where it regenerates in presence of air and produces flue gases (see Figure 1.1). The dense bed calculations provide the new values of catalyst temperature (Tcal) and coke on regenerated catalyst (Ccal) which are compared with the initial value of Trgn and Crgc. If Tcal and Ccal do not match with assumed Trgn and Crgc then one needs to start the reactor calculation with newly calculated values of Trgn and Crgc by using the successive substitution method. Finally all the reactor and regenerator equations are solved with converged

value of Trgn and Crgc. The tolerance for the convergence of Trgn and Crgc used are 1 ^{0}C and 10 $^{-4}$ kg of coke/kg of catalyst respectively.

3.4 MODEL VALIDATION AND PARAMETRIC SENSITIVITY ANALYSIS FOR FIVE LUMP KINETIC MODEL

A complete reactor regenerator FCC unit has been simulated using the reactor model equations given by Dave and Saraf, (2003) and the regenerator model equations from different literature sources (Kasat et al., 2002; Avidan et al., 1990; Krishna and Parkin, 1985; De Lasa and Grace, 1979). The data on activation energies, frequency factors and heat of reaction (Table 3.4) are also used from the literature Dave and Saraf, 2003.The plant data and the model predicted data are compared in Table 3.5 and the match was found to be satisfactory. This validated model was used for the parametric sensitivity of the model to operating conditions. The coupled reactor and regenerator models were used to study the effect of different independent and dependent parameters on the plant performance. In order to study the effect of changing one independent variable on the reactor performance, all others must be held constant. However, it is important that the reactor operates under steady state conditions at all times, and this may require some other variable to be varied simultaneously. The feed flow rate (F_{feed}) and feed preheat temperature (T_{feed}) are the two key independent variables in the FCC process. The effects of these operating variables on steady state FCC unit performance are calculated by varying air flow rate (F_{air}) and catalyst circulation rate (CCR) to keep either regenerated catalyst temp (T_{rgn}) or ROT constant. The air flow rate to the regenerator was also used as an independent variable and its effect on conversion and yield studied.

Table 3.5: Comparison of Plant Measured and Models Prediction Data

Parameters	Plant Measured	Model Predicted
Reactor Outlet Temp (K)	768.8	769.1
Gas Oil (wt %)	45.6	42.5
Gasoline (wt %)	34.0	36.7
LPG (wt %)	12.4	13.2
DG (wt %)	3.4	3.6
Coke (wt %)	4.6	4.0
Regenerator Temp(K)	937.5	937.2
Dense Bed Height(m)	-	6.5
Coke on Regenerated Catalyst (wt %)	-	0.12
O_2 (Vol %)	-	1.4
CO (Vol %)	-	10.3
CO_2 (Vol %)	-	6.4
N_2 (Vol %)	-	81.9
Flue Gas Temp(K)	-	939.0
Entrained Cat Flow Rate (kg/sec)	-	13.6

3.4.1 Effect of Feed Preheat Temperature on FCC Performance at Constant Feed Flow Rate (F_{feed})

a) At Constant CCR and Constant Regenerator Temperature (T_{rgn})

Feed preheat temperature plays an important role in controlling the temperature in the riser reactor and hence the cracking reactions (see Figures 3.2 and 3.3). Gas oil conversion as well as yield of all the products were found to increase linearly with increase in T_{feed} (Figure 3.2). Figure 3.3 shows that reactor outlet temperature (ROT) increases nearly linearly with T_{feed} but air flow rate to the regenerator decreases linearly. This is to be expected in view of the fact that with increased ROT, air flow rate must decrease in order to keep T_{rgn} fixed.

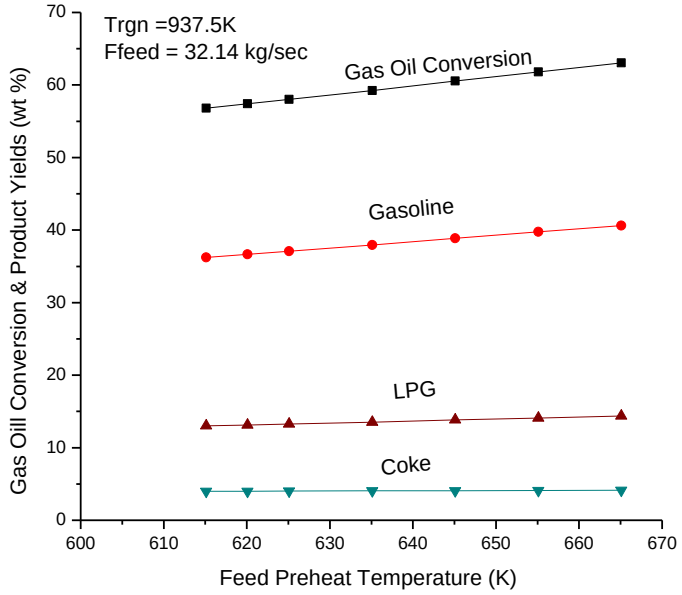

Figure 3.2: Effect of feed preheat temperature on gas oil conversion and product yields at fixed F_{feed} (32.14 kg/sec) and fixed regenerator temperature (937.5K)

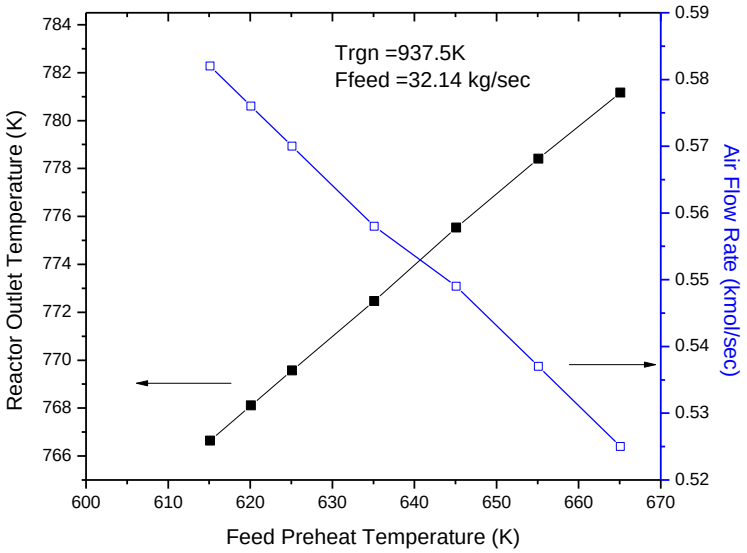

Figure 3.3: Effect of feed preheat temperature on riser outlet temperature (ROT) at fixed F_{feed} (32.14 kg/sec) and fixed regenerator temperature (937.5K)

b) At Constant Air Flow Rate (Fair) and Constant Reactor Outlet Temperature (ROT)

For ease of operation often the reactor outlet temperature is kept constant with the help of a controller. When feed preheat temperature is increased, regenerated catalyst flow rate (Frgc) must decrease to hold ROT constant (Figure 3.4). At constant feed

rate, this amounts to decreasing cat/oil ratio which leads to decrease in conversion and product yields (Figure 3.5). Figure 3.4 also shows that with increasing $T_{feed,}$ regenerator temperature increases initially rapidly and latter gradually. The change in slope seems to occur at feed preheat temperature 625K perhaps indicating an optimal condition of operation. At low T_{feed} the catalyst circulation rate is high giving rise of high conversion and high rate of coke formation. In view of this, regenerator temperature must increase rapidly, explaining the early sharp rise.

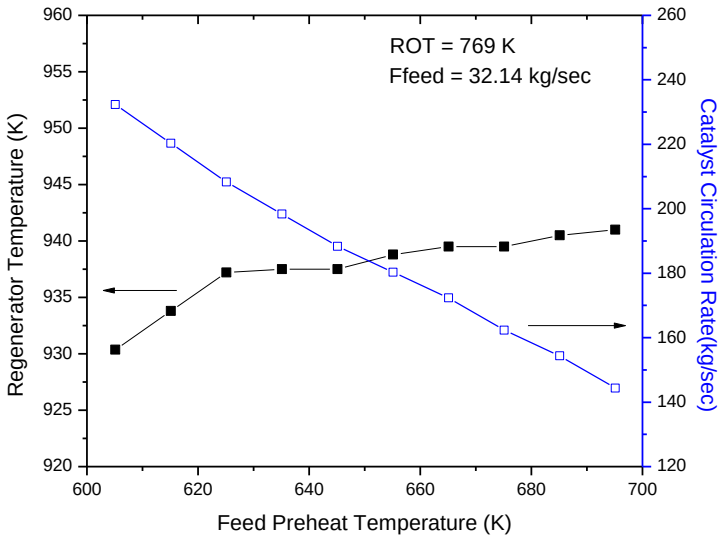

Figure 3.4: Effect of Feed Preheat Temperature on Regenerator Temperature (Trgn) at Fixed Feed Flow Rate (32.14 kg/sec) and Fix ROT (769 K)

From Figure 3.5 one can conclude that the effect of catalyst circulation rate (or cat/oil) is more pronounced as compared to that of Tfeed. Increasing Tfeed alone would have led to increase in conversion. The analysis showed that a decrease in feed preheat temperature by 10 K at fixed ROT and fixed feed could possibly result in 4% increase in gas oil conversion and 3.9 % gasoline yield. This corresponds to an increase in catalyst circulation rate from 208 to 220 kg/sec or an increase in cat/oil ratio from 6.5 to 6.9.

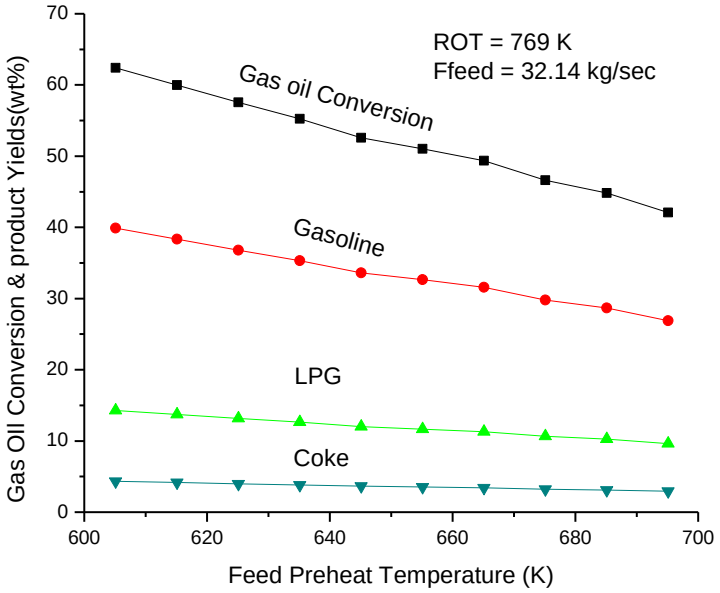

Figure 3.5: Effect of feed preheat temperature on gas oil conversion and product yields at fixed feed flow rate (32.14 kg/sec) and fix ROT (769 K)

3.4.2 Effect of Feed Flow Rate on FCC Performance at Constant T_{feed}

a) At Constant CCR and Constant Regenerator Temperature (T_{rgn})

As feed flow rate is increased keeping regenerator temperature and catalyst flow rate constant, the cat/oil ratio decreases which leads to decreased cracking activity and lower conversion and product yields (Figure 3.6).

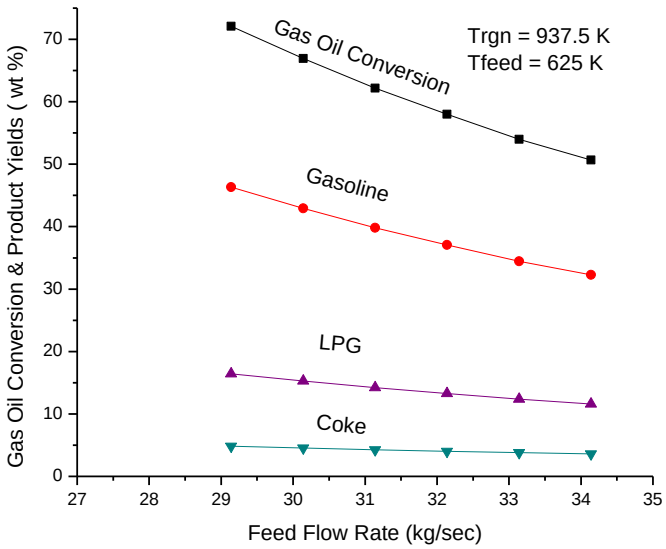

Figure 3.6: Effect of feed flow rate on the conversion and product yields at fixed feed preheat temperature (625K) and fixed regenerator temperature (937.5K)

Figure 3.7 shows that ROT decreases with increase in feed rate. While lower cat/oil ratio decreases conversion leading to less absorption of endothermic heat, higher feed absorbs more heat. The effect of feed rate being more pronounced as compared to cat/oil ratio, there is net decrease in ROT, which is to be expected since T_{rgn} is fixed. To keep Trgn constant, air flow rate must increase since sensible heat brought in the regenerator by the catalyst is less at lower ROT.

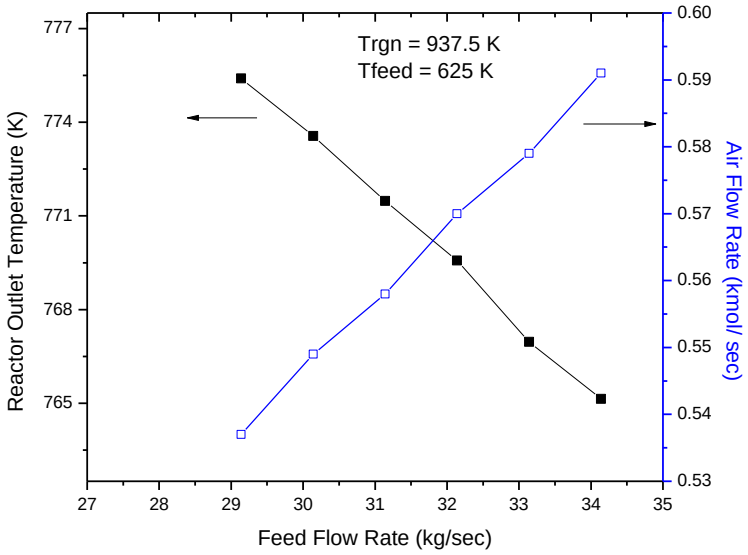

Figure 3.7: Effect of feed flow rate on the reactor outlet temperature (ROT) at fixed feed preheat temperature (625K) and fixed regenerator temperature (937.5K)

b) At Constant Air Flow Rate and Constant Reactor Outlet Temperature (ROT)

Figure 3.8 shows effect of change in feed rate on conversion and product yields at constant ROT and air flow rate. Under these conditions, T_{rgn} is expected to decrease because of extra amount of carbon coming in the regenerator (Figure 3.9). Catalyst circulation rate must increase to keep ROT constant. In the present case both catalyst flow rate and feed rate are increasing, the cat/oil ratio increasing gradually. This should lead to increase in conversion. However, Figure 3.8 shows a decreasing trend

in conversion as well as product yields. This can be explained in terms of sharp decrease in T_{rgn} amounting to less heat being available for endothermic cracking reactions, particularly when reactor outlet temperature must be maintained constant.

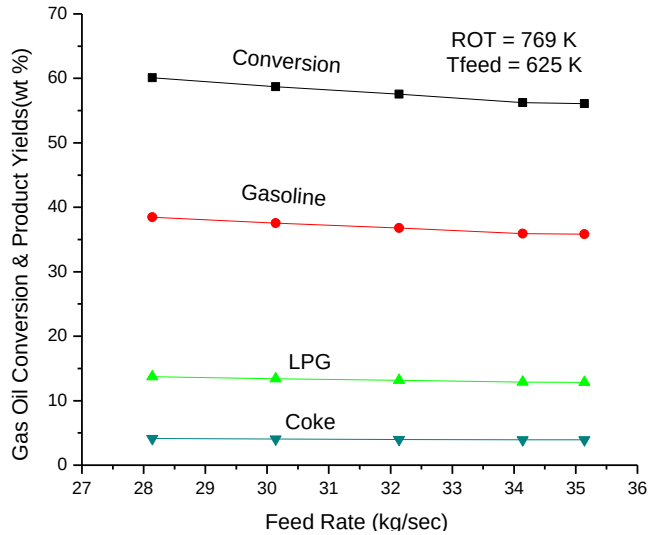

Figure 3.8: Effect of feed flow rate on the conversion and product yields at fixed reactor outlet temperature (768.8K) and fixed feed preheat temperature (625K)

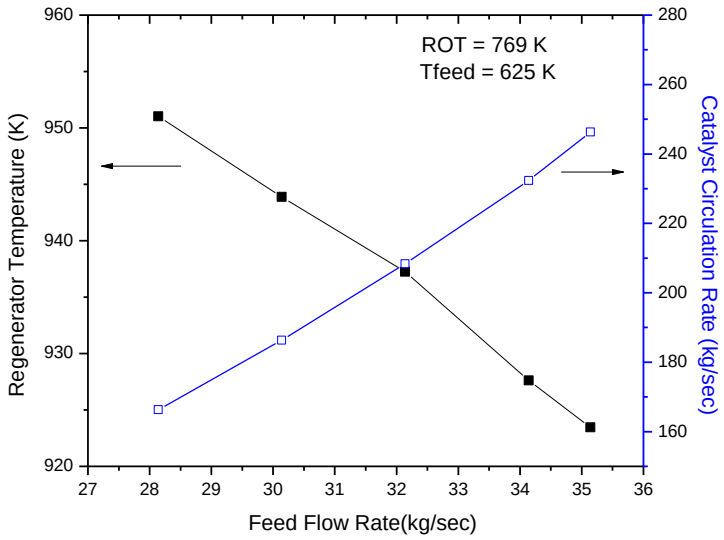

Figure 3.9: Effect of feed flow rate on the regenerator temperature (T_{rgn}) at fixed feed preheat temperature (625K) and fixed reactor outlet temperature (768.8K)

3.4.3 Effect of Air Flow Rate (F_{air}) on FCC Performance at Constant T_{feed}, F_{feed} and CCR:

Figure 3.10 shows that ROT as well as T_{rgn} increase initially with increasing air rate but become constant at higher air rates. More air rate leads to better coke combustion and hence higher T_{rgn} which in turn, increases ROT. Both T_{rgn} and ROT level off once coke combustion is nearly complete.

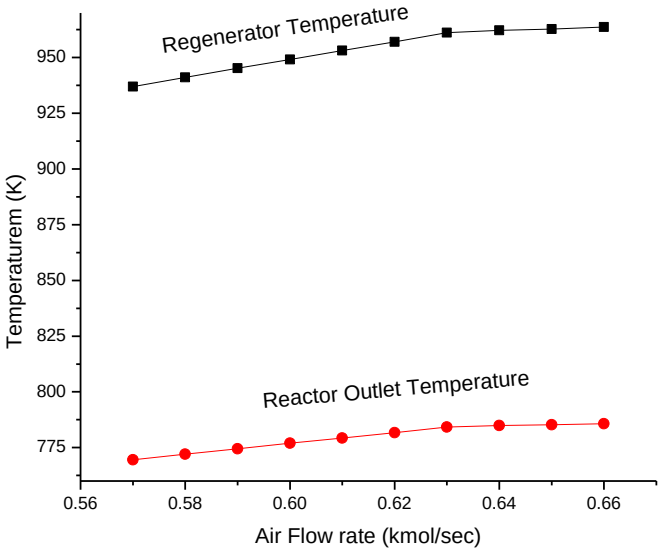

Figure 3.10: Effect of air flow rate on the regenerator temperature (T_{rgn}) and reactor outlet temperature (ROT)

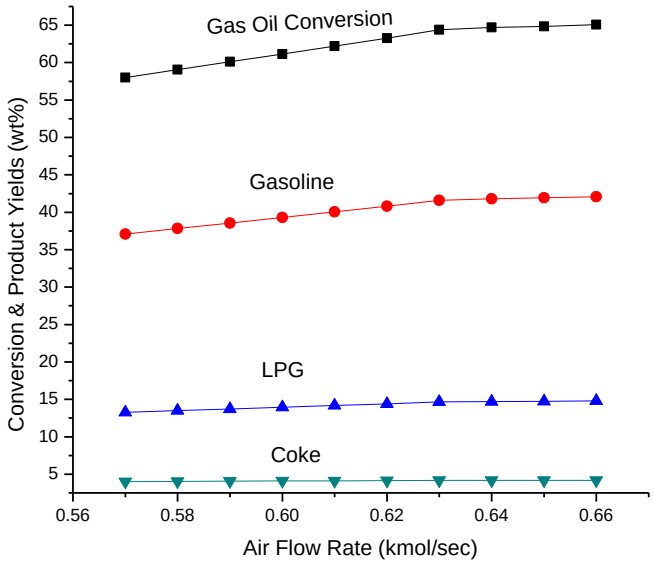

Figure 3.11: Effect of air flow rate on the conversion and product yields.

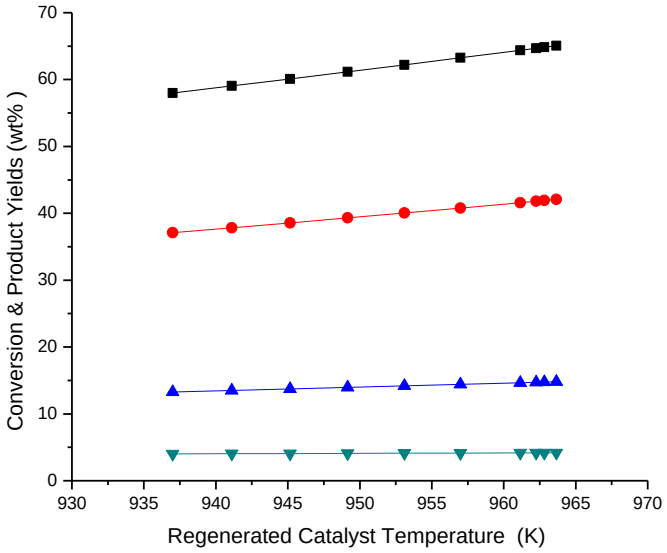

Figure 3.12: Effect of regenerated catalyst temperature (T_{rgn}) on the conversion and product yields.

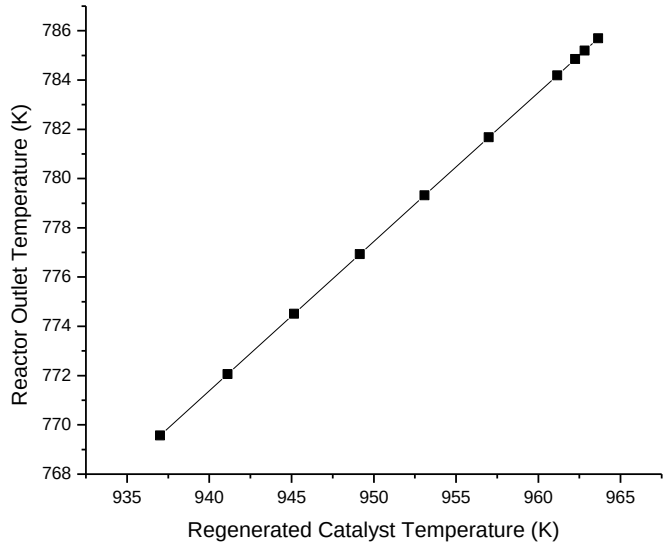

Figure 3.13: Effect of regenerated catalyst temperature (Trgn) on reactor outlet temperature (ROT)

Higher regenerated catalyst temperature provides higher reactor temperature and hence increased conversion and product yields (Figure 3.11). These plots suggest that it will be advantageous to increase ROT by 14 K, T_{rgn} by 24K by increasing air rate to 0.06 kmol/sec. The result of Figures 3.10 and 3.11 have been cross plotted in Figures

3.12 and 3.13 which show variation of conversion, product yields and reactor outlet temperature as a function of T_{rgn}.

Combining some of these observations as referred in Table 3.6, a decrease of say, 10K, in the feed preheat temperature (T_{feed}) and corresponding increase in air rate (F_{air}) and catalyst circulation rate (F_{rgc}) was found to increase gas oil conversion and product yields by 5 to 6 percent at constant reactor outlet temperature (ROT) and regenerated catalyst temperature (T_{rgc}). The economic visibility of such changes on the operating conditions can be explored by the refiners.

Table 3.6: Comparison of FCC Performance at Three Different Feed Preheat Temperatures with Increased Cat/Oil Ratio and Air Flow Rate

T_{feed}(K)	625.1	615.1	605.1
F_{rgc} (kg/sec)	208.3	220.3	232.3
F_{air} (kmol/sec)	0.57	0.63	0.63
ROT (K)	769.1	769.9	771.9
Gas oil conversion (wt %)	57.5	60.6	64.2
Gasoline (wt %)	36.8	38.8	41.2
LPG (wt %)	13.2	13.9	14.7
DG (wt %)	3.6	3.8	4.0
Coke (wt %)	4.0	4.2	4.4
T_{rgc} (K)	937.2	936.1	937.2

3.5 CONCLUDING REMARKS

An industrial FCC unit has been simulated by integrating kinetic models for the riser reactor and the regenerator. The model equations were solved using a computer based code in C-language. The calculated model results are compared with the plant data, which are found to be in agreement. This validated model is used to study parametric sensitivity such as effects of feed preheat temperature, feed flow rate and air flow rate (independent variables) on the FCC performance. Catalyst

circulation rate has stronger influence on gas oil conversion as compared to feed preheat temperature for a fixed reactor outlet temperature. On the other hand feed flow rate affects conversion more than catalyst circulation rate. Increase in air flow rate with other important parameters remaining constant leads to increased conversion. From above discussion of sensitivity analysis it appears that decreasing Tfeed and increasing catalyst circulation rate and air flow rate should lead to higher conversion and product yields. Table 3.6 shows the result of such computations. At given feed flow rate, a decrease in feed preheat temperature and increase in air flow rate may lead to increased conversion and product yields. However, this will require increased catalyst circulation rate. Trgn and ROT were found to remain essentially constant. The sensitivity analysis is useful for the refiners to understand the effects of individual parameters on the FCC performance for better productivity of the unit.

CHAPTER 4

EXPERIMENTAL WORK

The objectives of the present investigation include development of:

i) A predictive ANN model for estimation of detailed composition of FCC feeds in terms of paraffins, naphthenes and aromatics with routinely measured feed properties such as specific gravity, ASTM distillation temperatures etc, as inputs.

ii) A new ten lump kinetic model for cracking reactions in the FCC unit.

For the ANN model development, different FCC feed samples as well as individual blend constituents such as VGO, HVGO, OHCU Bottom samples were obtained from various Indian refineries processing indigenous crudes as well as low sulfur and high sulfur crudes from other sources such as Arab, Iran mix (Iran heavy and Iran light), Nigerian etc. and a mix thereof. The analysis of the all feed samples in terms of simple feed properties and their compositions in terms of three hydrocarbon groups were done in the R & D laboratory of Indian Oil Corporation Ltd, Faridabad.

Simple Feed Properties:

i) Specific gravity

ii) ASTM distillation temperatures

iii) Carbon residue

iv) Total sulfur

v) Total nitrogen

Feed Composition:

i) Paraffins (wt %)

ii) Naphthenes (wt %)

iii) Aromatics (wt %)

4.1 FCC FEED PROPERTIES

Routine laboratory measurements for specific gravity, ASTM distillation temperatures, Conradson carbon residue (CCR), total sulfur and total nitrogen were made for all the samples. A total of 28 feed samples were analyzed in the laboratory. All 28 samples were also analyzed for their detailed composition in terms of paraffins, naphthenes and aromatics. The results are shown in 4.1

Table 4.1: Properties of Different Heavy Gas Oil Samples

Sample No.	Sp. Gr	CCR	T.S	T.N	IBP	5 %	10 %	30 %	50 %	70 %	90 %	95 %	FBP	P	N	A
Units		wt %	wt %	wt %	^{0}C	^{0}C	^{0}C	^{0}C	^{0}C	^{0}C	^{0}C	^{0}C	^{0}C	wt %	wt %	wt %
1	0.9245	0.4	2.93	1401	37	317	342	392	423	454	498	514	538	8.3	24.1	67.6
2	0.996	1.55	4.35	200	42	409	428	458	477	494	514	523	537	7.8	25.3	66.8
3	0.8683	0.04	0.03	22	103	224	263	337	380	420	473	497	536	15.2	45.0	39.8
4	0.9136	0.04	1.54	329	111	276	318	368	391	407	427	436	460	14.8	15.5	70.5
5	0.9303	0.28	3.06	1161	169	257	320	402	438	474	519	535	574	11.2	23.3	65.6
6	0.8971	0.3	0.68	794	187	290	321	377	415	448	493	511	539	16.0	43.0	41.0
7	0.9382	0.3	3.28	1135	190	336	369	420	453	486	526	540	575	8.8	21.7	69.5
8	0.8386	0.04	0.02	5	253	354	379	411	434	464	508	524	543	46.2	35.6	18.1
9	0.940	1.48	3.1	1156	257	391	416	456	481	504	529	536	543	6.9	24.2	68.9
10	0.9528	0.73	2.82	1250	262	310	327	365	393	423	473	498	539	8.0	15.4	76.5
11	0.8516	0.05	0.01	589	277	355	373	411	437	464	503	518	541	27.7	55.9	16.5
12	0.8896	0.078	0.01 15	250	284	329	347	386	416	447	495	515	541	12.3	31.3	56.4
13	0.9734	1.61	2.8	700	294	388	412	455	480	504	534	544	579	7.5	25.9	66.5
14	0.9121	0.17	1.87	1150	298	352	372	414	442	468	506	522	542	11.8	25.6	62.5
15	0.9306	0.18	3.06	1466	320	368	385	425	455	489	530	544	579	8.8	24.3	66.9
16	0.9352	0.2	3.15	1268	325	377	396	439	472	503	538	552	580	8.7	25.3	66.1
17	0.9037	0.2	0.67	845	199	285	314	371	410	447	491	510	539	15.8	35.9	48.3
18	0.9119	0.24	3.35	842	215	327	352	400	434	466	508	523	541	14.4	23.3	62.2
19	0.9335	0.3	3.93	1240	298	374	393	435	463	489	518	528	541	4.9	21.1	74.0
20	0.8896	0.05	0.03 45	1100	291	342	361	400	429	459	504	523	542	10.9	29.9	59.2
21	0.9258	0.3	2.9	1077	303	367	385	421	448	478	517	531	549	10.4	18.5	71.0
22	0.9335	1.5	2.85	20	304	389	413	455	481	506	535	544	581	6.3	26.2	67.5
23	0.9269	0.42	3.04	1220	37	361	380	414	440	471	509	522	540	7.8	22.9	69.3
24	0.862	0.05	0.01 85	34	163	317	357	407	435	466	508	524	543	22.0	33.6	44.3
25	0.8896	0.15	0.6	900	251	343	363	404	431	461	506	523	542	15.7	36.3	47.9
26	0.9311	0.25	2.68	2089	294	366	383	421	451	482	519	529	544	12.7	22.4	64.8
27	0.9165	0.31	2.4	1348	299	364	379	414	443	475	526	528	544	13.7	24.0	62.2
28	0.9132	0.29	2.4	1626	301	371	388	427	458	490	524	533	544	12.6	25.2	62.1

4.1.1 Specific Gravity

Density is one of the most important physical properties of a fluid and defined as mass per unit volume of a fluid. Liquid densities decrease as temperature increases but the effect of pressure on liquid densities at moderate pressures is usually negligible. At low and moderate pressures (less than a few bars), saturated liquid density is nearly the same as actual density at the same temperature. Density may be expressed in the form of absolute density (ρ, kg/m^3), molar density (ρ_m, Kmol/m^3), specific volume (V, m^3/kg), molar volume (Vm, m^3/kmol). The liquid density at the reference conditions of 20 ^{0}C (293 K) and one atm is called absolute density (d) to distinguish it from relative density. Liquid density for hydrocarbons is usually reported in terms of specific gravity (SG) or relative density defined as

$$SG = \frac{\text{density of liquid at temperature T}}{\text{density of water at temperature T}}$$

Since the standard conditions adopted by the petroleum industry are 60 ^{0}F (15.5 ^{0}C) and 1 atm, specific gravities of liquid hydrocarbons are normally reported at these conditions. At a reference temperature of 60 ^{0}F (15.5 ^{0}C) the density of liquid water is 999 kg/m^3. Therefore, for a hydrocarbon or a petroleum fraction, the specific gravity is defined as

$$\text{SG}(60^0\text{ F}/60^0\text{ F}) = \frac{\text{density of liquid at } 60^0\text{F (kg/m}^3)}{999(\text{kg/m}^3)}$$

Water density at 60 ^{0}F is 999 or almost 1000 kg/m^3, therefore, values of specific gravities are nearly the same as the density of liquid at 15.5 ^{0}C (289 K) in kg/m^3. Since most of hydrocarbons found in reservoir fluids have densities less than that of water, specific gravities of hydrocarbons are generally less than 1. The American Petroleum Institute (API) defined the API gravity (degrees API) to quantify the quality of petroleum products and crude oils. ASTM D 4052 method was used to determine the specific gravity of FCC feed. The API gravity is defined as:

$$API\ gravity = \frac{141.5}{SG(at\ 60^0F)} - 131.5$$

4.1.2 Simulated Distillation Temperature

ASTM D86 is the standard method to measure distillation temperatures of petroleum fractions. However, more recently, it has been replaced by a distillation curve produced by gas chromatography (GC) and is called "simulated distillation (SD)". The method is described in ASTM D 2887 test method. Simulated distillation method is simple, consistent, and reproducible and can represent the boiling range of a petroleum mixture without any ambiguity. This method is applicable to petroleum fractions with a FBP of less than 538 ^{0}C (1000 ^{0}F) and a boiling range of greater than 55^{0}C (100 ^{0}F) and having a vapor pressure sufficiently low to permit sampling at ambient temperature. The ASTM D 2887 method is not applicable to gasoline samples and the ASTM D 3710 test method is recommended for such fractions. Distillation curves by SD are presented in terms of boiling point versus wt% of mixture vaporized because in gas chromatography, composition is measured in terms of weight fraction (wt%). Simulated distillation (SD) curves represent boiling points of compounds in a petroleum mixture at atmospheric pressure and very close to actual boiling points shown by TBP curves. These two types of distillation data are not identical and conversion methods should be used to convert SD to TBP curves. In comparison with ASTM D 86, the IBP from a SD curve of a petroleum mixture is less than IBP from ASTM D 86 curve, while the FBP from SD curve is higher than the FBP from ASTM D 86 of the same mixture. The percent vaporized for ASTM D 2887 (SD) is in wt % while for the ASTM D 86 curve is in vol %.

4.1.3 Carbon Residue (CR)

When a petroleum fraction is vaporized in the absence of air at atmospheric pressure, the nonvolatile compounds have a carbonaceous residue known as carbon

residue (CR). Therefore, heavier fractions with more aromatic contents have higher carbon residues while volatile and light fractions such as naphthas and gasolines have no carbon residues. CR is particularly an important characteristic of crude oils and petroleum residues. Higher CR values indicate low-quality fuel and less hydrogen content. There are two, older, different test methods to measure carbon residues, Ramsbottom (ASTM D 524) and the Conradson (ASTM D 189). The relationships between these methods are also given by the ASTM D 189 method. Oils that have ash forming compounds have erroneously high carbon residues by both methods. For such oils ash should be removed before the measurement. The most recent test method (ASTM D 4530) was used for present analysis that requires less sample amounts. In most cases carbon residues are reported in wt% by Conradson method, which is designated by % CCR. Carbon residue can be correlated to a number of other properties. It increases with an increase in carbon-to-hydrogen ratio (CH), sulfur content, nitrogen content, asphaltenes content, or viscosity of the oil. The most precise relation is between CR and hydrogen content in which as hydrogen content increases the carbon residue decreases.

4.1.4 Elemental Analysis (Total Sulfur and Total Nitrogen)

The main elements present in a petroleum fraction are carbon(C), hydrogen (H), nitrogen (N), oxygen (O), and sulfur(S). The most valuable information from elemental analysis that can be obtained is on the C/H ratio and sulfur content of a petroleum mixture from which one can determine the quality of oil. As boiling points of fractions increase or their API gravity decrease the amount of C/H ratio, sulfur content, nitrogen content, and the metallic constituents increase, signifying a reduction in the quality of an oil. Sulfur content of very heavy fractions can reach 6-8%. There are specific methods to measure these elements individually. However,

instruments do exist that can measure all these elements; these are called elemental analyzers. ASTM test methods for elemental analysis of petroleum products and crude oils include hydrogen content (ASTM D 1018, D 3178, D 3343), nitrogen content (ASTM D 3179, D 3228, D 3431), and sulfur content (ASTM D 129/IP 61, D 1266/IP 107, D 1552, D 4045). Infrared detector (IRD) detects CO2, H20, and SO2 in an elemental analyzer Model CHNS-932, while N2 is determined using the thermal conductivity detector (TCD) method. Generally, in heavier oils (lower API gravity) proportions of carbon, sulfur, nitrogen, and oxygen elements increase but the amount of hydrogen and the overall quality decrease. In the present work, total sulfur was measured by ASTM D2622 test method using X-ray fluorescence spectrometry (XRF) and total nitrogen was measured by the ASTM D4629 method (CHNS).

4.2 FCC FEED CHARACTERIZATION BY HYDROCARBON TYPE

Different test methods are available for the determination of hydrocarbons classes; NMR, HPLC and mass spectroscopy are some of important ones. High-performance liquid chromatography (HPLC) has found great utility in separating different hydrocarbon group types in nonvolatile feedstocks such as residue, and the molecular species in the asphaltene fraction (Chartier et al., 1986). However, a severe shortcoming of most high-performance liquid chromatographic approaches to a hydrocarbon group type of analysis is the difficulty in obtaining accurate response factors applicable to different distillate products. Nuclear magnetic resonance (NMR) has frequently been used for measurement of aromatics and saturated hydrocarbons (ASTM E-386) as well as hydrogen distributions. Beyond these results, both C and H in various structural groupings in a molecule can also be determined (Speight, 1994). As NMR (1H and 13C) is fast and relatively inexpensive, it has gained a prominent place for the structural group analysis of petroleum fractions especially in the heavy

gas oil range (Kapur et al., 2005; Bansal et al., 2007). Mass spectroscopy has proved to be highly successful in the petroleum industry, especially with the use of computerized techniques in determining, quantitatively, the percentage of paraffins, cycloparaffins and aromatics in heavy gas oil fractions. High-resolution mass spectrometry analysis (HRMS) was used for determining the hydrocarbon types in diesel range samples before and after the hydrocracking process and the results were compared with those from NMR (Bansal et al., 2004). Being very rapid method for obtaining full hydrocarbon type analysis for a wide range of fractions up to and including heavy gas oils, mass spectrometry is considered the most useful technique for PNA characterization of petroleum fractions.

There are several empirical correlations available in the literature (Sadeghbeigi, 2000, Riazi, 2005) for the hydrocarbon group characterization of heavy and light fuel oil fractions in terms of properties measured on regular basis such as specific gravity, distillation etc. The most commonly known procedures are the n-d-m method (ASTM D-3238, 1998) and API correlation. The n-d-m method (Van Nes and Van Westen, 1951) is used for estimating percentage carbon in aromatic, naphthenic and paraffinic structures with refractive index, density, average molecular weight and sulfur as input. However, this method is very sensitive to refractive index and can only be applied for samples with paraffin content greater than 25 wt%. The API method (API procedure 2B 4.1) is a generalized method that predicts mole fraction of paraffinic, naphthenic and aromatic compounds for an olefin-free hydrocarbon. Other procedures for the analysis of the composition of heavy and light petroleum fractions have been discussed by Waterman et al., 1958 and Riazi and Daubert, 1980. However, all the existing methods are accurate only for data on which the method is based and cannot be extrapolated for wide range of properties.

Moreover, most of these methods predict PNA composition in terms of mole or volume basis which is difficult to validate with mass spectroscopy, NMR or HPLC analysis obtained in weight basis.

All the FCC feed samples were analyzed for their hydrocarbon compositions through HC22 (22-hydrocarbon component class) analysis based on high-resolution mass-spectrometric method. Autospec Ultima High-Resolution mass spectrometer from Micromass UK was used for analysis. 5 µl of the sample was introduced into the mass spectrometer using the All Glass Heated Inlet System (AGHIS) and heated to desired temperature. The sample vapors were then allowed to homogenize in the bulb before being introduced into the source of the mass spectrometer.

The high-resolution mass spectra of the samples were acquired using OPUS software. Mass spectrometer with 5000 resolution is sufficient to distinguish masses up to 470 and to separate ions that differ in composition by +1 carbon and +2 hydrogen. The spectral data of minimum 7 or 8 scans were averaged and the averaged data were processed by Teeter's PCMASPEC - HC22 software (Teeter, 1985) for hydrocarbon type analysis. The method provides the quantification of 22 classes of hydrocarbons based on the number of hydrogen atoms relative to the number of carbon atoms as expressed by the letter z. The principal fragments formed from paraffin class in mass spectrometer are at odd masses with z+1. The seven saturated molecular species considered in this analysis have z values of 0,-2,-4, -6, -8, -10 and –12 respectively which correspond to cycloalkanes with one to seven rings (mono to heptacycloparaffins). The aromatic hydrocarbon groups starts with the alkyl benzene that has z number of –6 till z = 28 representing ten classes of aromatics. Four classes of sulfur-aromatics were also reported. This classification widely covers the

hydrocarbon classes present in the VGO range of samples. Representative analyses for four different samples are shown in Table 4.2

4.3 PLANT DATA FROM AN OPERATING REFINERY

For the development of the kinetic model, one needs to carry out the cracking reactions with different known feed compositions and at different operating conditions but using the same reactor design and catalyst.

Table 4.2: Mass Spectrometry Analysis for Different Samples

FCC Feed	**HSVGO**	**Mixed Feed**	**OHCU Bottom**	**HVGO**
Paraffins	10.9	10.4	31.4	33.8
Monocycloparaffins	9.8	4.6	23.8	9.3
Dicycloparaffins	7.3	4.7	15.3	5.5
Tricycloparaffins	5.8	5.3	10.5	5.1
Tetracycloparaffins	0.0	1.8	3.6	0.3
Pentacycloparaffins	0.0	0.0	0.0	0
Hexacycloparaffins	0.0	0.0	0.0	0
Heptacycloparaffins	0.0	0.0	0.0	0
Saturates	**33.8**	**26.8**	**84.6**	**54.0**
Alkylbenzenes	9.2	5.3	6.3	6.3
Benzocycloparaffins	4.7	5.0	4.2	5.1
Benzodicycloparaffins	3.7	4.9	1.6	3.7
Naphthalenes	3.2	9.3	2.2	5.8
Acenaphenes, biphenyls	2.4	6.9	0.0	3.0
Acenaphthylenes, fluorenes	4.3	12.9	0.7	8.6
Phenanthrenes	3.8	9.0	0.1	6.1
Pyrenes	5.4	9.5	0.1	4.2
Chrysenes	2.7	3.4	0.0	0.1
Benzopyrenes	3.1	0.1	0.0	0.0
Aromatics	**42.5**	**66.3**	**15.2**	**42.9**
Thiophenes	0.3	0.0	0.0	0.0
Benzothiophenes	12.8	4.6	0.1	2.6
Dibenzothiophenes	10.5	2.2	0.0	0.4
Naphthobenzothiophenes	0.0	0.0	0.0	0.0
Sulfur Compounds	**23.6**	**6.8**	**0.1**	**3.0**
PNA Composition of FCC Feed Samples				
Paraffins (wt %)	10.9	10.4	31.4	33.8
Naphthenes (wt %)	23.0	16.5	53.2	20.2
Aromatics (wt %)	66.1	73.1	15.4	46.0

This can either be achieved in an FCC pilot plant or the actual plant itself. The second option was considered to be more desirable in view of the complexity of the process. Plant data are also needed for validation of the developed model.

The capacity of the fluid catalytic cracking unit (FCCU) is 1.4 MMTPA. Three different test runs and one operating run were conducted at different operating conditions and with different feeds. A same commercial catalyst was used in FCC unit for all the cases. Extreme care was taken to ensure that data collected from the unit were true. The feeds were mainly a blend of hydrocracker bottom (OHCUB), Nigerian HVGO and BH VGO. The feed blend composition and their properties are given in Table 4.3. The feed unit design and operating data are given in Tables 6.1 to 6.3 in Chapter 6 and in Tables 7.1 in Chapter 7.

Table 4.3: Feed Properties for Different Blends

	Case I	**Case II**	**Case III**	**Case IV**
Feed Mix	**(Wt %)**	**(Wt %)**	**(Vol %)**	**(Wt %)**
OHCB	30	32.7	46.5	36
Nigerian HVGO	45	34.5	26.2	56
BH HVGO	25	32.8	27.3	8
Parameters	**Values**			
Specific gravity @ 15 ^{0}C	0.8896	0.8896	0.8858	0.8949
API Gravity	27.56	27.56	28.24	26.62
UOP K factor	12.35	12.26	12.33	12.21
Distillation, ASTM D-1160, ^{0}C				
0	288	268	253	282
5	370	357	358	352
10	386	383	384	372
30	425	417	416	408
50	450	438	445	437
70	483	464	466	475
90	530	505	509	517
95	542	517	519	536
100	546	525	526	555
CCR, wt%	0.15	0.22	0.21	0.38
Total sulpur, wt%	0.5	0.45	0.43	0.34
Basic Nitrogen, ppm	307	299	281	-
Total Nitrogen, ppm	900	717	672	-
Kinematic Viscosity, CSt @ 50 ^{0}C	28.82	28.67	-	-

CHAPTER 5

ESTIMATION OF FEED COMPOSITION THROUGH ANN MODELING

Modeling of FCC unit becomes complex due to the presence of large number of hydrocarbons in the feed which undergo a variety of reactions to yield cracking products. Laboratory analysis of these components at their molecular level is not an easy task and therefore, it is not possible to account for each individual feed component and its reactions in any realistic modeling exercise. Use of kinetic lumps has extensively been made by various researchers to model FCC units with varying success. The earliest attempt had only two lumps, one representing the feed and the second component was the product (Weekman and Nace, 1968). Three (Weekman., 1969), four (Lee et al., 1989) and five (Bollas et al., 2007) lump models have successively been used with improved success. Clearly, larger the number of lumps used, closer we approach to the real system.

In all these models, feed is represented by a single lump of average composition and molecular weight. If instead, feed analysis is available in terms of hydrocarbon groups and their relative proportions, the reaction kinetics can be better accounted for (Nace and Weekman, 1971). 10 and 12 lumps (Nace and Weekman, 1971; Jacob et al., 1976; Ellis et al 1998; Kumar et al., 1995; Cerqueira et al 1997) have been successfully used to model/simulate industrial FCC units with better prediction capabilities. Of these lumps, 6 to 8 were used to characterize feed and intermediate product (light fuel oil 221-343 0C) and remaining four for the final products namely gasoline, LPG, dry gas, and coke. Typically for the above models, accuracy of model prediction depends on realistic FCC feed characterization in terms of paraffins, naphthenes, aromatic rings and aromatic substituent groups. However, it

is not practical to undertake quantitative feed analysis in terms of hydrocarbon types before embarking on simulation every time particularly in a field laboratory, which is not usually equipped for such analysis.

The present work aims to develop an Artificial Neural Network based model which can use routinely measured properties of FCC feed such as density, ASTM distillation temperatures, Conradson carbon residue (CCR), sulfur and nitrogen content as inputs and provide detailed composition (wt percent of paraffins, naphthenes and aromatics) as output. Artificial neural network (ANN) type of modeling is most suited for this work since we do not know any functional relationship, even if it exists, between available inputs and desired outputs. Being a black box approach, ANN does not require, nor attempt to develop, any mathematical relation, linear or non linear, between input and output and yet can effectively serve as a tool to estimate the detailed composition of the feed required for FCCU modeling.

5.1 ARTIFICIAL NEURAL NETWORK (ANN) MODEL DEVELOPMENT

Artificial neural networks have been successfully implemented in the chemical industry, especially in the areas of dynamic modeling. Bhat and McAvoy, (1990) used neural network for dynamic modeling of pH in a CSTR and compared the results with traditional ARMA modeling. They found ANN models to be more accurate than ARMA models. Lately an increasing trend is observed to model the steady state processes also using ANN approach. The height equivalent of theoretical plate (HETP) and pressure drop for columns with structured packing were predicted by neural network model and the results were found to be more accurate than traditional semi-empirical model (Pollock and Eldridge, 2000; Whaley et al., 1999). Neural network models have also been developed for the prediction of heavy gas oil cracking

products (Sheikhattar and Zahedi, 2011) in hydrocracking (Elkamel et al., 1999), fluid catalytic cracking and catalytic reforming units (Zahedi et al., 2008). An ANN model was compared with a non-linear statistical model for FCC (Michalopoulos et al., 2001). The results showed the superiority of the ANN model in terms of prediction accuracy. An ANN model based optimizer to separate gas flow coming out of a hydrocracking reactor was developed (Altissimi et al., 1998) and the ANN results were compared with those obtained from the first principle models developed by Bayley et al, (1993). The ANN model was trained with data obtained from a commercial simulator (ASPEN PLUS) in absence of availability of sufficient plant data.

Neural networks have been used as soft sensors for the estimation of various parameters of crude petroleum column and prediction of product properties. (Ganguly et al., 2002; Murty et al., 1995; Lee and Chen, 1993). Presently, several refineries use ANN models as soft sensors to estimate output stream quality online and use this information to control distillation columns. Its applications are also shown in the chemical plants for detecting gross errors in the faulty sensors (Gupta and Narasimhan, 1993).

Conventionally, the desired network architecture is arrived at by a constructive (Wang et al, 1994) or a destructive (Bhat and McAvoy, 1992) method. With the development of evolutionary techniques such as genetic algorithm, it has become possible to design the network architecture optimally and directly (Boozarjomehry and Svrcek, 2001; Dam and Saraf, 2006). In the present study, however, the conventional constructive method has been used to design the networks starting from a small network and expanding it by adding more layers and neurons in the hidden layers.

A feed forward back propagation type of modeling approach has been followed in the present work which is most suited for numerical NN modeling. The number of neurons for feed forward neural networks is approximately proportional to the number of learning data sets (Fujita, 1992 and 1998). All neurons in the input layer carry information to the neurons in the hidden layers after multiplying each with corresponding synaptic weights. Each layer has mapping function (somatic operation) to be suitably chosen. Figure 5.1 shows a typical neural unit (neuron) with linear synaptic operation. Normally, one or two hidden layers are sufficient to estimate any function (Haykin, 1999). The hidden layer may consist of one or more layers which may be connected in series or parallel or a combination with the output layer.

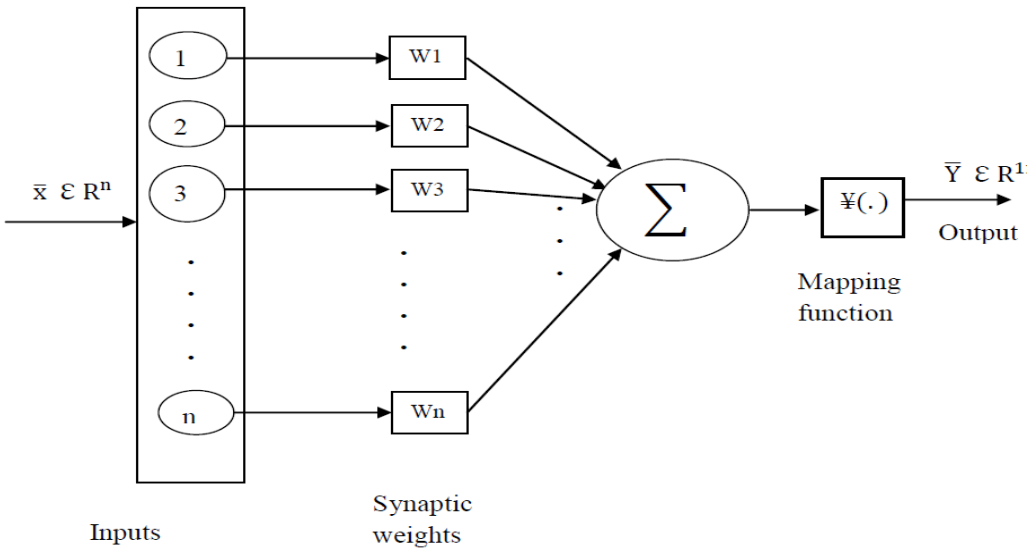

Figure 5.1: A typical neuron with linear synaptic operation.

In the present work, trial and error method was used to find near optimum ANN architecture for estimation of detailed feed composition (PNA). Neural Network Toolbox in MATLAB was used for the purpose. Various activation functions were investigated using different combinations for the hidden and the output layers. The numbers of neurons were also varied systematically in the hidden layers. The least

square error was optimized by addition of the neurons in the hidden layer. Finally, two hidden layers were found to be optimum.

In this algorithm, all information moves in the forward direction from input to output through hidden layers. Initial weights are arbitrarily assigned. During ANN training, the output is compared with the desired (experimental) known output and the error is back propagated to adjust the weights. Any non-linear optimization method whether local or global one can be used to optimize feed-forward neural network by changing the synaptic weights. The local searching optimization techniques are fundamentally limited to local solutions, while global ones attempt to avoid this limitation. The most popular optimization method has been Levenberg Marquardt algorithm based on variants of gradient, which was used in the present work. The training performance varies depending on the objective function and underlying error for a given problem and network configuration. After the network was fully trained and validated with new data sets, the network objective function was used to calculate the response to different inputs. Standard connections were used i.e network was fully connected between adjacent layers only. Figure 5.2 shows the ANN architecture used.

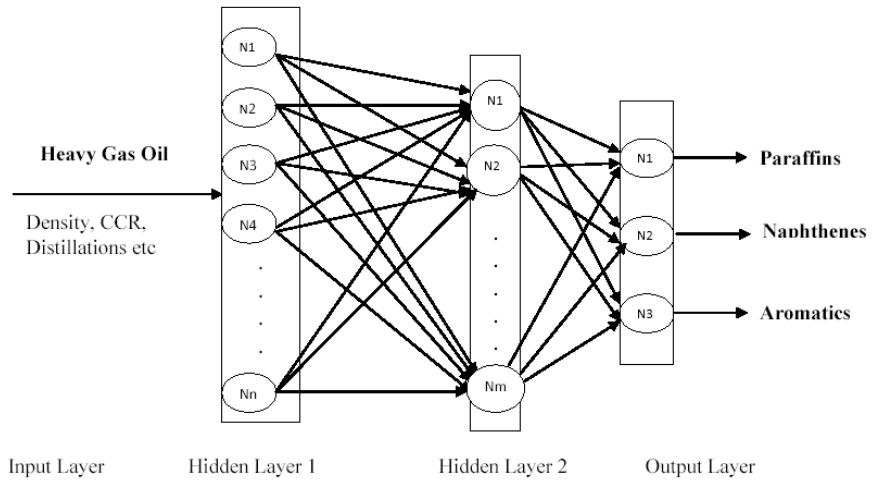

Figure 5.2: Neural network architecture with two hidden layers and an output layer.

5.2 MODEL PERFORMANCE EVALUATION CRITERIA

Following criteria were applied to evaluate the model performance

$$\text{Mean Square Error (MSE)} = \frac{1}{n}\sum_{n}\left(y_i^{obs} - y_i^{pred}\right)^2 \quad (5.1)$$

$$\text{Root Mean Square Error (RMSE)} = \sqrt{(\text{MSE})} \quad (5.2)$$

$$\text{Percent deviation (PD)} = \frac{y_i^{obs} - y_i^{pred}}{y_i^{obs}} * 100 \quad (5.3)$$

Coefficient of determination (also called R2) as defined below, was also included here as it reflects the accuracy of prediction. For the perfect model R2 = 1.

$$R^2 = \left(1 - \frac{SSE}{SST}\right) \quad (5.4)$$

Where SSE= sum of square error

$$SSE = \sum_n\left(y_i^{obs} - y_i^{pred}\right)^2 \quad (5.5)$$

SST= total sum of square deviation from the mean

$$SST = \sum_{n}\left(y_i^{obs} - \bar{y}_i^{obs}\right)^2 \quad (5.6)$$

A total of 28 samples were analyzed in the laboratory, of which 16 data sets covering the entire range of data (data range given in Table 5.1) were used for the development of ANN models (training). Another six data sets were used for testing the models and remaining 6 sets for model validation.

The developed ANN models are validated with remaining six data sets (input data range given in Table 5.2) representing FCC feeds with wide variation in compositions (paraffinic, naphthenic or aromatic in nature).

5.3 MODEL RESULTS

Two different ANN models (Model -1 and Model -2) have been developed in the present study. Model -1 predicts three output parameters: weight percents of

paraffin, naphthene and aromatic content of FCC feed from a single ANN architecture having three neurons in the output layer. Model -2 predicts the paraffin, naphthene and aromatic content individually from three different ANN architectures each with a single output neuron followed by normalization.

In ANN modeling there is always the big question about what should constitute the input parameters and there is no straight forward way to answer. One, therefore, tends to cautiously choose all possible inputs that are likely to influence the output. But this comes at a cost. Besides increasing computation load, particularly during training, it calls for larger data sets. Since all experimental data are prone to measurement errors, learning rates must be kept low resulting in further slowing down the training besides increasing model uncertainty and decreasing accuracy to convergence. It is therefore, desirable to use an optimal set of input parameters where the contribution of each input is more significant than the noise it adds.

Table 5.1: Range of Input Data sets Used for ANN Training

Parameters	**Minimum**	**Maximum**
Density, g/cc	0.8386	0.996
CCR (wt %)	0.04	1.61
Total Sulfur (wt %)	0.01	4.35
Total Nitrogen (ppm)	5	2089
SIMTBP (wt %)		
0 % (^{0}C)	37	325
5% (^{0}C)	224	409
10% (^{0}C)	263	428
30% (^{0}C)	337	458
50% (^{0}C)	380	481
70% (^{0}C)	407	506
90% (^{0}C)	427	538
95% (^{0}C)	436	552
100% (^{0}C)	460	581
Paraffins (wt %)	4.9	27.7
Naphthenes (wt %)	15.4	55.9
Aromatics (wt %)	16.5	76.5

Tables 5.3 and 5.4 provide the details of ANN model architecture used in the present study along with activation functions for the 13 and 8 inputs respectively. In the present study, initially all the 13 measured properties were chosen as input, namely: density, ASTM distillation temperatures - IBP, 5% ,10 %,30 % ,50% ,70 % , 90 % , 95 % and FBP, Conradson carbon residue (CCR), total sulfur and total nitrogen. Subsequently sensitivity of each variable was examined. Based on the sensitivity study and intuitive reasoning, five of the 13 variables were dropped. IBP and FBP can be seldom determined with any amount of certainty while CCR, Sulfur and nitrogen content in VGO are unlikely to influence its PNA composition. Remaining 8 – variables were used as inputs. Results are presented for both 13 as well as 8 inputs.

Table 5.2: Range of Input Datasets Used for Model Validation

Parameters	**Minimum**	**Maximum**
Density, g/cc	0.8896	0.9335
CCR (wt %)	0.05	1.5
Total Sulfur (wt %)	0.0345	3.93
Total Nitrogen (ppm)	20	1240
SIMTBP (wt %)		
0 % (^{0}C)	199	304
5% (^{0}C)	285	389
10% (^{0}C)	313	413
30% (^{0}C)	370	455
50% (^{0}C)	410	481
70% (^{0}C)	446	506
90% (^{0}C)	491	535
95% (^{0}C)	510	544
100% (^{0}C)	538	581

Table 5.3: Summary of ANN Model Architectures for 13 Input Variables

	Model 1	Model 2		
Output Parameters	**PNA**	**P**	**N**	**A**
No. of input variables	13	13	13	13
No. of hidden layers	2	2	2	2
No. of neurons in layer-1	14	13	12	9
No. of neurons in layer-2	14	14	14	10
Activation function of layer-1	tansig	tansig	logsig	tansig
Activation function of layer-2	logsig	logsig	logsig	logsig
Activation function output layer	purelin	purelin	purelin	purelin
Performance function	mse	mse	msereg	msereg
Training function	trainlm	trainlm	trainlm	trainlm

Table 5.4: Summary of ANN Model Architectures for 8 Input Variables

	Model 1	Model 2		
Output Parameters	**PNA**	**P**	**N**	**A**
No. of input variables	8	8	8	8
No. of hidden layers	2	2	2	2
No. of neurons in layer-1	8	12	12	9
No. of neurons in layer-2	9	13	12	9
Transfer function of layer-1	logsig	tansig	tansig	tansig
Transfer function of layer-2	logsig	logsig	logsig	logsig
Transfer function output layer	purelin	purelin	purelin	purelin
Performance function	mse	mse	mse	msereg
Training function	trainlm	trainlm	trainlm	trainlm

Table 5.5 gives a comparison between experimental values and model predictions of gas oil composition for 13 inputs using both the models. Also included in this table are the percent deviations of the predicted values from the measured ones, root mean square error and R^2 values. Table 5.6 shows a similar comparison with 8 input variables. These comparisons were made for the validation sets of input data which means these data were not shown to the networks earlier.

Table 5.5: A Comparison of Model Predictions with Experimental Observations for Two Different ANN Models with 13 Input Variables (Validation Set): (a) Model 1 (b) Model 2

(a) Model 1: RMS error = 2.97, R^2 value = 0.98,

	Paraffins			Naphthenes			Aromatics		
Sample ID	**Exp**	**Model 1**	**Dev %**	**Exp**	**Model 1**	**Dev %**	**Exp**	**Model 1**	**Dev %**
1	15.8	14.6	7.71	35.9	36.7	-2.17	48.3	48.7	-0.91
2	14.4	15.1	-5.12	23.3	23.2	0.53	62.2	61.7	0.83
3	4.9	5.0	-1.56	21.1	22.2	-5.09	74.0	72.8	1.55
4	10.9	16.7	-52.74	29.9	26.9	9.90	59.2	56.4	4.71
5	10.4	9.2	11.40	18.5	24.6	-33.21	71.0	66.1	6.84
6	6.3	6.5	-3.96	26.2	30.6	-16.75	67.5	62.9	6.87

(b) Model2: RMS error = 2.04 ; **R^2 value** = 0.993

	Paraffins			Naphthenes			Aromatics		
Sample ID	**Exp**	**Model 2**	**Dev %**	**Exp**	**Model 2**	**Dev %**	**Exp**	**Model 2**	**Dev %**
1	15.8	16.9	-6.95	35.9	31.7	11.63	48.3	51.4	-6.37
2	14.4	12.6	12.50	23.3	26.9	-15.47	62.2	60.5	2.74
3	4.9	5.4	-9.15	21.1	23.8	-12.75	74.0	70.9	4.24
4	10.9	11.9	-9.75	29.9	29.5	1.19	59.2	58.5	1.20
5	10.4	12.1	-16.23	18.5	19.1	-3.23	71.0	68.8	3.08
6	6.3	6.4	-1.18	26.2	26.6	-1.47	67.5	67.0	0.68

While both the models have acceptable levels of error, Model 2 scores over Model 1 in all respects. This is in line with the common knowledge that it is better to develop architectures with only one neuron in the output layer i.e. each model should preferably predict one parameter. For Model 1, maximum deviation is 52.7 % whereas it is only 16.2 % for Model 2. Figure 5.3 shows a parity plot between predicted and measured percent compositions for Models 1 and 2 using 13 input parameters.

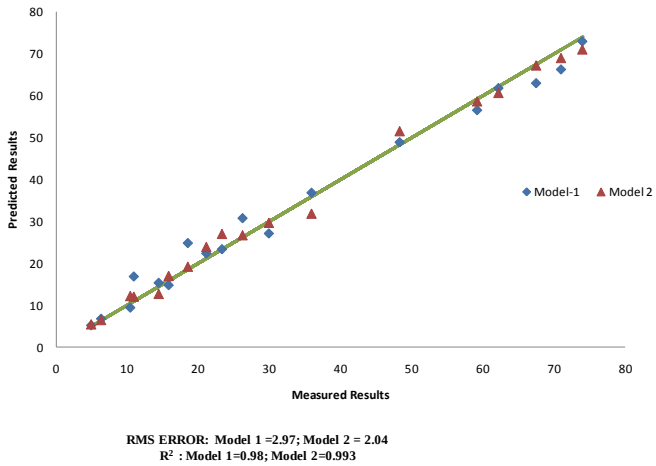

Figure 5.3: Parity plot between ANN predicted compositions and experimental values for models using 13 input variables.

Table 5.6 and Figure 5.4 provide similar information when only 8 inputs were used in place of 13. A comparison of Model 1 results for the two cases (with inputs 13 and 8) shows that fewer input parameters leads to less RMS error (2.09 against 2.97) and higher coefficient of determination, R^2 (0.993 against 0.98). Similar trend is observed for Model 2 also, however, less prominent.

Table 5.6: A Comparison of Model Predictions with Experimental Observations for Two Different ANN Models with 8 Input Variables (Validation Set)

Model 1: RMS error = 2.04; R2 value = 0.992,

	Paraffins			**Naphthenes**			**Aromatics**		
Sample ID	**Exp**	**Model 1**	**Dev %**	**Exp**	**Model 1**	**Dev %**	**Exp**	**Model 1**	**Dev %**
1	15.8	15.3	2.83	35.9	36.2	-0.71	48.3	48.5	-0.40
2	14.4	14.3	0.61	23.3	23.3	0.08	62.2	62.4	-0.33
3	4.9	4.8	2.31	21.1	20.8	1.20	74.0	74.4	-0.49
4	10.9	13.3	-22.03	29.9	26.2	12.40	59.2	60.5	-2.21
5	10.4	10.7	-3.27	18.5	23.3	-26.19	71.0	65.9	7.16
6	6.3	6.9	-9.92	26.2	24.6	6.17	67.5	68.5	-1.47
Model 2: RMS error = 1.71 ; R2 value = 0.994									
	Paraffins			Naphthenes				Aromatics	
Sample ID	Exp	Model 2	Dev %	Exp	Model 2	Dev %	Exp	Model 2	Dev %
1	15.8	15.8	0.19	35.9	36.4	-1.47	48.3	47.8	1.03
2	14.4	13.5	6.25	23.3	22.6	2.91	62.2	63.9	-2.70
3	4.9	4.5	7.64	21.1	23.3	-10.46	74.0	72.2	2.48
4	10.9	13.4	-22.99	29.9	32.3	-8.08	59.2	54.3	8.31
5	10.4	9.4	9.74	18.5	18.9	-2.14	71.0	71.7	-1.01
6	6.3	6.8	-7.25	26.2	26.7	-1.93	67.5	66.5	1.43

Clearly the dropped input parameters namely IBP, FBP, total sulfur, total nitrogen and CCR do not have noticeable role in predicting the FCC feed compositions but their associated measurement errors affect the network model performance.

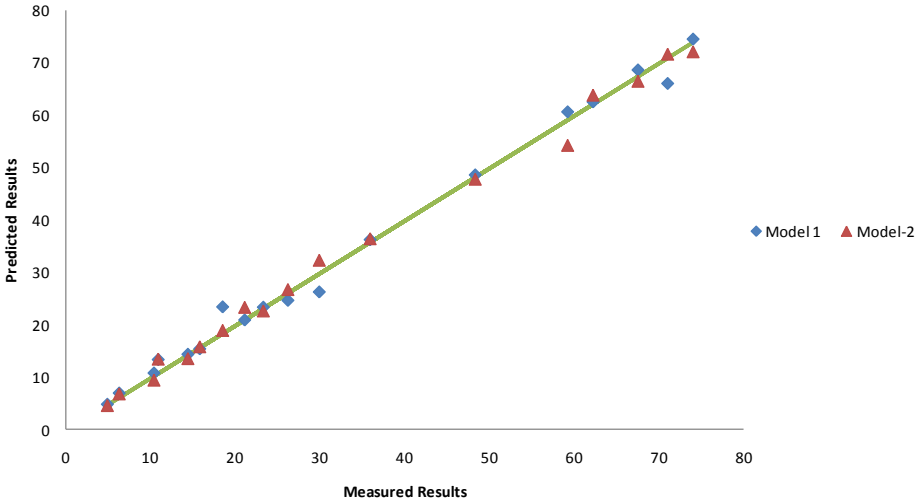

RMS ERROR: Model 1 =2.04; Model 2 =1.71
R2: Model 1=0.992; Model 2=0.994

Figure 5.4: Parity plot between ANN predicted compositions and experimental values for models using 8 input variables.

This chapter presents an artificial neural network (ANN) model to predict detailed composition of FCC feed using routinely measured simple properties such as density, ASTM distillation temperatures, Conradson carbon residue content (CCR), sulfur and total nitrogen as inputs to the model. 60% of all the laboratory data sets were used to train the different networks, 20% for testing and remaining 20% were used for the validation. Several feed forward back propagation networks with different number of neurons in hidden layers were studied using Levenberg Marquardt (LM) training algorithm. Among different investigated models, the ANN model with 8 inputs, namely density and distillation temperatures except IBP, FBP to predict paraffin, naphthene and aromatic contents individually shows best agreement with the experimental results within permissible limit.

CHAPTER 6
DEVELOPMENT OF A NEW TEN LUMP KINETIC MODEL

A new ten lump kinetic model for the FCC riser reactor is introduced which is based on the feed characterization in terms of 6 kinetic lumps, namely; heavy paraffins, heavy naphthenes, heavy aromatics, light paraffins, light naphthenes and light aromatics. The rate constants for a total of 25 cracking reactions have been estimated and these rate constants are invariant to feed gas oil composition. The model assumes a uniform two phase flow hydrodynamics but accounts for catalyst deactivation. The products yields, catalyst activity, and riser temperature are predicted all along the riser height. A combination of experimental data obtained from an operating plant and those generated from ASPEN FCC Simulator (ASPEN FCC, 2006) were regressed using an evolutionary optimization technique, genetic algorithm, to evaluate the rate constants. The detailed composition required as input to the 10 lump kinetic model was obtained from a validated ANN model requiring only routinely field laboratory measured feed properties as input (as detailed in Chapter 5). The product yields obtained by integrating the model equations using the present values of the rate constants were in close agreement with those measured in plant. Plant data from a refinery test run have been used for the validation of the developed model.

6.1 TEN LUMP KINETIC SCHEME

The present ten lump kinetic scheme is quite different from ten lump model proposed by Jacob et al., 1976 as in the current model, the heavy and light fuel oil are grouped in terms of three kinetic lumps such as paraffins, naphthenes and aromatics. Secondly, the present model uses LPG and dry gas as separate lumps. The detailed lumping scheme is shown in Figure 6.1.

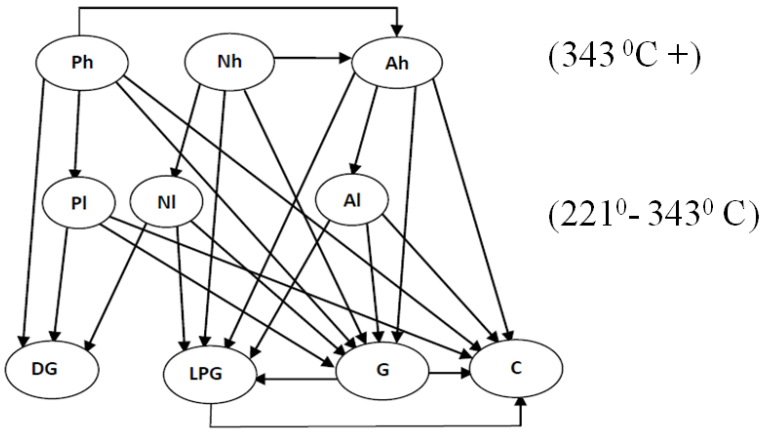

Figure 6.1: The ten lump kinetic scheme

1. P_h = Heavy paraffins, wt% paraffinic components in FCC feed $(343^{+}\,^{0}C)$
2. N_h = Heavy naphthenes, wt% naphthenic components in FCC feed $(343^{+}\,^{0}C)$
3. A_h = Heavy aromatics, wt% aromatic components in FCC feed $(343^{+}\,^{0}C)$
4. P_l = Light paraffins, wt% paraffinic components in light hydrocarbons (221- 343 ^{0}C)
5. N_l = Light naphthenes, wt% naphthenic components in light hydrocarbons (221-343 ^{0}C)
6. A_l = Light aromatics, wt% aromatics components in light hydrocarbons (221-343 ^{0}C)
7. G = wt% Gasoline
8. LPG = wt % Liquefied Petroleum Gas (Primary gaseous product)
9. DG= wt % Dry Gas (Secondary gaseous product)
10. C = wt % Coke

The present ten-lump model is developed on the basis of following assumptions which has also been used by others (Jacob et al., 1976; ASPEN FCC., 2006)

1) All cracking reactions are first order.
2) Reaction mass consists of only two phases, solid and gas phases.
3) Heat capacities and densities are constant throughout the length of the reactor.
4) Catalyst deactivation is non-selective and related to coke on catalyst only.
5) The solid catalyst particles are in thermal equilibrium with the gaseous mixture at all times.
6) The flow is uniform, that is, there is no slip between solid catalyst and vapors.
7) LPG and gasoline do not crack to produce dry gas and dry gas produce no coke.

6.1.1 Ten Lump Model Equations

Material Balance

The mass balance for the j[th] lump over a differential element of riser height (dh) can be written as follows:

$$\frac{dF_j}{dh} = A_{ris} H_{ris} (1 - \varepsilon) \rho_c \sum_{i=1}^{25} \left(\alpha_{kj}\right)_i r_i \tag{6.1}$$

where, A_{ris} = riser cross- sectional area in m^2,

i=1, 2…..25 are the number of reactions.

j=1, 2….10 and k=1, 2….10 are the kinetic lumps and k ≠ j.

$$\left(\alpha_{kj}\right)_i = stoichiometric\ coefficients = \frac{MW_k}{MW_j} = for\ k \rightarrow j\ in\ i^{th}\ reaction.$$

$$\text{dimensionless riser height (h)} = \frac{z}{H_{ris}} \tag{6.2}$$

z = axial height from the entrance of the riser in m.

Other properties such as rise void fraction (ε), oil vapor density (ρ_v in kg/m^3) and average molecular weight of gas oil are calculated by the following equations:

$$\rho_v = \frac{P_{ris} MW_g}{RT} \quad \text{and} \quad \varepsilon = \frac{F_{feed}/\rho_v}{F_{feed}/\rho_v + F_{rgc}/\rho_c} \tag{6.3}$$

$$MW_g = \sum_{j=1}^{10} x_j MW_j \tag{6.4}$$

where, MW_j is the molecular weight of j[th] kinetic lump and x_j is the mole fraction of j[th] lump.

R =Universal gas constant and T is the riser temperature at any axial height.

The rate equation for each i [th] reaction is as follows:

$$r_i = k_{0i} exp\left(-\frac{E_i}{RT}\right) C_j \phi \qquad for\ i = 1,2,3,4,5\ and\ j = 1 \tag{6.5}$$

$$r_i = k_{0i} exp\,(-\frac{E_i}{RT}) C_j \phi \quad for\ i = 6,7,8,9\ and\ j = 2 \tag{6.6}$$

$$r_i = k_{0i} exp\,(-\frac{E_i}{RT}) C_j \phi \quad for\ i = 10,11,12,13\ and\ j = 3 \tag{6.7}$$

$$r_i = k_{0i} exp\,(-\frac{E_i}{RT}) C_j \phi \quad for\ i = 14,15,16\ and\ j4 \tag{6.8}$$

$$r_i = k_{0i} exp\,(-\frac{E_i}{RT}) C_j \phi \quad for\ i = 17,18,19\ and\ j = 5 \tag{6.9}$$

$$r_i = k_{0i} exp\,(-\frac{E_i}{RT}) C_j \phi \quad for\ i = 20,21,22\ and\ j = 6 \tag{6.10}$$

$$r_i = k_{0i} exp\,(-\frac{E_i}{RT}) C_j\ \phi \quad for\ i = 23,24\ and\ j = 7 \tag{6.11}$$

$$r_i = k_{0i} exp\,(-\frac{E_i}{RT}) C_j\ \phi \quad for\ i = 25\ and\ j = 8 \tag{6.12}$$

The numbering scheme of the 25 reactions is shown below:

Reaction No. (i)	**Reaction**	**Reaction No. (i)**	**Reaction**	**Reaction No. (i)**	**Reaction**
1	Ph → Ah	10	Ah → Al	19	Nl → DG
2	Ph → Pl	11	Ah → G	20	Al → G
3	Ph → G	12	Ah → LPG	21	Al → LPG
4	Ph → DG	13	Ah → Coke	22	Al → Coke
5	Ph → Coke	14	Pl → G	23	G →LPG
6	Nh → Ah	15	Pl → DG	24	G → Coke
7	Nh →Nl	16	Pl → Coke	25	LPG → Coke
8	Nh → G	17	Nl → G		
9	Nh→ LPG	18	Nl → LPG		

j=1 to 10 represent; heavy paraffins, heavy naphthenes, heavy aromatics, light paraffins, light naphthenes, light aromatics, gasoline, LPG, dry gas and coke respectively. C_j is the concentration of j^{th} lump in kmol/m^3. E_i and k_{0i} are the activation energy and frequency factor of i^{th} reaction in the riser.

Φ is the catalyst deactivation function and depends only on the amount of coke on catalyst, and is given by following correlation (Yingxun, 1991).

$$\Phi = (1 + 51.C_c)^{-2.78} \tag{6.13}$$

where C_c is the coke on catalyst in wt % and is related to coke formation with time on stream (Voorhies, 1945) and Θ is the catalyst residence time in seconds; m and n are constants which depend upon feed, catalyst type and process conditions represented by the following equation. The exponent of Θ is close to 0.5.

$$C_c = m\,\Theta^{\,n} \tag{6.14}$$

Energy Balance:

The enthalpy balance across the same differential element of the riser height can be represented as follows:

$$\frac{dT}{dh} = \frac{A_{ris}H_{ris}\rho_c(1-\varepsilon)}{F_{rgc}C_{p_c} + F_{feed}C_{p_{fv}}}\sum_{i=1}^{25} r_i(-\Delta H_i) \tag{6.15}$$

$$T(h=0) = \frac{F_{rgc}C_{p_c}(T_{rgn} - 10.0) + F_{feed}C_{p_{fl}}T_{feed} - \Delta H_{evp}F_{feed} - Q_{loss,ris}}{F_{rgc}C_{p_c} + F_{feed}C_{p_{fv}}} \tag{6.16}$$

where ΔH_i is the heat of i^{th} reaction.

Equations (6.1) to (6.16) constitute the riser reactor model under steady state conditions. Equation (6.1), which actually represents 10 component material balances and Equation (6.15) representing enthalpy balance form a group of ordinary differential equations which need to be integrated simultaneously along the entire length of the reactor, the remaining equations are algebraic in nature. Equations (6.5) to (6.12) represent rate equations for the 25 reactions taking place. There are a total of 75 reaction parameters (including 25 frequency factors, 25 activation energies and 25 heat of reactions) which need to be evaluated before the model equations can be solved. The procedure used for the evaluation of these parameters is discussed below.

6.2 DETERMINATION OF REACTION PARAMETERS

The 10-lump kinetic scheme involving 25 reactions contains 75 kinetic parameters which need to be evaluated from experimental data before the model

equations can be integrated along the length of the reactor. The reactor output can, then, be compared with the plant production data in order to evaluate the adequacy of the proposed kinetic model

6.2.1 Refinery Test Run Data

For the evaluation of 75 parameters, enormous amount of data are required to be measured in the plant under test conditions. However, this is seldom possible in view of the high costs. A hybrid approach was, therefore adopted as described below. A few sets of test run data were collected using feeds of widely different compositions. One set of measured data consisting of feed compositions and properties is given in Table 6.1. Also included in Table 6.1 are the feed compositions in terms of PNA as obtained from the ANN model. The balance of requisite data were generated from a simulator. The plant operating conditions and other properties are given in Tables 6.2 and 6.3.

6.2.2 Data Generation from ASPEN FCC Simulator for Model Development

ASPEN FCC simulator (version 7.2) was first tuned with the test set of plant data. The ASPEN calculated parameters such as catalyst circulation rate, cat/oil ratio, coke on regenerated catalyst, delta coke etc and the product yields were compared with the plant data. The ASPEN model was tuned until a good match between predicted product yields and test data was obtained as shown in Table 6.4. The tuned ASPEN model was, then, used to generate yield data by varying riser outlet temperature (ROT). The data were collected at 11 different ROT at intervals of 3 to 5 ^{0}C. The cat/oil ratio and the coke on regenerated catalyst also varied as a result of variation in ROT. This is taken to be equivalent to collecting experimental data using a variety of feed stocks with different compositions.

6.2.3 Kinetic Parameters Estimation

The detailed kinetic lumping scheme proposed by different researchers ran into difficulty because of the non-availability of the kinetic data. A pattern search method was used to determine the rate constants using experimental data obtained from an isothermal micro activity test (MAT) at 482.22 ^{0}C (Jacob et al (1976). But the validity of these results in an industrial FCC plant working under very different and non-isothermal conditions raises serious doubts. In the present study some real data from an operating plant were collected and balance data were generated from a tuned industrial simulator. Initially, all physically possible 33 reaction pathways were considered for the ten kinetic lumps. An evolutionary optimization technique, Genetic Algorithm (GA) was used for minimization of the objective function given in Equation 6.17. GA is a random search technique and leads to global optimization even for highly non-linear problems and hence amply suited for estimation of kinetic parameters (Balasubramanian et al., 2003). Some computational details are given in Appendix A. The algorithm available in MATLAB Optimization Toolbox was used in the present study.

$$\mathrm{SSE} = \mathrm{Min}\left[\sum_{n=1}^{11}\sum_{i=1}^{10}\left(Y_{iexp} - Y_{ical}\right)_n^{\ 2} + \sum_{n=1}^{11}\left(T_{exp} - T_{cal}\right)_n^{\ 2}\right] \qquad (6.17)$$

The decision or manipulated variables are the kinetic parameters to be evaluated. The model equations form the equality constraints for the optimization problem. Y_{iexp} is the yield of the lumps as obtained either from plant data or ASPEN FCC Simulator and Y_{ical} is the yield obtained from the 10 lump kinetic model by integrating the model equations. The double summation on right hand side of Equation 6.17 is overall 10 lumps and 11 sets of data. The additional term in the objective function is to ensure a match in reactor outlet temperature also. Those reactions, which were found to have very low rate constants, were dropped from the reaction scheme. Finally, 25 reaction pathways were found to be sufficient for the

proposed ten lump reaction scheme. The parameter estimation exercise was then repeated for these 25 reactions pathways and the results are shown in Table 6.5. These final rate constants are used for the model validation with actual plant test run data from a refinery FCC unit.

Table 6.1: Feed Composition and Properties Measured in the Lab

Feed mix	**(w/w %)**
OHCB	30
Nigerian HVGO	45
BH HVGO	25
Parameters	**Values**
Specific gravity @ 15 ^{0}C	0.8896
Distillation, ASTM D-1160, ^{0}C	
0	288
5	370
10	386
30	425
50	450
70	483
90	530
95	542
100	546
Metal, ppm	
V	<0.2
Ni	<0.2
Fe	0.36
Cu	<0.2
CCR, wt%	0.15
Total sulfur, wt%	0.5
Basic nitrogen, ppm	307
Total nitrogen, ppm	900
Kinematic viscosity, cSt @ 50 ^{0}C	28.82
Lab RI	1.49
Paraffins ,wt%	15.7
Naphthenes ,wt%	36.3
Aromatics, wt%	47.9

6.2.4 Solution of Model Equations

Using the kinetic parameters from Table 6.5, the model equations were solved to calculate product yields and temperature at the reactor outlet. Equations

(6.1) and (6.15) representing material and energy balances were integrated using fourth order Runge-Kutta method and the remaining non-linear algebraic equations were solved using Successive Substitution method. The programming was done in C language and the problem was solved on an Intel Core i3 with 4.0 GB installed physical memory (RAM) CPU laptop. The code is available with the first author.

Table 6.2: Plant Operating / Design Data Used in Simulation

Description	**Test Run**
Feed rate (F_{feed}), kg/s	49.3
Feed preheat temp (T_{feed}), K	621.9
Reactor outlet temp (T), K	767.3
Cat/Oil	4.6
Cat circulation rate(F_{rgc}), kg/sec	225
Catalyst density($\rho_{c)}$, kg /m^3	817.0
Reactor pressure (P_{ris}), kPa	229.5
Regenerator pressure(P_{rgn}), kPa	256.9
Regenerator dense phase temp (T_{rgn}), K	938.0
Regenerator dilute phase temp(T_{dil}), K	958.2
Riser height (H_{ris}), m	37.0
Riser diameter (D_{ris}), m	0.7

Table 6.3: Thermodynamic and Other Parameters Used in Simulation

Description	**Test Run**
Catalyst heat capacity(C_{pc}), kj/kg.K	1.32[a]
Liquid feed heat capacity (C_{pfl}), kj/kg.K	3.43[a]
Vapor feed heat capacity (C_{pfv}), kj/kg.K	3.39[a]
Heat of vaporization of oil feed (ΔH_{evp}), kj/kg	349[a]
Molecular weight of kinetic lumps, kg/kmol	
Ph, Nh, Ah	339
Pl, Nl, Al	240
G	114
LPG	54
DG	30
C	12

[a]Data from Arbel et al., 1995.

Table 6.4: Comparison of Tuned ASPEN Model Outputs with Plant Test Run Data

Parameters	Test Run	ASPEN FCC Model
Inputs Parameters		
Feed Rate ,kg/sec	49.3	49.3
Reactor Outlet Temp (ROT), K	767	767
Regenerator Bed Temp, K	938	938
Regenerator Cyclone Temp, K	958	958
Regenerator Flue Gas Temp, K	958	958
Air Rate, kg/hr	81594	81594
Calculated Parameters		
Cat/Oil Ratio, wt/wt	4.6	4.4
Cat Circulation Rate, Tons/min	14.88	14.26
Coke on Regenerator Cat, wt %	-	0.009
Coke on Spent Cat, wt %	-	0.925
Delta Coke, wt %	0.93	0.92
Product Yields, wt %		
DG	1.54	1.54
LPG	11.40	11.79
Gasoline	51.47	50.87
LCO(221 -343) 0C	17.15	17.59
CLO (343+) 0C	14.45	14.15
Coke	3.99	4.06
Flue Gas Composition, mol %		
O2	0.2	0.2
CO	9.0	9.0
CO2	10.7	10.7
CO2/CO	1.19	1.19

6.2.5 Validation of 10-Lump Kinetic Model

Table 6.6 shows a comparison between plant test data and the model calculated values. Also included in the Table 6.6, are results from the ASPEN FCC

Simulator. A good match of the calculated values from the present model with both the plant data and ASPEN Simulator validates the ten lump kinetic constants as part of the present study. A more detailed validation of the present simulator with different plant data sets will be reported at a future date. We present a parametric sensitivity analysis of kinetic constants in the next section.

Table 6.5: Calculated Frequency Factors, Apparent Activation Energies and Heat of Reactions

Reaction Number (i)	Reaction	Frequency Factor (m^3 /kg_{cat}.sec)	Activation Energy(kJ/kmol)	Heat of Reactions (kJ/kmol)
1	Ph → Ah	0.54	10207	4079
2	Ph → Pl	9.19	11374	144003
3	Ph → G	0.45	21583	58250
4	Ph → DG	0.33	8743	10715
5	Ph → Coke	1.96	15725	544
6	Nh → Ah	1.92	8038	15122
7	Nh →Nl	0.85	15015	3647
8	Nh → G	0.80	16210	30121
9	Nh→ LPG	2.00	44570	274344
10	Ah → Al	0.90	19473	3281
11	Ah → G	0.40	8119	6605
12	Ah → LPG	0.35	14286	193822
13	Ah → Coke	0.59	43132	3856
14	Pl → G	3.73	19239	70246
15	Pl → DG	0.33	22925	1207
16	Pl → Coke	0.45	22332	4024
17	Nl → G	1.70	21532	4179
18	Nl → LPG	0.30	26919	86646
19	Nl → DG	0.10	13253	854
20	Al → G	1.57	25049	527
21	Al → LPG	0.56	28050	12016
22	Al → Coke	0.19	25549	2632
23	G →LPG	0.29	37330	50885
24	G → Coke	0.49	33808	169116
25	LPG → Coke	0.35	24103	10133

Table 6.6: Comparison of Model Calculated Values with Plant Data.

	Plant Data	Calculated Values		% Deviation	
		ASPEN Simulator	Present Model	ASPEN	Present Model
Riser Bottom Temp , K		788.460	788.02		
Riser Outlet Temp, K	767.3	767.440	767.95	-0.02	-0.08
Heavy Paraffins (Ph), wt %	-	0.000	0.00		
Heavy Naphthenes (Nh), wt %	-	0.035	0.05		
Heavy Aromatics (Ah), wt %	-	14.116	13.64		
Total Heavy Fraction(343^{+} ^{0}C), wt %	14.45	14.15	13.69	2.07	5.26
Light Paraffins (Pl), wt %	-	2.681	2.34		
Light Naphthenes (Nl), wt %	-	3.264	2.57		
Light Aromatics (Al), wt %	-	11.646	11.35		
Total Light Fraction (221- 343 ^{0}C), wt %	17.15	17.59	16.26	-2.59	5.17
Gasoline (C5 - 221 ^{0}C), wt %	51.47	50.87	52.10	1.18	-1.21
LPG, wt %	11.40	11.79	12.17	-3.44	-6.76
Dry Gas, wt %	1.54	1.54	1.65	-0.32	-7.36
Coke, wt %	3.99	4.06	4.12	-1.64	-3.21

6.3 SENSITIVITY OF RATE CONSTANTS IN TEN LUMP KINETIC MODEL

All the 25- frequency factors and 25- activation energies were varied in steps of ± 10 %, ± 20 % and ± 40 % from their mean position, one at a time to see how sensitive are the gas- oil conversion and yields of gasoline, LPG, dry gas and coke to these parametric variations. While a gradual variation of the output is expected, unusually high sensitivity may reflect adversely on the validity of the kinetic parameters. Alternatively, such analysis also helps in designing appropriate control systems. Given below is the outcome of the sensitivity study; Figure 6.2 shows the variation of gas oil conversion and product yields with respect to frequency factor ($k_{0,i}$). The results included in this figure are only for most sensitive reactions.

In order to avoid crowding, the reactions whose rates are not affected significantly by variation in the values of frequency factors are not plotted. As shown in Figures 6.2(a) and 6.2(b), the k_0 value for reaction (Ah $\rightarrow$ G) is most sensitive for conversion and

gasoline yield, for which maximum percentage variations are 10 and 18 percent respectively, when k_0 value is varied from its original value by – 40 %. The k_0 values for other reactions in these two figures are less sensitive, showing less than 5 % deviation in gas oil conversion and gasoline yield from original value with variation in k_0 up to ±40 %. Figure 6.2(c) shows the maximum variation on LPG yield is 32 percent with varying the k_0 (Ah → LPG) from its original value by – 40 %. Figure 6.2(d), shows that the coke yield is most sensitive to variation in frequency factors (k_0 values) of two reactions (Ph → Pl and Ph → Coke) resulting in a decrease of 11 % and increase of 9 %, when k_0 values for these two reactions changed from their original value by – 40 %.

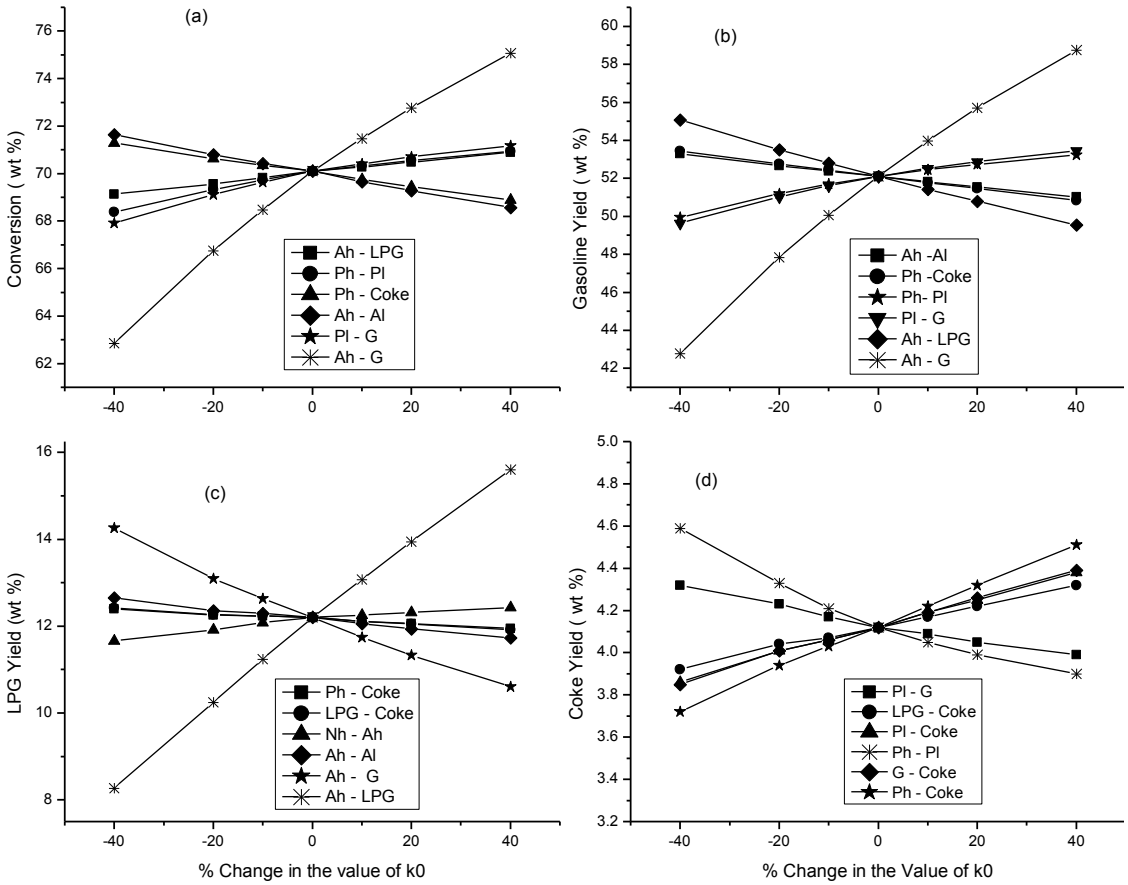

Figure 6.2: Sensitivity as a function of frequency factors (a) conversion (b) gasoline yield (c) LPG yield (d) coke yield

Figures 6.3(a) to 6.3(d) show variation of conversion and product yields with respect to variation in activation energies of different reactions. Again reactions showing significant sensitivity have been plotted. Figures 6.3(a) and 6.3(b), show maximum variation in conversion and gasoline yield of 11 and 19 percent respectively with – 40 % variation in E value (Ah ⇾ G) from its original value. Percent variation in LPG yield is very high (88 percent) with – 40 % decrease in value of E (Ah ⇾ LPG) from original value as shown in Figure 6.3(c). The coke yield increased by 89 percent with moving the E value (G ⇾ Coke) from its original value by – 40 %. Several other reaction rates also show significant sensitivity to coke yield when activation energy is varied (Ah ⇾ Coke, Ph⇾ Coke etc) as seen in Figure 6.3(d).

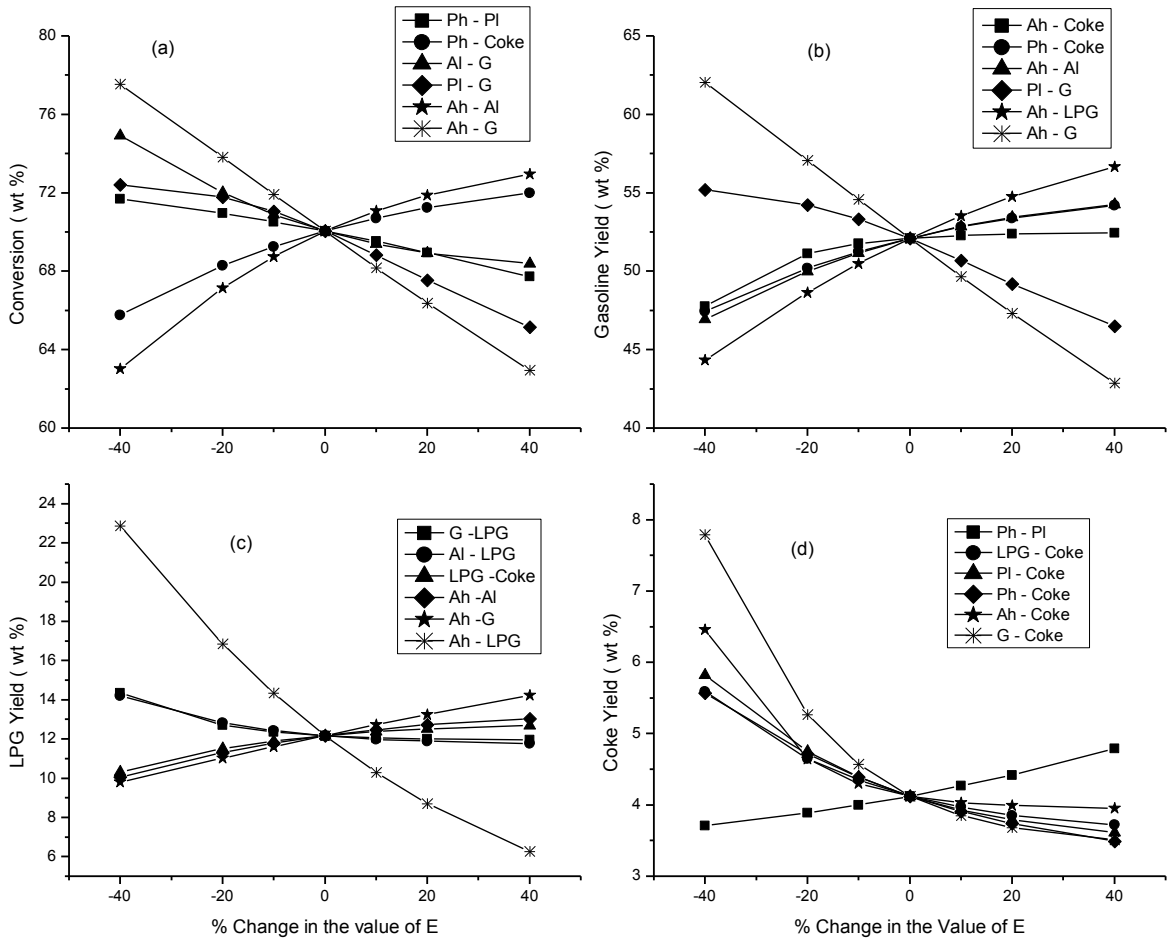

Figure 6.3: Sensitivity as a function of activation energies (a) conversion (b) gasoline yield (c) LPG yield (d) coke yield

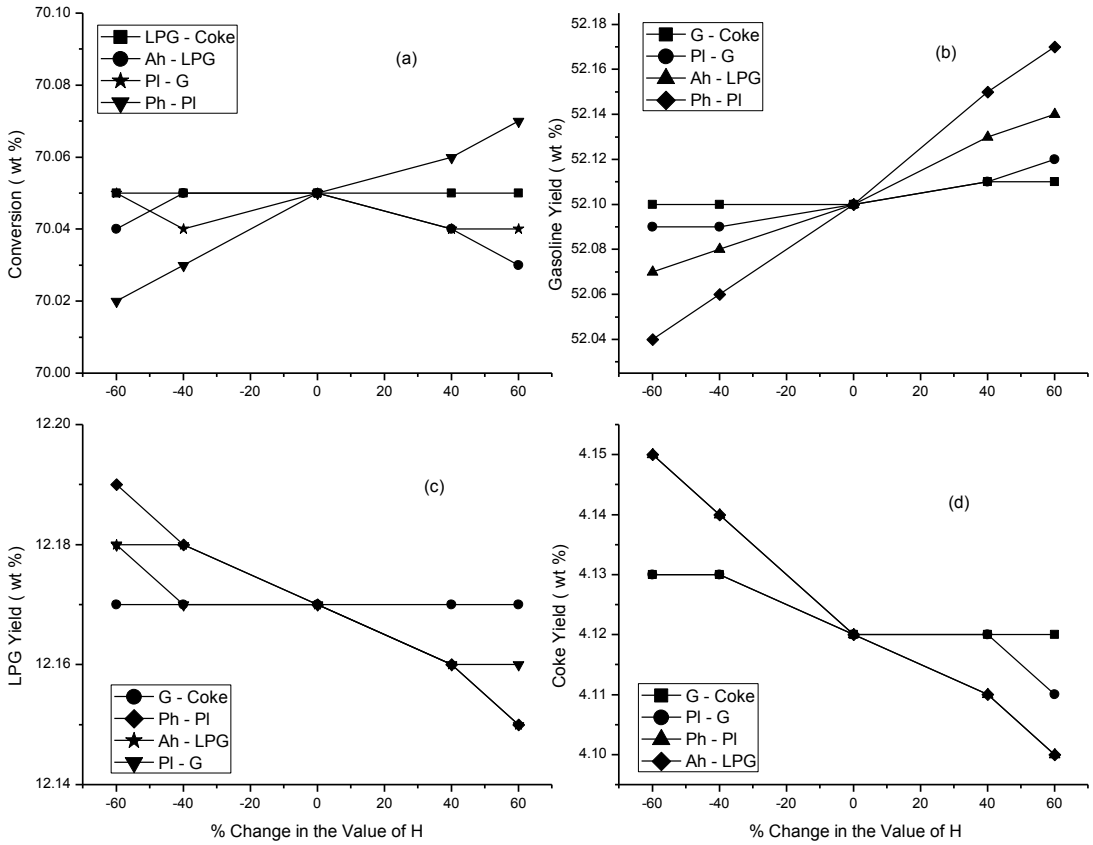

Figure 6.4: Sensitivity as a function of heat of reactions (a) conversion (b) gasoline yield (c) LPG yield (d) coke yield.

All the plots in Figures 6.2 and 6.3, confirm the non-linear behavior of the process because deviation in conversion and product yields are more with decreased values of k0 and E (towards -40 % from the original value) while these variations are less pronounced with increased values of k_0 and E (towards +40 % from the original value) .

The 25- heat of reactions (ΔH_i) were also varied in steps of ± 40 %, and ± 60 % from their mean position, one at a time, to study the sensitivity of ΔH_i on gas- oil conversion and yields of gasoline, LPG, dry gas and coke. Figure 6.4 shows no change or very small change in the gas- oil conversion and product yields with the variation in ΔH from original value by up to ± 60 %.

CHAPTER 7

VALIDATION OF FCC SIMULATOR USING 10- LUMP KINETIC MODEL AND ITS COMPARISON WITH THAT USING A 5-LUMP MODEL

A simulator for FCC unit has been developed by integrating FCC riser reactor and regenerator models. The kinetic model for the riser reactor involves lumped species based on feed characterization in terms of PNA (paraffins, naphthenes and aromatics) in both light and heavy fuel oil fractions and products (Dasila et al., 2012a). The detailed composition required as input to the 10 lump kinetic model was obtained from a validated ANN model, requiring only field laboratory measured feed properties as input (Dasila et al., 2012b). The kinetic parameters were estimated from experimental data supplemented with additional data generated from ASPEN FCC simulator. The product yields were obtained by integrating the model equations using the estimated values of the rate constants (see Table 6.5). This simulator includes the regenerator model from literature (Krishna and Parkin, 1985 and Arbel et al., 1995

7.1 Validation of FCC Model with Plant Data

Several sets of test run data and one set of normal operating data were obtained from an operating FCC plant in a refinery for validation of the developed simulator. The performance of the model has been evaluated by comparing the model predicted values of the conversion and yields with the plant data at the riser outlet. The feed for all the cases were the mixture of three different heavy gas oils in different proportions.). The plant refinery data on detail feed composition and operating conditions of different heavy gas oils were used for the simulation (Table 7.1)

Table 7.1: Data Used in Simulation of Ten Lump Model

Description	Case I	Case II	Case III	Case IV
Feed composition (wt%) from ANN model				
Paraffins	17.7	11.8	12.7	17.2
Naphthenes	23.2	36.6	34.0	21.4
Aromatics	59.0	51.6	53.3	61.5
Operating parameters				
Feed rate, kg/s	49.31	50.16	46.72	47.22
Feed preheat temp, K	621.89	621.00	616.00	614.34
Reactor outlet temp, K	767.30	767.43	767.32	767.17
Cat circulation rate, kg/sec	225.00	250.81	237.78	211.78
Catalyst density, kg/m3	817.00	831.00	850.00	800.00
Regenerator dense phase temp, K	938.00	935.00	935.00	945.01
Reactor pressure, KPa	327.54	220.65	219.67	221.90

7.1.1 Case I

The model predicted yields were compared with the first set of refinery plant data and the results were found to be in good agreement as shown in Table 7.2.

Table 7.2: Comparison of Model Calculated Values with Plant Data (Case I)

	Case I	Calculated Values from Simulation		% Deviation	
		ASPEN FCC	Present Model	ASPEN	Present Model
Riser Outlet Temp, K	767.3	767.440	767.95	-0.02	-0.08
Heavy Paraffins (Ph)		0.000	0.00		
Heavy Naphthenes (Nh)		0.035	0.05		
Heavy Aromatics (Ah)		14.116	13.64		
Total Heavy Fraction(343+ ^{0}C)	14.45	14.15	13.69	2.07	5.26
Light Paraffins (Pl)		2.681	2.34		
Light Naphthenes (Nl)		3.264	2.57		
Light Aromatics (Al)		11.646	11.35		
Total Light Fraction (221-343 ^{0}C)	17.15	17.59	16.26	-2.59	5.17
Gasoline (C5-221 ^{0}C)	51.47	50.87	52.10	1.18	-1.21
LPG	11.40	11.79	12.17	-3.44	-6.76
Dry Gas	1.54	1.54	1.65	-0.32	-7.36
Coke	3.99	4.06	4.12	-1.64	-3.21

The percent deviation between the plant and model were also calculated. The heavy and light fractions deviated about 5 percent where as the other four products namely, Gasoline, LPG, Dry Gas and Coke showed a maximum deviation of 7 percent. The results from ASPEN FCC Simulator have also been included in the same Table. Similar deviations are seen except with smaller magnitude.

7.1.2 Case II

The model was again validated with second test run data from the same FCC unit but with different feed composition. Table 7.3 shows comparison with plant as well ASPEN calculated values. The comparison shows a good match between present model and plant test run with deviation less than 4.5 % except for the LPG yield (10.9 %). The performance of ASPEN Simulator shows more deviation with plant data for heavy fraction (16.7%) than present model.

Table 7.3: Comparison of Model Calculated Values with Plant Data (Case II)

	Case II	Calculated Values from Simulation		% Deviation	
		ASPEN FCC	Present Model	ASPEN	Present Model
Riser Outlet Temp, K	767.43	767.45	770.85	0.00	-0.45
Heavy Paraffins (Ph)		0.00	0.00		
Heavy Naphthenes (Nh)		0.00	0.03		
Heavy Aromatics (Ah)		10.77	12.75		
Total Heavy Fraction(343^{+} ^{0}C)	12.93	10.77	12.78	16.75	1.19
Light Paraffins (Pl)		1.28	1.25		
Light Naphthenes (Nl)		1.45	2.23		
Light Aromatics (Al)		13.70	11.74		
Total Light Fraction (221-343 ^{0}C)	15.62	16.43	15.22	-5.21	2.55
Gasoline (C5-221 ^{0}C)	54.31	54.80	53.31	-0.89	1.84
LPG	12.39	12.61	13.74	-1.76	-10.89
Dry Gas	1.18	1.60	1.22	-35.13	-3.30
Coke	3.56	3.80	3.72	-6.62	-4.40

7.1.3 Case III

A new set of daily operating data was used to simulate the model. The results on yields and reactor outlet temperature from plant and model calculated are shown in Table 7.4. This case also shows a good match between present model and plant operating data for all the values except dry gas. Dry gas content being small (~1.5 %), its measured values is likely to be uncertain to a larger extent because of measurement errors. It may be noted that for this case, ASPEN model performance is quite inferior as compared to the present model.

Table 7.4: Comparison of Model Calculated Values with Plant Data (Case III)

	Case III	Calculated Values from Simulation		% Deviation	
		ASPEN FCC	Present Model	ASPEN	Present Model
Riser Outlet Temp, K	767.32	767.59	770.73	-0.04	-0.44
Heavy Paraffins (Ph)		0.00	0.00		
Heavy Naphthenes (Nh)		0.00	0.03		
Heavy Aromatics (Ah)		7.77	13.00		
Total Heavy Fraction($343^{+}{}^{0}$C)	12.08	7.77	13.03	35.65	-7.86
Light Paraffins (Pl)		0.42	1.39		
Light Naphthenes (Nl)		0.56	2.10		
Light Aromatics (Al)		15.08	11.70		
Total Light Fraction (221-343 ^{0}C)	13.90	16.06	15.19	-15.52	-9.27
Gasoline (C5-221 ^{0}C)	55.89	56.68	53.12	-1.42	4.95
LPG	12.88	14.23	13.61	-10.43	-5.64
Dry Gas	1.55	1.95	1.25	-25.82	19.52
Coke	3.69	3.31	3.79	10.45	-2.61

7.1.4 Case IV

The model was finally simulated with yet another set of plant data to facilitate wider comparison between model calculated values and plant data and the results are shown in Table 7.5. The matches were found to be in the range of acceptable limit. From above study with four different cases of plant data obtained with different feed

compositions it can be seen that the present model represents the FCC riser reactor reasonably well. The predictions from present model are as good as those of ASPEN FCC simulator and at times, even better.

Table 7.5: Comparison of Model Calculated Values with Plant Data (Case IV)

	Case IV	Calculated Values from Simulation		% Deviation	
		ASPEN FCC	Present Model	ASPEN	Present Model
Riser Outlet Temp, K	767.16	767.4	771.67	-0.03	-0.59
Heavy Paraffins (Ph)		0	0		
Heavy Naphthenes (Nh)		0	0.09		
Heavy Aromatics (Ah)		15.1	15.44		
Total Heavy Fraction($343^{+}\ ^{0}C$)	14.47	15.10	15.53	-4.35	-7.32
Light Paraffins (Pl)		1.05	2.42		
Light Naphthenes (Nl)		1.41	1.94		
Light Aromatics (Al)		17.29	13.29		
Total Light Fraction (221-343 ^{0}C)	20.23	19.74	17.65	2.40	12.73
Gasoline (C5-221 ^{0}C)	48.64	48.85	50.79	-0.42	-4.41
LPG	11.13	11.33	10.82	-1.79	2.79
Dry Gas	1.40	1.47	1.44	-4.80	-2.66
Coke	4.13	3.52	3.77	14.71	8.66

7.2 PARAMETRIC SENSITIVITY STUDY FOR TEN LUMP MODEL WITH RESPECT TO OPERATING CONDITIONS

Earlier sensitivity studies were carried with respect to operating conditions for the five lump kinetic model as discussed in Chapter 3 (Dasila et al., 2012c). The validated ten lump steady state FCC simulator was also used for parametric sensitivity studies with respect to the operating variables. The same independent variables, feed flow rate (F_{feed}) and feed preheat temperature (T_{feed}) were varied for the ten lump FCC model. The effects of these operating variables on steady state FCC unit performance are calculated at constant regenerator temperature and constant reactor outlet temperature. The air rate and catalyst circulation rate (CCR) were varied to keep the regenerator temperature and reactor outlet temperature (ROT) constant respectively.

7.2.1 Effect of Feed Flow Rate on FCC Performance at Constant Feed Preheat Temperature (T_{feed})

(a) At Constant CCR and Constant Regenerator Temperature (T_{rgn})

As feed flow rate is increased keeping regenerator temperature and catalyst flow rate constant, the cat/oil ratio decreases which leads to decreased cracking activity and lower conversion and product yields (Figure 7.1).

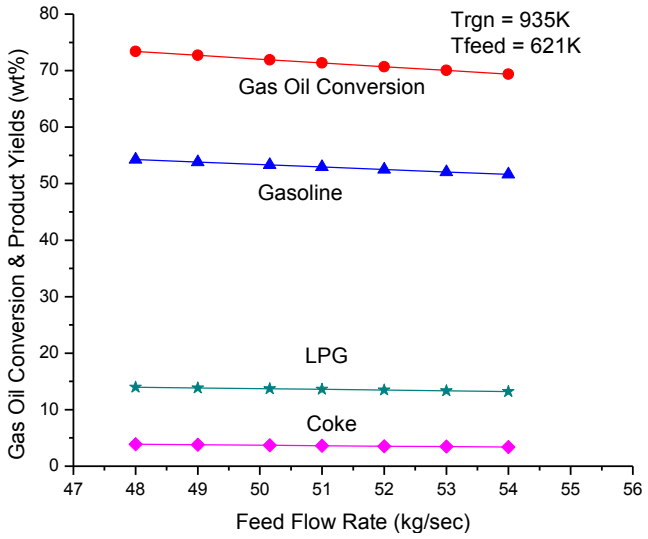

Figure 7.1: Effect of feed flow rate on the conversion and product yields at fixed feed preheat temperature (621K) and fixed regenerator temperature (935K)

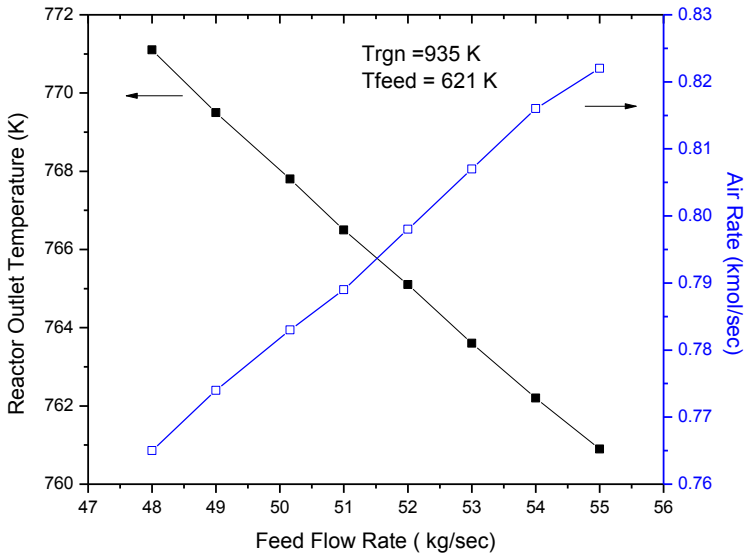

Figure 7.2: Effect of feed flow rate on the reactor outlet temperature (ROT) at fixed feed preheat temperature (621K) and fixed regenerator temperature (935K)

Reactor outlet temperature also decreases with increase in feed rate due to more heat absorption. However, air flow rate to the regenerator must increase with increase in feed rate to burn the coke and maintain regenerator temperature constant (Figure 7.2). These trends in Figures 7.1 and 7.2 are similar as in Figures 3.6 and 3.7, which were obtained with 5-lump model.

(b) At Constant Air Flow Rate and Constant Reactor Outlet Temperature (ROT)

Figure 7.3 shows the gas oil conversion and product yields, all of which decrease, with increase in feed rate at constant ROT and constant air flow rate. The catalyst circulation rate must increase to keep ROT constant when feed rate is increased. However, regenerator temperature decreases because of extra amount of carbon coming in the regenerator due to more catalyst circulation rate leads the less residence time to burn coke in the regenerator (shown in Figure 7.4). These plots also show similar trends as in Figures 3.8 and 3.9.

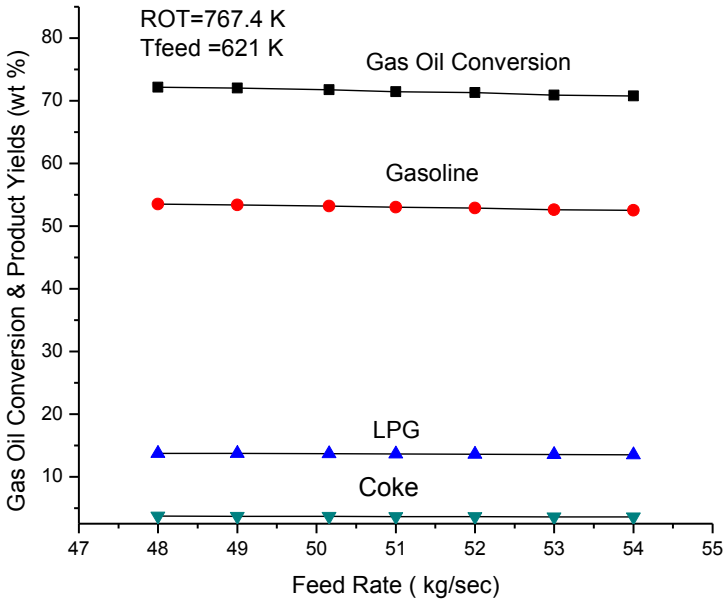

Figure 7.3: Effect of feed flow rate on the conversion and product yields at fixed reactor outlet temperature (767.4 K) and fixed feed preheat temperature (621 K).

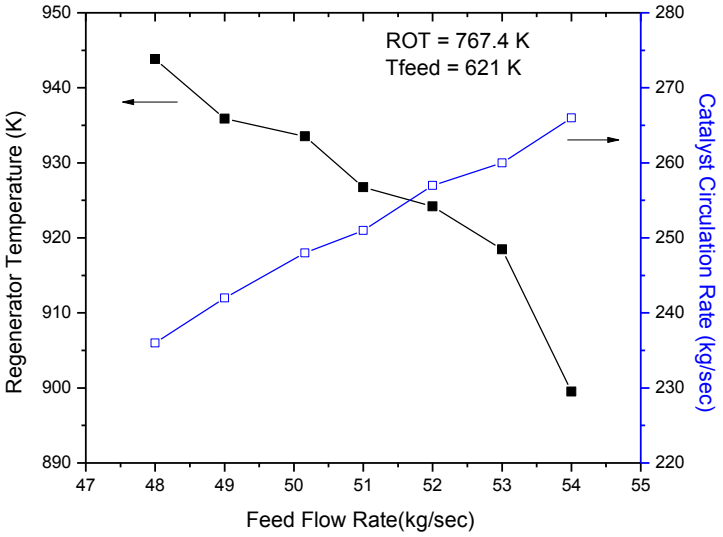

Figure 7.4: Effect of feed flow rate on the regenerator temperature (Trgn) at fixed feed preheat temperature (621 K) and fixed reactor outlet temperature (767.4K).

7.2.2 Effect of Feed Preheat Temperature on FCC Performance at Constant Feed Flow Rate (F_{feed})

(a) **At Constant CCR and Constant Regenerator Temperature (T_{rgn})**

The LPG and coke yields were found to marginally increase with increase in T_{feed} while the gasoline yield and gas oil conversion slightly decreased. However as seen in Figure 7.5, the changes are very small.

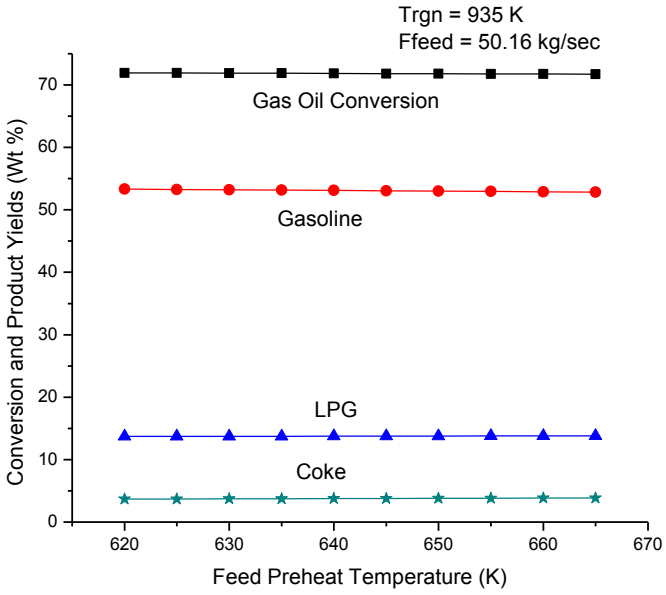

Figure 7.5: Effect of feed preheat temperature on gas oil conversion and product yields at fixed Ffeed (50.16 kg/sec) and fixed regenerator temperature (935K)

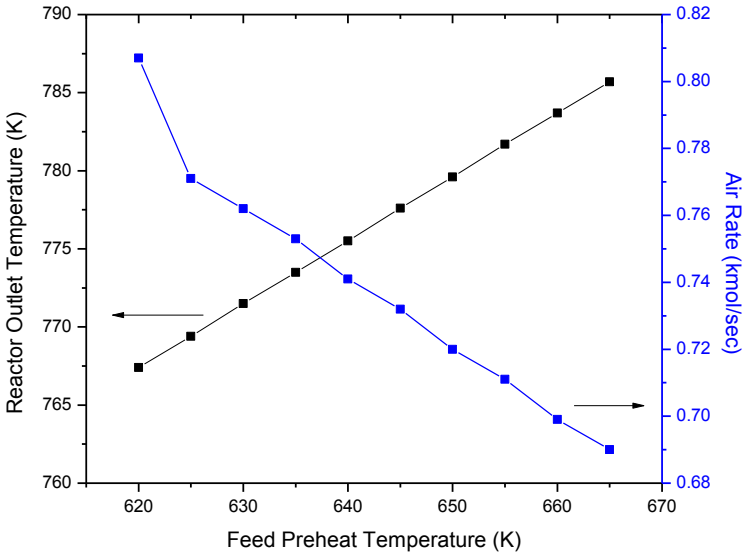

Figure 7.6: Effect of feed preheat temperature on riser outlet temperature (ROT) at fixed F_{feed} (50.16 kg/sec) and fixed regenerator temperature (935K)

The decrease in gasoline yield and gas oil conversion may be small. This decrease in gasoline yield and gas oil conversion may be due to more amount of coke on regenerated catalyst. These results are at variance from those obtained using 5-lump model (see Figure 3.2). The reasons are not obvious but one may expect that a more detailed kinetic model would result in more accurate trends. The reactor outlet temperature (ROT) increases linearly with T_{feed} but air flow rate to the regenerator decreases to maintain the Trgn constant as shown in Figure 7.6.

(b) At Constant Air Flow Rate (Fair) and Constant Reactor Outlet Temperature (ROT)

As feed preheat temperature is increased, catalyst circulation rate (CCR) must decrease to hold ROT constant. At constant feed rate, decreasing CCR, (cat/oil ratio) leads to decrease in conversion and product yields as shown in Figure 7.7. These Figures 7.7 and 7.8 show similar trends as for the five lump model in Figures 3.4 and 3.5 respectively. The slopes in Figure 7.7 are gentler and perhaps more accurate than

those in Figure 3.4, It is however, not possible to verify these results experimentally in an operating plant.

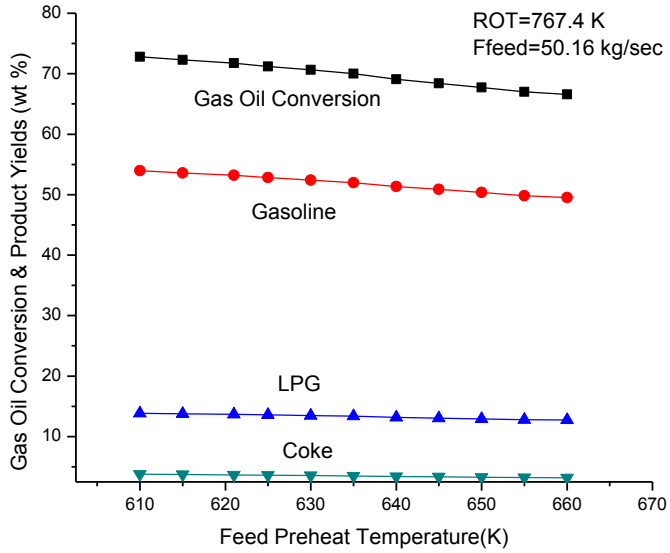

Figure 7.7: Effect of feed preheat temperature on gas oil conversion and product yields at fixed F_{feed} (50.16 kg/sec) and fix ROT (767.4 K)

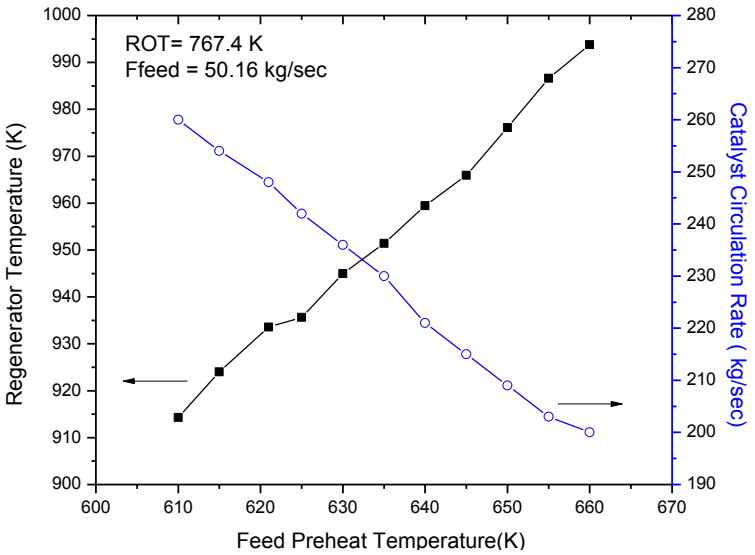

Figure 7.8: Effect of feed preheat temperature on regenerator temperature (Trgn) at fixed feed flow rate (50.16 kg/sec) and fix ROT (767.4 K)

7.3 KINETIC PARAMETERS REESTIMATION FOR FIVE LUMP MODEL

The data that were regressed to obtained kinetic parameters for the 10 - lump model were reused to calculate kinetic parameters for the 5- lump model to facilitate a realistic comparison between the two models. The 5- lump kinetic scheme consists of

9 reactions, shown in Figure 3.1 has been used for the estimation of kinetic parameters. An evolutionary optimization technique, Genetic Algorithm (GA) was used to minimize the objective function given in Equation 7.3. The algorithm available in MATLAB Optimization Toolbox was used in the present study.

$$SSE = Min\left[\sum_{n=1}^{11}\sum_{i=1}^{5}\left(Y_{iexp} - Y_{ical}\right)_n^{\ 2} + \sum_{n=1}^{11}\left(T_{exp} - T_{cal}\right)_n^{\ 2}\right] \qquad (7.3)$$

Y_{iexp} is the yield of i^{th} lump as obtained from ASPEN and Y_{ical} is the yield obtained from the 5 lump kinetic model by integrating the model equations 3.1 to 3.12. The double summation on right hand side of Equation 7.3 is over all 5 lumps and 11 sets of data. The additional term in the objective function is to ensure a match in reactor outlet temperature also. The material balances in Equation (3.1) and enthalpy balance in Equation 3.5 form a group of ordinary differential equations which need to be integrated simultaneously along the entire length of the reactor, the remaining model equations for riser reactor are algebraic in nature. There are a total of 27 reaction parameters (including 9 frequency factors, 9 activation energies and 9 heat of reactions) which need to be evaluated before the model equations can be solved. The calculated data on activation energies, frequency factors and heat of reaction are shown in Table 7.6. Using these kinetic parameters, the 5-lump model equations were integrated for the same cases shows in Table 7.1. Model results provided the riser outlet temperature (ROT) and the weight percent concentration of each lump in the product stream. The performance of the model has been evaluated by comparing the model predicted values of conversions and product yields with the plant data.

Table 7.6: Calculated Kinetic Parameters for 5-Lump Model

Reaction Number (i)	Reactions	Frequency Factor ($m3/kg_{cat}.sec$)	Activation Energy (kJ/kmol)	Heat of Reactions (kJ/kmol)
1	Gas Oil → Gasoline	38842.4	49928	61176
2	Gas oil → LPG	3984.7	45587	196892
3	Gas Oil → DG	345.5	43575	252494
4	Gas Oil → Coke	81.4	28496	300409
5	Gasoline →LPG	65.6	62699	31598
6	Gasoline → DG	0.1	38033	39681
7	Gasoline → Coke	1.8	44810	1182
8	LPG→ DG	2.0	47446	2670
9	LPG → Coke	0.3	32762	1542

7.3.1 COMPARISON OF TEN LUMP FCC KINETIC MODEL WITH FIVE LUMP KINETIC MODEL AND PLANT DATA

Tables 7.7 to 7.9 show comparison of model calculated values using both 10 - lump and 5-lump kinetics and plant measured experimental values. While maximum deviation in unconverted gas oil was only 8.6 % for 10- lump model, it was as high as 15.7 % for the 5 - lump model (Table 7.9)

Table 7.7: Comparison of Ten Lump and Five Lump Model Calculated Values with Plant Data (Case I)

	Plant Data	Model Calculated Value		% Deviation	
	Case I	Ten Lump	Five Lump	Ten Lump	Five Lump
Riser Outlet Temp, K	767.3	767.95	767.75	-0.08	-0.06
Heavy Paraffins (Ph)		0			
Heavy Naphthenes (Nh)		0.05			
Heavy Aromatics (Ah)		13.64			
Total Heavy Fraction($343^{+}\ ^{0}C$)	14.45	13.69		5.26	
Light Paraffins (Pl)		2.34			
Light Naphthenes (Nl)		2.57			
Light Aromatics (Al)		11.35			
Total Light Fraction (221-343 ^{0}C)	17.15	16.26		5.17	
Total Unconverted Gas Oil ($221^{+}\ ^{0}C$)	31.60	29.95	30.84	5.21	2.45
Gasoline (C5-221 ^{0}C)	51.47	52.10	51.92	-1.21	-0.86
LPG	11.40	12.17	11.94	-6.76	-4.52
Dry Gas	1.54	1.65	1.47	-7.36	4.55
Coke	3.99	4.12	3.82	-3.21	4.50

Table 7.8: Comparison of Ten Lump and Five Lump Model Calculated Values with Plant Data (Case II)

	Case II	Model Calculated Value		% Deviation	
		Ten Lump	Five Lump	Ten Lump	Five Lump
Riser Outlet Temp, K	767.43	770.85	769.45	-0.45	-0.26
Heavy Paraffins (Ph)		0			
Heavy Naphthenes (Nh)		0.03			
Heavy Aromatics (Ah)		12.75			
Total Heavy Fraction(343+ ^{0}C)	12.93	12.78		1.19	
Light Paraffins (Pl)		1.25			
Light Naphthenes (Nl)		2.23			
Light Aromatics (Al)		11.74			
Total Light Fraction (221-343^{0}C)	15.62	15.22		2.55	
Total Unconverted Gas Oil (221+ ^{0}C)	28.55	28.00	31.51	1.94	-9.38
Gasoline (C5-221 ^{0}C)	54.31	53.31	51.45	1.84	5.56
LPG	12.39	13.74	11.83	-10.89	4.74
Dry Gas	1.18	1.22	1.46	-3.30	-19.11
Coke	3.56	3.72	3.76	-4.40	-5.23

Table 7.9: Comparison of Ten Lump and Five Lump Model Calculated Values with Plant Data (Case III)

	Plant Data	Model Calculated Value		% Deviation	
	Case III	Ten Lump	Five Lump	Ten Lump	Five Lump
Riser Outlet Temp, K	767.32	770.73	769.35	-0.44	-0.26
Heavy Paraffins (Ph)		0			
Heavy Naphthenes (Nh)		0.03			
Heavy Aromatics (Ah)		13			
Total Heavy Fraction(343+ ^{0}C)	12.08	13.03		-7.86	
Light Paraffins (Pl)		1.39			
Light Naphthenes (Nl)		2.1			
Light Aromatics (Al)		11.70			
Total Light Fraction (221-343 ^{0}C)	13.90	15.19		-9.27	
Total Unconverted Gas Oil (221$^+$ ^{0}C)	25.98	28.22	30.83	-8.61	-15.72
Gasoline (C5-221 ^{0}C)	55.89	53.12	51.85	4.95	7.79
LPG	12.88	13.61	12.00	-5.64	7.36
Dry Gas	1.55	1.25	1.48	19.52	4.94
Coke	3.69	3.79	3.84	-2.61	-3.81

Deviation in gasoline yield was higher at 7.8 % for 5 -lump model as compared to 5 % for the 10-lump model (Table 7.9). Although the 10 - lump model predictions were generally better than those using 5-lump model but not significantly differently. This is because the same data were regressed to obtain the kinetic parameters in both cases. However, if we use kinetic parameter values for five lump model from literature (Table 3.4) the deviation are glaring as seen in Table 7.10 and 7.11.

Table 7.10: Five Lump Model Calculated Values with Literature Kinetic Parameters (Case I)

	Case I	Five Lump Model	% Deviation
Riser Outlet Temp, ^{0} K	767.3	776.97	-1.26
Heavy Paraffins (Ph)			
Heavy Naphthenes (Nh)			
Heavy Aromatics (Ah)			
Total Heavy Fraction(343+ ^{0}C)	14.45		
Light Paraffins (Pl)			
Light Naphthenes (Nl)			
Light Aromatics (Al)			
Total Light Fraction (221-343 ^{0}C)	17.15		
Total Unconverted Gas Oil (221$^+$ ^{0}C)	31.60	56.63	-79.23
Gasoline (C5-221 ^{0}C)	51.47	27.56	46.46
LPG	11.40	9.92	12.98
Dry Gas	1.54	2.77	-80.23
Coke	3.99	3.12	21.84

Table 7.11: Five Lump Model Calculated Values with Literature Kinetic Parameters (Case II)

	Case II	Five Lump Model	% Deviation
Riser Outlet Temp, K	767.43	778.42	-1.43
Heavy Paraffins (Ph)			
Heavy Naphthenes (Nh)			
Heavy Aromatics (Ah)			
Total Heavy Fraction(343+ ^{0}C)	12.93		
Light Paraffins (Pl)			
Light Naphthenes (Nl)			
Light Aromatics (Al)			
Total Light Fraction (221-343 ^{0}C)	15.62		
Total Unconverted Gas Oil (221$^+$ ^{0}C)	28.55	57.26	-100.54
Gasoline (C5-221 ^{0}C)	54.31	27.19	49.94
LPG	12.39	9.78	21.07
Dry Gas	1.18	2.72	-130.30
Coke	3.56	3.06	14.12

CHAPTER 8

CONCLUSIONS AND RECOMMENDATIONS

8.1 CONCLUSIONS

The aim of this research project was to develop a mathematical model that can simulate the behaviour of an FCC unit with significant accuracy yet use only feed properties measured routinely in field laboratory for input. The developed model incorporates detailed ten lump kinetics for the riser reactor where feed is described in terms of hydrocarbon types, further subdivided as heavy and light fractions. The riser reactor model was integrated with a robust catalyst regenerator model, also developed in house, to complete the FCC simulator development. An ANN based feed module was able to predict the PNA composition of the heavy fraction ($343^{+}\ ^{0}C$) satisfactorily with use of only specific gravity and distillation temperatures of the feed. The simulator was subsequently used in studies on parametric sensitivity.

A novel ten lump kinetic description was introduced in the present work to model heavy gas oil cracking in an FCC unit. Of a total of 33 feasible reactions, 25 were found to suffice for the calculation of gas oil conversion and the product yields. Use of genetic algorithm for evaluation of kinetic parameters ensured that a global solution was found as compared to gradient methods which usually converge to a local solution. A simulation algorithm using the calculated rate constants predicted gas oil conversion as well as product yields which were in good agreement with plant data as well as ASPEN FCC Simulator predictions validating the results.

A parametric sensitivity analysis of estimated kinetic parameters was done by varying all the 25- frequency factors and 25- activation energies in steps of ± 10 %, ± 20 % and ± 40 % from their mean position, one at a time, to see how sensitive are the gas- oil conversion and yields of gasoline, LPG, dry gas and coke to these parametric

variations. All changes were found to be gradual as expected. The 25- heat of reactions (ΔH_i) were also varied in steps of ± 40 %, and ± 60 % from their mean position, one at a time, which showed very small change in gas- oil conversion and product yields.

In order to enhance application of the developed model in refineries, the present work also aimed to predict detailed composition of heavy gas oil feeds to FCCU in terms of hydrocarbon types such as weight percent of paraffins, naphthenes and aromatics from routinely measured feed properties such as density, distillation, CCR, total sulfur, total nitrogen. Of the various ANN architectures developed and tested, the one with 8 input parameters namely density and distillation temperatures using three separate models with single output neurons for paraffins, naphthenes and aromatics followed by normalization of predicted compositions was found to be in close agreement with experimental results.

The developed ten lump kinetic model was integrated with a rigorous regenerator model, also developed during the present work, for the simulation of the entire FCC unit. Several sets of test run data and one set of normal operating data were obtained from an operating FCC plant in a refinery for validation of the developed simulator. Because of detailed characterization of the feed in terms of hydrocarbon types (paraffin, naphthenes and aromatics), the simulator was found to be independent of the source of feed, as long as it was in the range of heavy gas oil.

To establish better prediction accuracy of the developed 10 lump kinetic model, a reference riser-reactor simulator was rebuilt based on five lump kinetic scheme available in literature. The data that were used to obtain kinetic parameters for the 10 - lump model were reused to calculate kinetic parameters for the 5- lump model to facilitate comparison between the two models. The 5- lump model predicted

values deviated significantly as compared to the 10- lump model predictions which were found to be in good agreement with the plant data for all the cases investigated.

Finally a parametric sensitivity study was undertaken in respect of operating conditions such as effect of feed preheat temperature, feed flow rate and air flow rate (independent variables) on the industrial FCC performance. Catalyst circulation rate was found to have stronger influence on gas oil conversion as compared to feed preheat temperature for a fixed reactor outlet temperature. On the other hand feed flow rate affected the HGO conversion more than catalyst circulation rate. Increase in air flow rate with other important parameters remaining constant, led to increased conversion. From above discussion of sensitivity analysis it appears that decreasing T_{feed} and increasing catalyst circulation rate and air flow rate should lead to higher conversion and product yields. Few case studies have been performed to illustrate such scenarios. The sensitivity analysis is useful for the refiners to understand the effects of individual parameters on the FCC performance and to perform optimization study for better productivity of the unit.

8.2 RECOMMENDATIONS FOR FUTURE WORK

The following aspects of the work encountered during the present study, but not accounted for, should be incorporated in future developments.

1. The present model assumes that partially vaporized feed enters at the bottom of the reactor gets completely vaporized instantaneously, resulting in a two phase flow throughout the reactor height. In real plants, this cannot happen and to a certain height, three phase flow must exist. The hydrodynamics, along with heat and mass transfer can have profound influence on the performance of the FCC unit even if such conditions prevail over relatively short length of the reactor. This

region needs to be investigated in detail so that the gross assumption of blanket two phase model can be dispersed with.

2. The assumption of uniform flow of vapors of reaction mass and catalyst particles is questionable. These exists a velocity profile in vapor as well as catalyst flow across the reactor cross- section, the flow being faster in the axial region as compared to that near the wall. Catalyst particles being heavier are likely to move slower than the vapors. Small particles can agglomerate to form loose clusters offering resistance to flow of reactants to the catalyst surface. Some larger agglomerates near the wall may even move in reverse direction. These aspects need to be investigated.
3. While the present kinetic model is valid for feeds of different compositions owing to a more detailed description of the feed, this will not hold good for units using different catalysts because of the pseudo – homogeneous kinetic model used in this study. Development of a heterogeneous kinetic model is therefore, necessary which takes into account, the catalyst characterization also.
4. In the present investigation only feeds in heavy gas oil range were considered , which includes – HGO, HVGO, HCO,CLO etc and their blends. However , in industry the operators often add some amounts of resid to the FCC feed. The present model can not account for this. If the resid is used, the feed entering the reactor will be vaporized to a lesser extent and larger reactor length will be used up by three phase flow. In the liquid phase, thermal cracking of resid will be significant and needs to be accounted for.

References

1. Abul-Hamayel, M. A., Kinetic Modeling of High-Severity Fluidized Catalytic Cracking, *Fuel*, **82**, 1113–1118 (2003).
2. Ali, H., Rohani, S. and Corriou, P., Modeling and Control of a Riser Type Fluid Catalytic Cracking (FCC) Unit, *Chem. Eng. Res. Des*., **75**, 401- 412 (1997).
3. Alsabei, R., Nagy, Z.K. and V. Nassehi., Process Simulators Based Control Design for a Fluid Catalytic Cracking Unit. *18th International Congress of Chemical and Process Engineering(*CHISA), Prague, Czech Republic (2008).
4. Altissimi, R., Brambilla, A., Deidda, A. and Semino, D., Optimal Operation of a Separation Plant using Artificial Neural Networks, *Comput. Chem. Eng*., **22**, 939-942(1998).
5. Ancheyta, J. J., Lopez, I.F. and Aguilar, R.E., 5-Lump Kinetic Model for Gas Oil Catalytic Cracking, *Appl. Catal. A*., **177**, 227-235 (1999).
6. Ancheyta, J. J., Lopez, I.F., Aguilar, R.E. and Moreno, J.C.M., A Strategy for Kinetic Parameter Estimation in the Fluid Catalytic Cracking Process, *Ind. Eng. Chem. Res*., **36**, 5170-5174(1997).
7. Ancheyta, J. J., Lopez, l. F. and Aguilar, R. E., Correlations for Predicting the effect of Feedstock Properties on Catalytic Cracking Kinetic Parameters, *Incl. Eng. Chem. Res.*, **37**, 4637- 4640 (1998).
8. Ancheyta, J.J., "Modeling and Simulation of Catalytic Reactors for Petroleum Refining", First edition, John Wiley and Sons, Inc., New Jersey, USA (2011).
9. Annual Book of ASTM Standards. "American Society for Testing and Materials", West Conshohocken, PA (1998).
10. Arandes, J.M., Alkoiti, M.J., Bilbao, J. and de Lasa, H.L., Modeling FCC Units under Steady and Unsteady State Conditions, *Can. J. Chem. Eng*., **78**, 111-123(2000).
11. Arbel, A., Huang, Z., Rinard, I.H., Shinnar, R. and Sapre, A.N., Dynamics and Control of Fluidized Catalytic Crackers. 1. Modeling of the Current Generation FCC's, *Ind. Eng. Chem. Res*., **34**, 1228-1243(1995).
12. Aspen FCC 2006.5. User's Guide. Aspen Technology Inc. (Version 7.2), Burlington, MA. USA. URL: http://www.aspentech.com.

13. ASTM D-1319. "Test Method for Hydrocarbon Types in Liquid Petroleum Products by Fluorescent Indicator Adsorption". American Society for Testing and Materials, West Conshohocken, PA (1998).
14. Avidan, A. A. O., Development and Scope of FCC Catalysis. In Fluid Catalytic Cracking: Science and Technology. Studies in Surface Science and Catalysis; Magee, J. S., Mitchell, M. M., Jr., Eds., Elsevier: Amsterdam, Netherlands, **76**, 1-39 (1993).
15. Avidan, A. A., Edwards, M. and Owen, H., Innovative Improvements Highlight FCC's Past and Future. *Oil Gas J.*, **88**, 33 (1990).
16. Avidan, A. A., Shinnar, R., Development of Catalytic Cracking Technology. A Lesson in Chemical Reactor Design, *Ind. Eng. Chem. Res*., **29**, 931-942(1990).
17. Bai, D., Zhu, J-X., Jin, Y. and Yu, Z., Simulation of FCC Catalyst Regeneration in a Riser Regenerator, *Chem. Eng. J.*, **71** , 97-109 (1998).
18. Balasubramanian, P., Bettina, S. J., Pushpavanam, S. and Balaraman. K. S., Kinetic Parameter Estimation in Hydrocracking using a Combination of Genetic Algorithm and Sequential Quadratic Programming, *Ind. Eng. Chem. Res*, **42**, 4723-4731(2003).
19. Bansal, V., Krishna, G. J., Chopra, A. and Sarpal, A.S., Detailed Hydrocarbon Characterization of RFCC Feed Stocks by NMR Spectroscopic Techniques, *Energy Fuels*., **21**, 1024-1029 (2007).
20. Bansal,V., Vatsala, S., Kapur, G.S., Basu, B. and Sarpal, A.S., Hydrocarbon Type Analysis of Middle Distillates by Mass Spectrometry and NMR Spectrometric Technique - A Comparison, *Energy Fuels*., **18**, 1505-1511(2004).
21. Bartholomew, C. H. and Farrauto, R. J., "Fundamentals of Industrial Catalytic Processes", Second edition, Wiley-AIChE: Hoboken, NJ (2005).
22. Bayerlein, R.A., Tamborski, G.A. and Marshall, C.L., *Proceedings of the Symposium on Advances in FCC Technology II*, ACS Meeting, 694-702 (1990).
23. Bayley, J.K., Hrymak, A.N., Treiber, S.S. and Hawkins, R.B., Nonlinear Optimization of a Hydrocracker Fractionation Plant, *Comput. Chem. Eng*., **17**, 123-138(1993).
24. Berry, T.A., McKeen, T.R., Pugsley, T.S. and Dalai, A.K., Two-Dimensional Reaction Engineering Model of the Riser Section of a Fluid Catalytic Cracking Unit, *Ind. Eng. Chem. Res*., **43**, 5571-5581(2004).

25. Bhat, N. and McAvoy T. J., Determining Model Structure for Neural Models by Network Stripping, *Comput. Chem. Eng.*, **16**, 271-281(1992).
26. Bhat, N. and McAvoy, T. J., Use of Neural Nets for Dynamic Modeling and Control of Chemical Process Systems, Comput. Chem. Eng., 14, 573-583(1990).
27. Blasetti, A. and de Lasa, H.I., FCC Riser Unit Operated in the Heat-Transfer Mode: Kinetic Modeling, *Ind. Eng. Chem. Res*., **36**, 3223-3229 (1997).
28. Bollas, G.M., Lappas,A.A., Iatridis,D.K. and Vasalos, I.A., Five Lump Kinetic Model with Selective Catalyst Deactivation for the Prediction of the Product Selectivity in the Fluid Catalytic Cracking Process, *Catal. Today.*, **127**, 31-43(2007a).
29. Bollas, G.M., Vasalos,I.A., Lappas, A.A., Iatridis, D.K., Voutetakis, S.S. and Papadopoulou, S.A., Integrated FCC Riser - Regenerator Dynamics Studied in a Fluid Catalytic Cracking Pilot Plant, *Chem. Eng. Sci*., **62**, 1887-1904 (2007b).
30. Boozarjomehry, R. B., and Svrcek, W.Y., Automatic Design of Neural Network Structures, *Comput. Chem. Eng.,* **25**, 1075–1088(2001).
31. Brereton, C.M.H. and Stomberg, L., Some Aspects of the Fluid Behavior of Fast Fluidized Beds. In Circulating Fluid Bed Technology, Basu, P., Ed, Permagon Press: Toronto, 133-143(1986).
32. Cerqueira, H.S., Caeiro, G., Costa, L. and Ribeiro, F. R., Deactivation of FCC Catalysts, *J. Mol. Catal. A: Chem*. **292**, 1–13(2008).
33. Cerqueira, S. H., Biscaia Jr. E.C. and Sousa-Aguiar, E.F., Mathematical Modeling and Simulation of Catalytic Cracking of Gas Oil in a Fixed Bed: Coke Formation, *Appl. Catal. A.*, **164**, 35-45 (1997).
34. Chartier, P., Gareil, P., Caude, M., Rosset, R. and Neff, B., Bourgognon, H. F. and Husson, J. F., *J. Chromatogr*. 357:381(1986).
35. Chen,C., Yang,B., Yuan,J., Wang,Z. and Wang,L., Establishment and Solution of Eight-Lump Kinetic Model for FCC Gasoline Secondary Reaction using Particle Swarm Optimization, *Fuel*, **86**, 2325–2332(2007).
36. Christensen, G., Apelian, M. R., Hickey, K. J. and Jaffe, S. B., Future Directions in Modeling the FCC Process: An Emphasis on Product Quality, *Chem. Eng. Sci.,* **54**, 2753- 2764 (1999).
37. Corella , J. and Menedez, M., The Modelling of the Kinetics of Deactivation of Monofunctional Catalysts with and Acid Strength Distribution in their Non-

Homogeneous Surface. Application of the Deactivation of Commercial Catalysts in the FCC Process, *Chem. Eng. Sci.*, **41**, 1817-1826 (1986).

38. Corella, J., Bilbao, R., Molina, J.A. and Artigas, A., Variation with Time of the Mechanism, Observable Order, and Activation Energy of the Catalyst Deactivation by Coke in the FCC Process., *Ind. Eng. Chem. Process Des. Dev*., **24**, 625-636 (1985).
39. Corella, J., Fernandez, A. and Vidal, J.M., Pilot Plant for the Fluid Catalytic Cracking Process: Determination of the Kinetic Parameters of Deactivation of the Catalyst, *Ind. Eng. Chem. Process Des. Dev*., **25**, 554-562(1986).
40. Corella, J., On the Modeling of the Kinetics of the Selective Deactivation of Catalysts, Application to the Fluidized Catalytic Cracking Process, *Ind. Eng. Chem. Res*., **43**, 4080 - 4086 (2004).
41. Coxon, P.G. and Bischoff, K.B., Lumping Strategy, 1. Introduction Techniques and Application of Cluster Analysis, *Ind. Eng. Chem. Res.*, **26**, 1239-1248(1987).
42. Dam, M. and Saraf, D. N., Design of Neural Networks Using Genetic Algorithm for On-Line Property Estimation of Crude Fractionator Products, *Comput. Chem. Eng*., **30**, 722–729(2006).
43. Dasila, P.K ., Choudhury I.R., Saraf D.N., Singh,S., Rajagopal, S. and Chopra, S.J ., A New Ten Lump Kinetic Model for Fluid Catalytic Cracking Unit: Determination of Rate Constants, Communicated to Fuel , Dec 2012a
44. Dasila, P.K., Choudhury I.R ., Saraf D.N., Kagdiyal,V., Rajagopal, S. and Chopra, S.J ., Estimation of FCC Feed Composition from Routinely Measured Lab Properties through ANN Model, Communicated to Fuel Processing Technology, Nov, 2012b.
45. Dasila, P.K., Choudhury, I., Saraf, D., Chopra,S. and Dalai, A., Parametric Sensitivity Studies in a Commercial FCC Unit, *Adv. Chem. Eng. Sci*., **2**, 136-149 (2012c).
46. Dave, D.J. and Saraf, D.N., Model Suitable for Rating and Optimization of Industrial FCC Units, *Indian. Chem. Eng. Sec. (A*)., **45**, 7-19 (2003).
47. de Lasa, H. I. and Grace, J. R., The Influence of the Freeboard Region in a Fluidized Bed Catalytic Cracking Regenerator, *AIChE J.*, **25**, 984 (1979).

48. de Lasa, H. I., Errazu,. A., Barrezro, E. and Solzoz , S., Analysis of Fluidized Bed Catalytic Cracking Regenerator Models in an Industrial Scale Unit, *Can. J. Chem. Eng.*, **59**, 549-553 (1981).
49. Dewachtere, N.V., Froment, G.F.,Vasalos, I., Markatos,N. and Skandalis,N., Advanced Modeling of Riser-Type Catalytic Cracking Reactors, *Appl. Therm. Eng.*, **17**, 837-844 (1997).
50. Dooley, J. E., Thompson, C. J., Hirsch, D. E. and Ward, C. C., Analyzing Heavy Ends of Crude, *Hydrocarbon Process.*, **53**, 187-194 (1974).
51. Elkamel, A., Al-Ajmi, A. and Fahim, M., Modeling the Hydrocracker Process using Artificial Neural Networks, *Pet. Sci. Technol.*, **17**, 931-954(1999).
52. Ellis, R. C., Li, X. and Riggs, J. B., Modeling and Optimization of a Model IV Fluidized Catalytic Cracking Unit, *AIChE J*, **44**, 2068-2079 (1998).
53. Errazu, A. F., de-Lasa and Sarti, F., A Fluidized Bed Catalytic Cracking Regenerator Model. Grid Effects, *Can. J. Chem. Eng*., **57**, 191-197(1979).
54. Ewell, R.B.and Gadmer G., Design Cat Crackers by Computer. Hydrocarbon process., 4, 125-134 ,1978.
55. Faltsi-Saravelou, O., Vasalos, I. A., A Model for Fluidized Bed Simulation -II. Simulation of an Industrial Fluidized Catalytic Cracking Regenerator, *Comput. Chem. Eng.*, **15**, 647- 656 (1991b).
56. Faltsi-Saravelou, O., Vasalos, I. A., A Model for Fluidized Bed Simulation I. Dynamic Modeling of an Adiabatic Reacting System of Small Gas Fluidized Particles, *Comput. Chem. Eng*., **15**, 639 - 646(1991a).
57. Farag, H., de Lasa, H. and Ng, S., Kinetic Modeling of Catalytic Cracking of Gas Oils Using in Situ Traps (FCCT) To Prevent Metal Contaminant Effects, *Ind. Eng. Chem. Res*., **32**, 1071- 1080 (1993).
58. Fei W, Xing, R., Rujin, Z., Guohua, Luo., and Yong, J., A Dispersion Model for Fluid Catalytic Cracking Riser and Downer Reactors, *Ind. Eng. Chem. Res.*, **36**, 5049-5053(1997)
59. Feng, W., Vynckier, E and Froment, G. F. Single Event Kinetics of Catalytic Cracking. *Ind. Eng. Chem. Res*., **32**, 2997-3005(1993).
60. Fernandes, J. L., Verstraete, J. J., Pinheiro, C. I. C., Oliveira, N. M. C and Ramoa Ribeiro, F., Dynamic Modelling of an Industrial R2R FCC Unit, *Chem. Eng. Sci*., **62**, 1184-1198 (2007).

61. Froment, G. F. and Bischoff, K. B., “Chemical Reactor Analysis and Design”, Willey: New York, (1979).
62. Froment, G. F. Modeling of Catalyst Deactivation. *Appl. Catal. A: Gen,* **212**, 117(2001).
63. Fujita O. Optimization of the Hidden Unit Function in Feedforward Neural Networks, *Neural Networks*, **5**, 755–764(1992).
64. Fujita O. Statistical Estimation of the Number of Hidden Units for Feedforward Neural Networks, *Neural Networks*, **11**, 851–859(1998)
65. Ganguly, S., Sadhukhan, J. and Saraf, D. N., Artificial Neural Network based Estimation of Petroleum and Product Properties, *Indian Chem. Eng*., **44**, 294–299(2002).
66. Gao, J., Xu, C., Lin, S., Yang, G., and Guo, Y., Advanced Model for Turbulent Gas-Solid Flow and Reaction in FCC Riser Reactor, *AIChE J*., **45**, 1095-1113(1999).
67. Gao, J., Xu, C., Lin, S., Yang, G., and Guo, Y., Simulation of Gas-Liquid-Solid 3-Phase Flow and Reaction in FCC Riser Reactors, AIChE J., 47, 677-692(2001).
68. Gianetto, A., Farag, H. I., Blasetti, A. P. and de Lasa, H. I., Fluid Catalytic Cracking Catalyst for Reformulated Gasolines: Kinetic Modeling. *Ind. Eng. Chem. Res*., **33**(12), 3053-3062(1994).
69. Gidaspow, D., and Huilin, L., Equation of State and Radial Distribution Functions of FCC Particles in a CFB, *AIChE J*., **44**, 279-293(1998).
70. Gross, B., Jacob, S. M., Nace, D. M. and Voltz, S. E., “Simulation of Catalytic Cracking Process”, US Patent 3960707, (1976).
71. Guisnet, M and Magnoux, P., Organic Chemistry of Coke Formation, *Appl. Catal. A: Gen.,* **212**, 83-86 (2001).
72. Guisnet, M. and Magnoux, P., Deactivation by Coking of Zeolite Catalysts. Prevention of Deactivation. Optimal Conditions for Regeneration, *Catal. Today*, **36**, 477-483(1997).
73. Gupta R.K. and Kumar V., Fluid Catalytic Cracking Riser Modeling in Heat Transfer Mode, *Chem. Prod. Process. Model*., **3**(1), Article 11(2008).
74. Gupta, A. and Subba, R. D. Model for the Performance of a Fluid Catalytic Cracking (FCC) Riser Reactor: Effect of feed atomization, *Chem. Eng. Sci*., **56**, 4489-4503(2001).

75. Gupta, G., and Naraasimhan, S., Application of Neural Networks for the Gross Error Detection, *Ind. Eng. Chem. Res.*, **32**, 1651-1657(1993).
76. Gupta, R.K., Kumar, V. and Srivastava, V.K., A New Generic Approach for the Modeling of Fluid Catalytic Cracking (FCC) Riser Reactor, *Chem. Eng. Sci.*, **62**, 4510-4528(2007).
77. Haykin, S., "Neural Networks: A Comprehensive Fundation", Second edition, Upper Saddle Rever, New Jersey, Prentice Hall (1999).
78. Jacob, S. M., Gross, B., Voltz, S.E. and Weekman, V.W.Jr., A Lumping and Reaction Scheme for Catalytic Cracking, *AIChE J.*, **22**, 701-713(1976).
79. Jin, Y., Yu, Z., Qi, C. and Bai, D., The Influence of Exit Structures on the Axial Distribution of Voidage in Fast Fluidized Bed. In Fluidization: Science and Technology, Kwauk, M. and Hasatani, M., Eds., **88**, 165-173 (1988), Science Press: Beijing.
80. Kapur, G.S., Chopra, A. and Sarpal, A. S., Estimation of Total Aromatic Content of Vacuum Gas Oil (VGO) Fractions (370-560 °C) by 1H NMR Spectroscopy, Energy *Fuels.*, **19**, 1065-1071 (2005).
81. Kasat, R.B., Kunzru, D., Saraf, D.N. and Gupta, S.K., Multiobjective Optimization of Industrial FCC Units Using Elitist Non-dominated Sorting Genetic Algorithm, *Ind. Eng. Chem. Res.*, **41**, 4765-4776 (2002).
82. Kraemer, D., Larocca, M., and de Lasa, H.I., Deactivation of Cracking Catalyst in Short Contact Time Reactors: Alternative Models, Can. J. Chem. Eng., 69, 355- 360 (1991).
83. Krishna, A. S., Parkin, E. S., Modeling the Regenerator in Commercial Fluid Catalytic Cracking Units, *Chem. Eng. Prog.*, **81**, 57-62 (1985).
84. Krishnaiah, D., Gopikrishna,V., Bono, A. and Sarbatly, R., Steady State Simulation of a Fluid Catalytic Cracking Unit, *J. Appl. Sci.*, **7**(15), 2137-2145(2007).
85. Kumar, S., Chadha A., Gupta, R. and Sharma, R., CATCRACK: A Process Simulator for an Integrated FCC- Regenerator System, *Ind. Eng. Chem. Res.*, **34**(11), 3737-3748 (1995).
86. Kung, H.H., Williams,B.A., Babitz , S.M.. Miller, J.T., Haag, W.O. and Snurr, R.Q., Enhanced Hydrocarbon Cracking Activity of Y Zeolites , *Top. Catal.*, **10** , 59–64(2000)

87. Kunii, D. and Levenspiel, O., Fluidized Reactor Models. 1. For Bubbling Beds of Fine, Intermediate, and Large Particles. 2. For the Lean Phase: Freeboard and Fast Fluidization, *Ind. Eng. Chem. Res.*, **29**, 1226 -1234(1990).
88. Landeghem, F. Van., Nevicato,D., Pitault,I., Forissier,M., Turlier,P., Derouin, C. and Bernard, J.R., Fluid Catalytic Cracking: Modelling of an Industrial Riser. *Appl. Catal., A* **138**, 381- 405(1996).
89. Lappas, A. A., Patiaka, D. D., Dimitriadis, V. D. and Vasalos, I. A., Separation and Characterization and Catalytic Cracking Kinetics of Aromatic Fraction obtained from FCC Feedstocks, *Appl. Catal. A,* **152,** 7-26 (1997a).
90. Lappas, A. A., Patiaka, D. D., Dimitriadis, V. D. and Vasalos, I. A., Separation and Characterization of Paraffins and Naphthenes from FCC Feedstocks, *Ind. Eng. Chem. Res*., **36**, 3110-3115 (1997b).
91. Larocca, M., Ng, S. and de Lasa, H., Ctalytic Cracking of Heavy Gas Oils: Modelling Coke Deactivation, *Ind. Eng. Chem. Res*., **29**(2), 171-180 (1990).
92. Lee, L., Chen, Y., Huang, T. and Pan, W. Four Lump Kinetic Model for Fluid Catalytic Cracking Process, *Can. J. Chem. Eng*., **67**, 615-619 (1989a).
93. Lee, L., Yu, S., Cheng, C., and Pan, W., Fluidized Bed Catalytic Cracking Regenerator Modeling and Analysis, *Chem. Eng. J*., **40**, 71-82 (1989b).
94. Lee, M and Chen, J., Fluid Property Predictions with the Aid of Neural Networks, *Ind. Eng. Chem. Res*., **32**, 995-997(1993).
95. Li, C., Yang, C. and Shan, H., Maximizing Propylene Yield by Two-Stage Riser Catalytic Cracking of Heavy Oil, Ind. Eng. Chem. Res., 46, 4914 – 4920 (2007).
96. Liguras, D.K. and Allen, D. T. Structural Models for Catalytic Cracking. 1. Model Compound Reactions, *Ind. Eng. Chem. Res*., **28**, 665 -673 (1989).
97. Maya-Yescas, R., Villafuerte-Maciasb, E.F., Aguilar, R. and Salazar-Sotelo, D., Sulphur Oxides Emission During Fluidised-Bed Catalytic Cracking, *Chem. Eng. J.*, **106,** 145–152 (2005).
98. McFarlane, R.C., Reineman, R.C., Bartee, J.F. and Georgakis, C., Dynamic Simulation for a Model IV Fluid Catalytic Cracking Unit-V: Static and Dynamic Bifurcation, *Chem. Eng. Sci,* **50**, 1635-1643 (1995).
99. Michalopoulos, J., Papadokonstadakis,S., Arampatzis, G. and Lygeros, A., Modelling of an Industrial Fluid Catalytic Cracking Unit using Neural Networks, *Trans. IChemE*, **79**(A) (2001).

100. Morley, K. and de Lasa, H. I., On the Determination of Kinetic Parameters for the Regeneration of Cracking Catalyst, *Can. J. Chem. Eng*., **65**, 773 (1987).
101. Morley, K. Lasa and H. I. de. Regeneration of Cracking Catalyst Influence of the Homogeneous CO Post Combustion Reaction. *Can. J. Chem. Eng*., **66**, 428(1988).
102. Murcia, A. A., Numerous Changes Mark FCC Technology Advance, *Oil Gas J*., **90**, 68-71 (1992)
103. Murty, B.S.N., Dutt, N.V.K. and Reddy, P.J., Estimation of Flash Point from Normal Boiling Point using the Artificial Neural Network Technique, *Indian Chemi. Eng. Sec. A.* **37**, 63 (1995).
104. Nace, D. M.,Voltz, S. E. and Weekman, V. W., Application of a Kinetic Model for Catalytic Cracking Effects of Charge Stocks, *Ind. Eng. Chem. Process Des. Dev*., **10**(4), 530-538 (1971).
105. Nace, D.M., Catalytic Cracking Over Crystalline Aluminosilicates. Micro-Recator Study of Gas Oil Cracking, *Ind. Eng. Chem. Process Des. Dev.,* **9**, 203-209(1970).
106. Nam, I. S. and Kittrell, J. R., Use of Catalyst Coke Content in Deactivation Modeling, *Ind. Eng. Chem. Process Des. Dev.,* **23**, 237-242 (1984).
107. Otterstedt, J. E., Gevert, S. B., Jaas S. G. and Menon, P. G., Fluid Catalytic Cracking of Heavy (Residual) Oil Fractions: a Review, *Appl. Catal.,* **22**, 159-179(1986)
108. Paraskos, J. A., Shah, Y.T., McKinney, I.D. and Carr, N.L., A Kinematic Model for Catalytic Cracking in a Transfer Line Reactor, *Ind. Eng. Chem. Process Des. Dev*., **l5**, 165-169 (1976).
109. Penteado, J. C., Rossi, L.F. S. Negr ao, C. O. R. Numerical Modeling of a FCC Regenerator. *In 17th International Congress of Mechanical Engineering (COBEM 2003),* Sao Paulo, Brazil, Associacao Brasileira de Ciencias Mecanicas (ABCM): Sao Paulo, Brazil (2003)
110. Pinheiro, C.I.C., Fernandes, J.L., Domingues, L., Chambel, A. J.S., Graca, I., Nuno, M. C. Oliveira, N. M. C., Cerqueira, H.S and Ribeiro, F.R., Fluid Catalytic Cracking (FCC) Process Modeling, Simulation, and Control, *Eng. Chem. Res*., **51**, 1-29(2012).

111. Pitault, I., Nevicato, D., Forissier, M. and Bernard, J.R., Kinetic Model on a Molecular Description for Catalytic Cracking of Vacuum Gas Oil, *Chem. Eng. Sci.*, **49**, 4249-4262 (1994).
112. Pollock, G., and Eldridge, R., Neural Network Modeling of Structured Packing Height Equivalent of a Theoretical Plate, *Ind. Eng. Chem. Res.*, **39**, 1520-1525 (2000).
113. Quann, R. J. and Jaffe, S. B. Building Useful Models of Complex Reaction Systems in Petroleum Refining, *Chem. Eng. Sci.*, **51**, 1615 (1996).
114. Quann, R. J. and Jaffe, S. B., Structure-Oriented Lumping: Describing the Chemistry of Complex Hydrocarbon Mixtures, *Ind. Eng. Chem. Res*., **31**, 2483(1992).
115. Quintana-Solorzano, R., Thybaut, J. W., Galtier, P. and Marin, G. B., Simulation of an Industrial Riser for Catalytic Cracking in the Presence of Coking using Single-Event Micro Kinetics, *Catal. Today*., **150**, 319- 331(2010).
116. Riazi, M. R., "Characterization and Properties of Petroleum Fractions Handbook", First edition, ASTM Manual Eeries: West Conshohocken, PA (2005).
117. Riazi, M.R., Daubert, R. and Thomas, E., Prediction of the Composition of Petroleum Fractions, *Ind Eng Chem Process Des Dev*., **19**, 289 - 294 (1980).
118. Sa, Y., X. Chen, J. Liu, H. Weng , Z. Zhu and X, Mao. Investigation of the Lumped Kinetic Model for Catalytic Cracking and the Establishment of the Physical Model, *Acta Pet. Sin.* (Pet. Process. Sect.) **1**, 3 (1985).
119. Sa, Y., X. Liang, Chen, X. and Liu, J., Study on the 13-Lump Kinetic Model for Residual Catalytic Cracking, *Memorial of 30th Anniversary of the Fluid Catalytic Cracking Process*, Luoyan Petrochemical Engineering Corporation. Luoyang, China, p. 145(1995).
120. Sadeghbeigi, R., "Fluid Catalytic Cracking Handbook", Second edition, Gulf Professional Publishing: Houston (2000).
121. Schnitzlein, M.G. and Weinstein, H., Flow Characterization in High-Velocity Fluidized Beds using Pressure Fluctuations., *Chem. Eng. Sci*., **43**, 2605-2614(1988).
122. Shah, Y. T., Huling, G. T., Paraskos, J. A. and McKinney, J. D., A Kinematic Model for an Adiabatic Transfer Line Catalytic Cracking Reactor, *Ind. Eng. Chem. Process. Des. Dev.*, **16**, 89-94 (1977).

123. Sheikhattar, L., Zahedi, H. H. G., Artificial Neural Network Simulation and Sensitivity Analysis of Heavy Oil Cracking Unit, *Int. J. Chem. Environ. Eng.*, **2**(1), 7-14 (2011).
124. Shuyan, W. Y.H., Huilin, L., Ding, J., Lijie, Y. and Wentie, L., Simulation of Performance of Cracking Reactions of Particle Clusters in FCC Risers, *Ind. Eng. Chem. Res.*, **47**, 4632-4640 (2008).
125. Speight, J. G., In: Asphaltenes and Asphalts, 1. Developments in Petroleum Science, 40. T. F. Yen and G. V. Chilingarian., Eds, Elsevier Science Publishers., Amsterdam, The Netherlands. Chapter 2, (1994).
126. Speight, J.G., "Handbook of Petroleum Analysis" John Wiley and Sons., Canada (2001).
127. Standard Test Method for Calculation of Carbon Distribution and Structural Group Analysis of Petroleum Oils by the n-d-M Method, ASTM Annual Books of Standard, ASTM International Publishing Co.:West Conshohocken, USA, 5 (2004).
128. Stockwell, D.M. and Wieland, W.S., Proceedings of the Second International Symposium on Deactivation and Testing of Catalysts, *219th ACS National Meeting, Preprints*, pp. 310–316 (2000).
129. Takatsuka, T., Sato, S., Morimoto, Y. and Hashimoto, H., A Reaction Model for Fluidized-Bed Catalytic Cracking of Residual Oil, *Int. Chem. Eng*., **27**, 107-116(1987).
130. Teeter, Richard. M., High Resolution Mass Spectrometry for Type Analysis of Complex Hydrocarbon Mixtures, *Mass Spectrom. Rev*., **4**, 123-143(1985).
131. Theologos, K.N., Lygeros, A.I.and Markatos, N.C. Feedstock Atomization Effects on FCC Riser Reactors Selectivity. Chem. Eng. Sci., 54, 5617-5625(1999).
132. van der Meer, E.H., Thrope, R.B. and Davidson, J.F., Dimensionless Groups for Practicable Similarity of Circulating Fluidised Beds, *Chem. Eng. Sci*., **54**, 5369-5376 (1999).
133. van der Meer, E.H., Thrope, R.B., and Davidson, J.F., Flow Patterns in the Square Cross-Section Riser of a Circulating Fluidized Bed and Effect of Riser Exit Design, *Chem. Eng. Sci.,* **55**, 4079-4099 (2000).
134. Van Nes, K., and Van Westen, H. A., "Aspects of the Constitution of Mineral Oils". Houston-Ainsterdam: Elsevier Press, 484, (1951).

135. Voorhies, A., Carbon Formation in Catalytic Cracking. *Ind. Eng. Chem*., **37**, 318- 322 (1945)
136. Wang, G., Xu, C. and Gao, J., Study of Cracking FCC Naphtha in a Secondary Riser of the FCC Unit for Maximum Propylene Production, *Fuel Process. Technol*., **89**, 864 - 873 (2008).
137. Wang, Z., Massimo, C. D., Tham, M. T., and Morris, J. A Procedure for Determining the Topology of Multilayer Feedforward Neural Networks, *Neural Networks*, **7**, 291–300(1994).
138. Waterman, H. I., Boehower, C., and Cornelissen, J. "Correlation between Physical Constants and Chemical Structure", Elsevier Publishing Co. Inc., New York (1958).
139. Weekman ,V. W. Jr., Kinetics and Dynamics of Catalytic Cracking Selectivity in Fixed Bed Reactors, *Ind. Eng. Chem. Process Des. Dev*., **8**(3), 385-391 (1969).
140. Weekman, V. W. Jr. and Nace, D. M., Kinetics of Catalytic Cracking Selectivity in Fixed, Moving and Fluid Bed Reactors, *AIChE J*., **16**(3), 397- 404, (1970).
141. Weekman, V. W., Lumps, Models, and Kinetics in Practice, *AIChE Monogr. Ser.,* **75**(11), 3 (1979).
142. Weekman, V.W. Jr., A Model of Catalytic Cracking Conversion in Fixed, Moving, and Fluid-Bed Reactors, *Ind. Eng. Chem. Process Des. Dev*., **7**, 90 - 95(1968).
143. Wei, J. and Prater, C.D., A New Approach to First-Order Chemical Reaction System, *AIChE J*., **9**, 77-81 (1963).
144. Weisz, P.B., Combustion of Carbonaceous Deposits within Porous Catalyst Particles, III. The CO2/CO Product Ratio, *J. Catal.*, **6**, 425- 430 (1966).
145. Whaley, A., Bode, C., Ghosh, J., and Eldridge, R., HETP and Pressure Drop Prediction for Structured Packing Distillation Columns using a Neural Network Model, *Ind. Eng. Chem. Res*., **38**(4), 1736-1739(1999).
146. Wojciechowski, B.W., A Theoretical Treatment of Catalyst Decay, *Can. J. Chem. Eng*., **46**,48-52 (1968).
147. Yingxun, Sha., Deactivation by Coke in Residuum Catalytic Cracking. Catalysts Deactivation; C.H. Bartholomew, and J.B. Butt, Eds., Elsevier: Amsterdam, 327-331 (1991).

148. Zahedi, G., Mohammadzadeh, S. and Moradi, G., Enhancing Gasoline Production in an Industrial Catalytic-Reforming Unit using Artificial Neural Networks, *Energy Fuels*., **22**, 2671-2677(2008).
149. Zheng, Y.Y., Dynamic Modeling and Simulation of a Catalytic Cracking Unit, *Comput. Chem. Eng.* **18**, 39 (1994).
150. Zhou J., Grace, J.R., Lim, C.J. and Brereton, C.M.H., Particle Velocity Profiles in a Circulating Fluidized Bed Riser of Square Cross-Section, *Chem. Eng. Sci.,* **50**, 237-244 (1995).
151. Zhou J., Grace, J.R., Qin, S., Brereton, C.M.H., Lim, C.J. and Zhu, J. Voidage Profiles in a Circulating Fluidized Bed of Square Cross-Section. *Chem. Eng. Sci.*, **49**, 3217-3226 (1994).
152. Zhu, K., Mao, X., Weng, H., Zhu, Z. and Liu, F., Investigation of the Lumped Kinetic Model for Catalytic Cracking: II. A Prior Simulation for Experimental Planning, *Acta. Pet. Sin.* (Pet. Process. Sect), **1**, 47 (1985).

APPENDICES

APPENDIX A: Details of Genetic Algorithm (GA)

The constrained optimization problem with objective function given in Eq^n (17) and equality constraints given in eqn (1) to (16) was solved using Genetic Algorithm available in MATLAB Optimization Toolbox. The constraints were multiplayed with Lagrangian multipliers and an augmented unconstrained optimization problem was solved in real variables and not the commonly used binary coded variables. For an efficient use of this technique, several parameters are required to be selected judiciously. These include: population type and size, crossover and mutation probabilities and termination criterion such as number of generations. The choice of these parameters depends on the size and type of problem to be solved. The population is represented by an m x n matrix where m denotes the population size and n denotes the number of variables. For the present problem n is 75. If value of m, the population size, is too small, GA may not explore enough of the solution space to find good solution. After some trial and error following parameters were chosen.

Evolution Parameter

Parameter	Value
Population Type	Real values
Crossover rate	0.8
Population size	900
Maximum Generation	50

Algorithm for Kinetic Parameter Estimation

Step1. Choose the coding parameters: Population size, Crossover probability, max allowable generation t_{max}, lower and upper bounds of kinetic parameters.

Step2. Initial kinetic parameters (LB), t = zero.

Step3. Calculate the yields at riser outlet by solving the material and energy balance equations.

Step4. Minimize the fitness function value

Fitness function is the same as the augmented optimization function.

Step5. If $t > t_{max}$ or any other termination criterion is satisfied, (**Terminate) else Update** the parameters using GA operators and go to **Step3.**

APPENDIX B: Simulation Code for 5-Lump Model

Available with the author

APPENDIX C: Simulation Code for 10-lump Model

Available with the author

LIST OF PUBLICATIONS

1. **Dasila, P.K**., Choudhury I.R., Saraf D.N., Chopra, S.J. and Dalai, A.K., Parametric Sensitivity Studies in a Commercial FCC Unit. Advances in Chemical Engineering and Sciences, 2,136-149 (2012).

2. **Dasila, P.K.,** Choudhury I.R., Saraf D.N., Kagdiyal,V., Rajagopal, S and Chopra, S.J ., Estimation of FCC Feed Composition from Routinely Measured Lab Properties through ANN Model., (Communicated to Fuel Processing Technology, Oct 2012).

3. **Dasila, P.K** ., Choudhury I.R ., Saraf D.N., Singh,S., Rajagopal, S. and Chopra, S.J ., A New Ten Lump Kinetic Model for Fluid Catalytic Cracking Unit: Determination of Rate Constants (Communicated to Fuel , Nov 2012).

4. **Dasila, P.K**., Choudhury I.R., Saraf D.N., Singh, S., Rajagopal, S. and Chopra, S.J., A New Ten Lump Kinetic Model for FCC Riser Reactor, its Validation and Comparison with Five Lump Model (Manuscript under preparation).